**Title**
Limit shapes in two-dimensional lattice models arising from physics and combinatorics

**Permalink**
https://escholarship.org/uc/item/67j1b2kx

**Author**
Keating, David

**Publication Date**
2021

Peer reviewed|Thesis/dissertation

Limit shapes in two-dimensional lattice models arising from physics and combinatorics

by

David A Keating

A dissertation submitted in partial satisfaction of the

requirements for the degree of

Doctor of Philosophy

in

Mathematics

in the

Graduate Division

of the

University of California, Berkeley

Committee in charge:

Professor Nicolai Reshetikhin, Chair
Professor Mark Haiman
Professor John Lott
Professor Alistair Sinclair

Spring 2021

Limit shapes in two-dimensional lattice models arising from physics and combinatorics

Abstract

Limit shapes in two-dimensional lattice models arising from physics and combinatorics

by

David A Keating

Doctor of Philosophy in Mathematics

University of California, Berkeley

Professor Nicolai Reshetikhin, Chair

In this thesis we study aspects of the limit shape phenomenon for two-dimensional lattice models. The three models that will be of greatest interest to us are the six vertex model, the dimer model on the hexagonal lattice, and bounded lecture hall tableaux. Chapter 1 presents a brief overview of the these objects and their relations to one another, as well as the techniques we will use to study them. In Chapter 2, we give a more detailed description of the six vertex model, and describe the Bethe ansatz method for computing the free energy in the thermodynamic limit. We show that there is an infinite family of commuting Hamiltonians governing the evolution of the limiting height function of the inhomogeneous six vertex model on a cylinder. In Chapter 3, we describe the Kasteleyn theory for dimer models on the hexagonal lattice. This dimer model can be seen as a degeneration of the six vertex model from the previous chapter. We study the asymptotic behavior of the dimer correlation functions. In Chapter 4, we turn to the study of an object arising from combinatorics known as bounded lecture hall tableaux. We show that these can be seen as a lattice model of non-intersecting paths on a certain graph. Equivalently, we show how they can be described as a dimer model. We study limit shape formation in the non-intersecting lattice path setting and conjecture formula for the arising Arctic curves. Throughout this thesis many numerical simulations of lattice models are presented. In Chapter 5, we describe an algorithm for numerically simulating lattice models utilizing the parallel processing capabilities of graphical processing units. This method of simulation applies to the previous models studied in this thesis, as well as to many other two-dimensional lattice models. Several examples are given.

# Contents

# List of Figures

# List of Tables

# Chapter 1

# Introduction

## 1.1 Preface

This thesis presents some new results on the statistical mechanics of certain two-dimensional lattice models. In particular, we focus on the limit shape phenomenon. We will discuss the classical integrability of partial differential equations governing limit shape formation (Chapter 2), correlations between fluctuations about the limit shape (Chapter 3), and the computation of Arctic curves separating phase boundaries within the limit shape (Chapter 4). We are most interested in the six vertex model and dimer models (particularly, dimers on the hexagonal lattice). We will also discuss bounded lecture hall tableaux, a combinatorial object that can be expresses as a dimer model or as a collection of non-intersecting paths. Chapter 5 concentrates on technical aspects of numerically simulating lattice models.

Below we briefly describe some aspects of the various models and techniques that will be used in this thesis. We then outline the rest of the thesis and highlight the main results.

## 1.2 The six vertex model

The six vertex model is a prototypical example of a two-dimensional lattice model. It was first introduced by Pauling [77] as a way to model ice in two dimensions. Early results describing the free energy in the thermodynamic limit were obtained by E. Lieb [67]. Given a domain of the square lattice, assign an arrow to each edge such that for any vertex the number of incoming and outgoing arrows are equal. This condition leaves six possible configurations of arrows around each vertex, giving the model its name. To each of these local configurations we assign a weight. Fixing an orientation of the arrows, these configurations can be drawn as a collection of paths, shown in bold in Figure 1.1. Here we choose our orientation so that up and right pointing arrows are drawn as paths, and down and left pointing arrows are not. It is well-known that, on a simply connected domain of the square lattice with fixed boundary conditions, the set of possible path configurations is in bijection with integer valued functions on the faces of the domain. These functions are known as height functions.

The height functions can be defined so that given a six vertex configuration with height function $h$, the paths correspond to the boundaries between level sets of $h$.
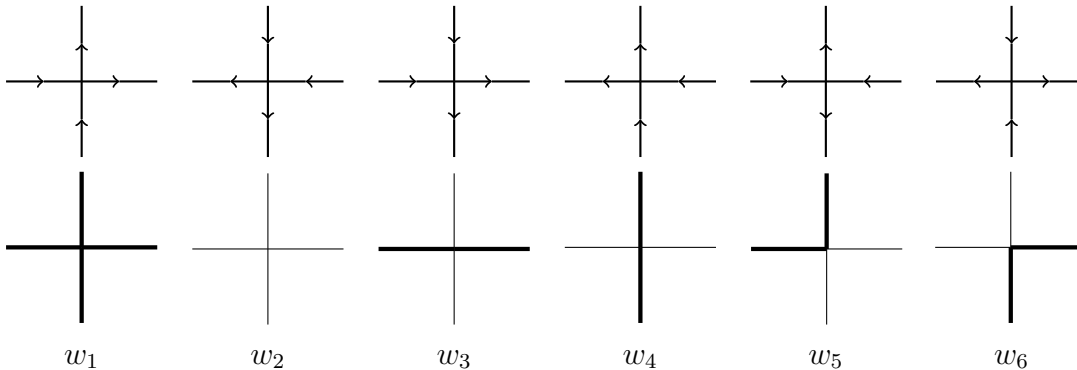


Figure 1.1: Local six vertex configurations as arrows and paths.

## Integrability

The six vertex model on a cylinder was shown by Baxter [5] to be quantum integrable in the sense that there exist an infinite family of commuting row-to-row transfer matrices. The root of this commutativity was the fact that the transfer matrix could be constructed as a tensor product of solutions to the Yang-Baxter equation (YBE) known as quantum $R$-matrices. A representation theoretic origin of the the YBE and its solutions came in the form of quantum groups [47]. In the case of the six vertex model, one is concerned with tensor products of the spin-$\frac{1}{2}$ representation of the quantum group $\mathcal{U}_q(\widehat{\mathfrak{sl}}_2)$. Baxter was able to diagonalize the row-to-row transfer matrix using the coordinate Bethe ansatz. Later an algebraic formulation of the ansatz was developed in [38].

Using these techniques Nicolai Reshetikhin and Ananth Sridhar [83] were able to relate the quantum integrability of the transfer matrices of the homogenous six vertex model to the classical notion of Liouville integrability in Hamiltonian systems. They were able to construct, in the thermodynamic limit, an infinite family of Poisson commuting Hamiltonians that describe the evolution of the height function of the model from one end of a cylinder to the other.

## Limit shape phenomena and Arctic curves

The six vertex model also exhibits what is known as the limit shape phenomenon. As an example, consider the six vertex model on an $N \times N$ square domain with domain wall boundary conditions (DWBC). With these boundary conditions a path enters the domain at every edge along the top boundary and a path exits the domain at every edge along the right boundary. In the limit $N \to \infty$, the height function as a random variable converges to a deterministic function known as the limit shape. The limit shape for the DWBC six
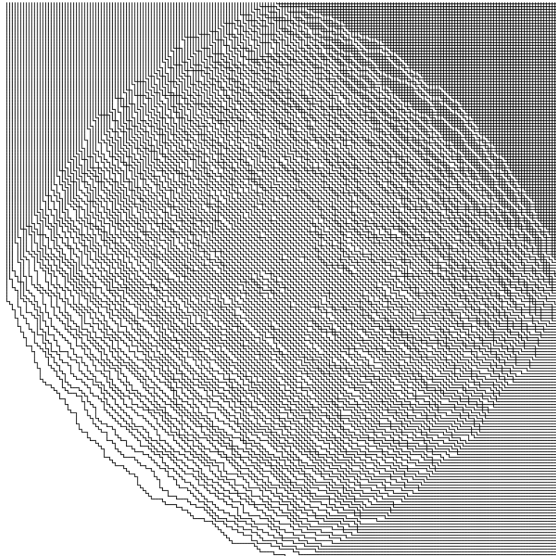
Figure 1.2: A randomly sample configuration of the DWBC six vertex model.

vertex model possesses striking geometric features. This limiting height function exhibits phase separation: the corners of the domain contain certain frozen phases while the interior is in a disordered 'liquid' phase. See Figure 1.2 for an example configuration. These phases are separated by a deterministic boundary known as the Arctic curve. Phase separation also occurs in the Ising model [35] and in dimer models [20]. In both of these cases it was shown that the limiting height function solves a variational problem. A version of the variational principle for the limit shape is believed to hold for the six vertex model as well. For the six vertex model with DWBC the full limit shape is not known except for some very specific choices of vertex weights. However, in [22, 24] the authors were able to calculate an explicit expression for the Arctic curve.

## 1.3   Dimer models

Another class of lattice models are the dimer models. Given graph $G = (V, E)$, a dimer cover $D$ is a subset of edges in which each vertex is adjacent to exactly one edge. This is also known as a perfect matching. The collection of all dimer covers $\mathcal{D}$ defines the configuration space of the model. Commonly one considers bipartite graphs in which we can color the vertices black and white in such a way that each edge connects a black vertex to a white vertex.

Often one is interested in adding weights to the edges. The partition function is defined as

$$Z = \sum_{D \in \mathcal{D}} \prod_{e \in D} w(e)$$
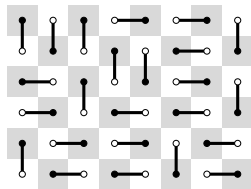
Figure 1.3: A dimer cover of a portion of the square lattice.

where $w : E \to \mathbb{R}_{\geq 0}$ is the weight function. The Gibbs distribution for the dimer model is defined such that the probability of a dimer cover $D \in \mathcal{D}$ occurring is given by $P(D) = w(D)/Z$ where $w(D) = \prod_{e \in D} w(e)$.

See Figure 1.3 for an example of a dimer cover of a portion of the square lattice. Dimer covers of the square lattice are equivalent to domino tilings of a checkerboard.

## Kasteleyn theory

In [50] Kasteleyn proved that the partition function of the planar bipartite dimer model could be written as a determinant of a matrix $K$ known as the Kasteleyn matrix, a signed weighted adjacency matrix for the underlying graph of the dimer model. Similar results for dimer models on surfaces can be found in [18].

The inverse of the Kasteleyn matrix gives information on the statistics of the model [58]. For example, the probability of a particular edge occurring in a dimer cover (sampled according to the Gibbs distribution) depends only on a single entry of the inverse

$$P(e_{w_i b_j}) = |K^{-1}_{w_i b_j}|$$

where the edge connects white vertex $w_i$ with black vertex $b_j$. Similar results hold for the probability of a collection of edges occurring as well.

Understanding the asymptotic behavior of the inverse Kasteleyn matrix allows one to understand the asymptotic density of dimers in the model and is important in understanding the limit shape phenomena and phase separation in dimer models. For example, see [61] where the authors classify the possible phases for bipartite dimer modes and [87, 20] where the authors use the asymptotic behavior of the inverse Kasteleyn matrix on a torus in order to prove that the limit shape of a planar bipartite dimer model solves a variational problem.

## Relation to the six vertex model

Dimer models and the six vertex model share many avenues of research. The study of limit shapes and the fluctuation around these limiting configuration is an active area of research for both systems. In many ways the six vertex model can be seen as a generalization of bipartite dimer models. In fact, at the free fermionic point ($w_1 w_2 + w_3 w_4 - w_5 w_6 = 0$), the six vertex model is equivalent to a certain bipartite dimer model, see Figure 1.4. Certain limits of the six vertex model result in dimer models as well. For example, setting $w_1 = 0$
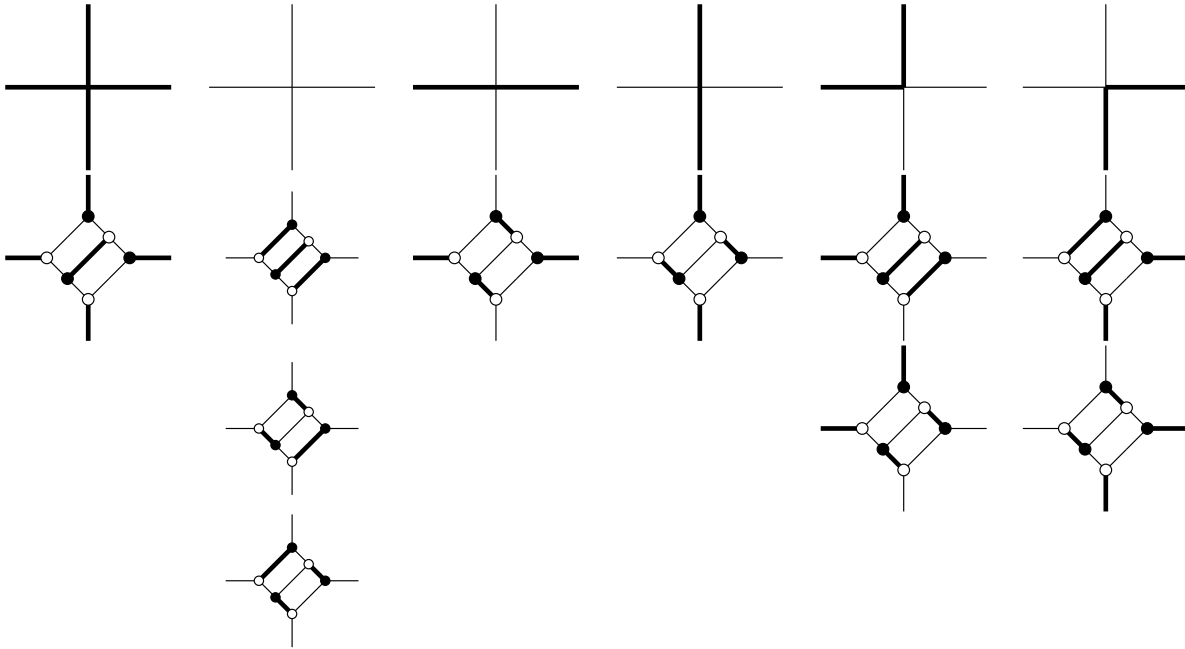
Figure 1.4: Six vertex configurations and the corresponding dimer configuration of the dimer fundamental domain.

results in the five vertex model, which is related to dimers on a hexagonal lattice (Figure 1.5).
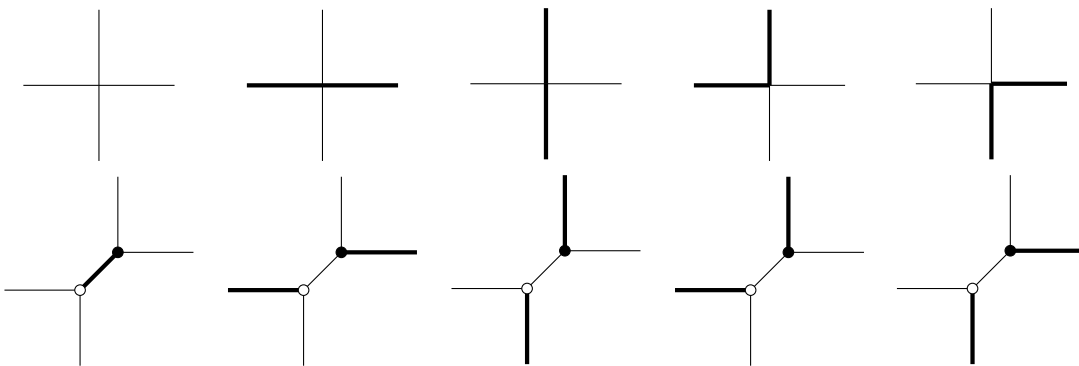
Figure 1.5: Five vertex configurations and the corresponding dimer configuration of the hexagonal lattice fundamental domain.

Many of the results which are known to be true for bipartite dimer models are believed to carry over to the six vertex model as well. In particular, the limit shape for the six vertex model is believed to solve a variational problem, as is the case for planar bipartite dimer models. Further, many results on the structure of the spectrum of the six vertex model

transfer matrix are only proven to be true in the free-fermionic case. For recent progress in generalizing some of these results see [42].

## 1.4   The tangent method

In [21] the authors described a new way to study Arctic curves. Known as the tangent method, it provides a heuristic that can be used to describe the Arctic curve for any system that can be modeled as a collection of non-intersecting paths. By computing certain one-point boundary correlation functions, one is able to obtain a parametrization of the Arctic curve. This new method sacrifices power, one cannot compute the full limit shape, but gains an ease of use and generally applicability. Since its inception the tangent method has been used to calculate Arctic curves for many models, including the six vertex model and dimer models (for example, see [1, 29, 30]). In every case for which the Arctic curve is known by other means, the Arctic curve given by the tangent method is in agreement.

### Heuristic argument

This method relies on two assumption. First, that a portion of the Arctic curve is described in the thermodynamic limit by the trajectory of one of the outermost paths of the model. Second, the tangency assumption: if we vary the endpoint of this path, its new trajectory will follow the arctic curve until it is able to move in a straight line tangent to the arctic curve towards its new endpoint. (There are models in which the path follows a geodesic rather than a straight line [31].) These assumption have been proven in a certain case of the six vertex model [1].

### Boundary correlation function

In practice, using the tangent method requires computing a certain boundary correlation function. This is easiest to explain in picture, see Figure 1.6. Given a DWBC six vertex model, we move the left most paths endpoint to the right by $s$ and down by $z$. We consider the point at which the path crosses the original right boundary of the domain, calling the distance from this point to the paths original endpoint $r$. We then calculate the critical value $r = r*$ that maximizes the probability of finding a configuration in which the path crosses the right boundary of the domain at $r$, fixing $z$ and $s$. The critical point $(0, -r^*)$ and the point $(s, -z)$ define a line which by assumption is tangent to the Arctic curve in the thermodynamic limit. Varying $z$ allows one to find a family of lines which form an envelope of a portion of the Arctic curve. This can then be turned into a parametric description of this portion of the curve. Usually one can use various symmetries of the model at hand in order to obtain the other portions of the Arctic curve.

Adapting this method we were able to describe the Arctic curves in combinatorial objects know as bounded lecture hall tableaux [27].
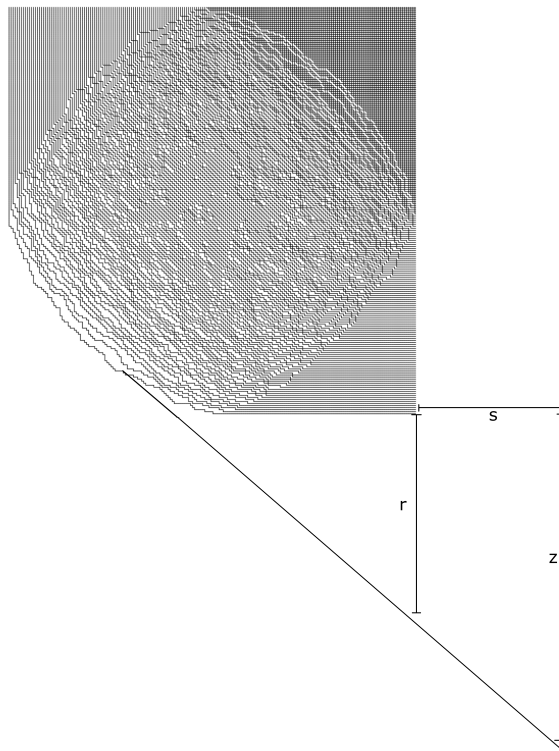
Figure 1.6: Extending the last path in the tangent method. In the thermodynamic limit, one assumes that the path will travel in a straight line tangent to the Arctic curve.

## 1.5 Lecture hall tableaux

### Bounded lecture hall tableaux

Lecture hall tableaux were first introduced [26] in a combinatorial context, where the authors were interested in studying multivariate little $q$-Jacobi polynomials. The authors later introduced bounded lecture hall tableaux (BLHT) [25]. These tableaux are fillings of a Young diagram satisfying certain inequalities depending on two parameters $(n, t)$. In particular, given a Young diagram with filling $T$ one must have

$$\frac{T(i,j)}{n-i+j} \geq \frac{T(i,j+1)}{n-i+j+1}, \qquad \frac{T(i,j)}{n-i+j} > \frac{T(i+1,j)}{n-i-1+j}, \qquad \frac{T(i,j)}{n-i+j} < t$$

where $T(i,j)$ is the filling of the cell in row $i$ and column $j$ and $j-i$ is the content of the cell $(i,j)$. As an example see Figure 1.7.

In [25] the authors showed that, fixing the shape of the Young diagram, the number of BLHT is closely related to the more well-known standard and semi-standard Young tableaux. For example, consider the following expansion of Schur polynomials

$$s_\lambda(t+x_1,\ldots,t+x_n) = \sum_{\mu \subseteq \lambda} |LHT_{\lambda/\mu}(n,t)| s_\mu(x_1,\ldots,x_n),$$

Figure 1.7: On the left is a possible filling $T$ of a bounded lecture hall tableau with $n = 5$, $t = 4$, and $\lambda = (4, 3, 1, 0, 0)$. The diagram on the right shows the numbers $T(i, j)/(n - i + j)$.

where $|LHT_{\lambda/\mu}(n, t)|$ is the number of BLHT of shape $\lambda/\mu$. When $\mu$ is the empty partition, the enumeration is particularly simple and takes the form

$$|LHT_\lambda(n, t)| = t^{|\lambda|} \prod_{1 \le i < j \le n} \frac{\lambda_i - i - \lambda_j + j}{j - i}$$

where $\lambda = (\lambda_1, \ldots, \lambda_n)$.

## Lattice paths

In [25] the authors also described a bijection between the set of BHLT of fixed shape and a collection of non-intersecting paths on a certain irregular graph $\mathcal{G}_t$. The vertices of the $\mathcal{G}_t$ are

- $(i, j/(i + 1))$ for $i \ge 0$ and $0 \le j < t(i + 1)$.

and the directed edges are

- from $(i, k + r/(i+1))$ to $(i+1, k+(r+1)/(i+1))$ for $i \ge 0$ and $0 \le r \le i$ and $0 \le k < t$.

- from $(i, k + (r + 1)/(i+1))$ to $(i, k + r/(i+1))$ for $i \ge 1$ and $0 \le r \le i$ and $0 \le k < t$.

Each path represents a row of the diagram. The path corresponding to the $i^{th}$ row begins at $(n - i, t - 1/(n - i + 1))$ and ends at $(n + \lambda_i - i, 0)$. The number of cells under the horizontal step of the $i^{th}$ path in column $n - i + j$ is given by $T_{ij}$.

In the example given in Figure 1.7, the corresponding collection of non-intersecting paths is given in Figure 1.8. Numerical simulations with large $n, t$ (for example, see Figure 1.9) indicate the presence of a limit shape.

The simplicity of the enumeration, as well as the formulation as a collection of non-intersecting paths make it possible to compute the Arctic curve using the tangent method.

## Relation to dimer models

It is an interesting to note that bounded lecture hall tableaux can be seen as a bipartite dimer model on a non-regular graph. See Figure 1.10. When $t = 1$ this simplifies and one can see bounded lecture hall tableaux as lozenge covering of a trapezoid, equivalently dimers
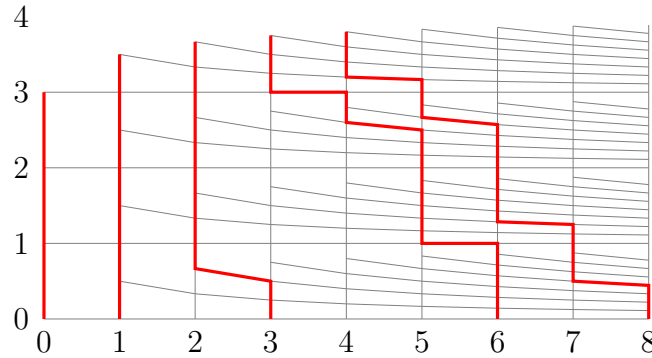
Figure 1.8: Non-intersecting lattice paths on $\mathcal{G}_4$ for $n = 5$ and $\lambda = (4, 3, 1, 0, 0)$.
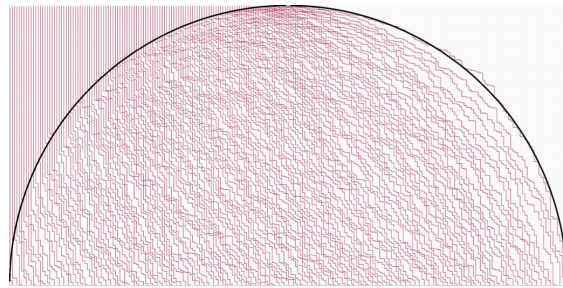


Figure 1.9: Randomly generated configuration for a bounded lecture hall tableaux of shape $\lambda = (n, n - 1, \ldots, 2, 1)$, with $t = n = 120$.
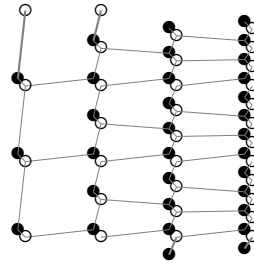


Figure 1.10: The bipartite graph for the dimer model describing bounded lecture hall tableaux for $t = 3$. Here $\lambda = (2, 2)$ and $\mu = (0, 0)$.

on a domain of the hexagonal lattice, Figure 1.11. We see that bounded lecture hall tableaux are closely related to the other models we have discussed. In Chapter 4 we focus on their formulation as non-intersecting paths.
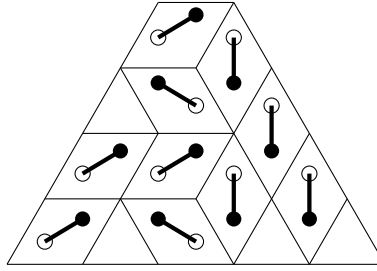
Figure 1.11: Bounded lecture hall tableaux of shape $\lambda/\mu$ with $t = 1$ are equivalent to lozenge tilings of a trapezoid. Above is an example of a possible filling of a bounded lecture hall tableaux with $\lambda = (2,2,1)$, $\mu = (1,0,0)$, $n = 3$ and $t = 1$, along with the corresponding tiling and dimer cover.

## 1.6 Numerical methods

Numerical experiment and numerical evidence has a long history [70, 44] of aiding the study of statistical mechanical systems. Limit shapes for DWBC six vertex model were studied in [4, 64]. For dimer models, and more generally Schur processes, an exact sampling algorithm was given in [8]. As limit shape formation occurs in the thermodynamic limit, it is necessary to have numeric simulations on large domains. Because of this it is useful to have fast sampling algorithms.

### The Metropolis-Hastings algorithm

For lattice models, it is generally the case that on a simply connected domain with fixed boundary conditions the space of possible configurations is connected by a set of local moves. By randomly executing these local moves from a starting configuration one can sample from the space of configurations. As an example consider the Metropolis-Hastings algorithm [70, 44]. This is a Markov chain Monte Carlo method used to randomly generate configuration of some statistical mechanical model. For such a model there is a natural probability measure on the set of configuration, known as the Gibbs distribution. To any configuration $C$ associate the probability $P(C) = W(C)/Z$, where $W(C)$ is the weight of the configuration and $Z$ is a normalization constant known as the partition function.

Given a starting configuration $C_0$, a single step in the Markov chain is given by first proposing a new configuration $C_1$ according to some distribution $p(C_1|C_0)$ and then choosing to accept the proposal according to some distribution $a(C_1, C_0)$. For the cases we are interested in, for which the set of configurations is connected under local moves (see Figure 1.12), the proposal step consists of proposing to execute a particular local move chosen uniformly at random from all possible local moves. The acceptance probability is given by

$$a(C_1, C_0) = \min\left(1, \frac{W(C_1)p(C_0|C_1)}{W(C_0)p(C_1|C_0)}\right).$$
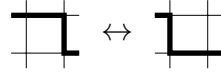
Figure 1.12: The local move for the six vertex model is given by a flipping a single corner.

Note that if the proposal distribution is symmetric this algorithm always accepts a move to a higher weight state. It can be shown that as the number of step goes to infinity, this algorithm samples uniformly from the Gibbs distribution of the model.

## 1.7 Outline of thesis

This section outlines the remaining chapters of this thesis and summarizes the main results within each chapter.

### Chapter 2

In Chapter 2 we give a more detailed overview of the six vertex model on a cylinder with inhomogenieties. We describe the transfer matrix and its use in constructing the partition function of the model, the Bethe ansatz construction of the spectrum of the transfer matrix, the thermodynamic limit of the Bethe ansatz eigenvalues, and the free energy of the six vertex model on the cylinder and on the torus.

The main results of this chapter is the construction of an infinite family of Poisson commuting Hamiltonians for the inhomogeneous six vertex model on a cylinder [52]. This generalizes the result of [83] which held for the homogeneous six vertex model.

**Theorem 1.7.1.** *Let $H_u(\pi, h)$ be the Hamiltonian describing the evolution of height function of the six vertex model form one end of a cylinder to the other. Suppose the position dependent inhomogeneities $u(y)$ are sufficiently small and smooth. Then*

$$\{H_u, H_w\} = 0.$$

This requires a detailed analysis of the properties of the integral kernels coming from the limit of the Bethe equations. We show that the free energy of the inhomogeneous six vertex model satisfies some surprising identities.

### Chapter 3

In Chapter 3 we first recall basic facts about dimer models on the hexagonal lattice. We study the Kasteleyn operator and its description in terms of Kasteleyn fermions. We also study its inverse. The main result of this chapter is a formula for the asymptotic of the inverse to the Kasteleyn operator computed in two different ways: from the integral formula and from its definition in terms of a difference equation.

**Theorem 1.7.2.** *As the lattice spacing $\epsilon \to 0$ the inverse Kasteleyn operator has the following asymptotic*

$$R(h,t|h't') = (e^{\frac{S(z_0)-S(w_0)}{\epsilon}} \frac{\sqrt{\frac{\partial z_0}{\partial \chi_1} \frac{\partial w_0}{\partial \chi_2}}}{z_0 - w_0} + e^{\frac{S(\bar{z}_0)-S(w_0)}{\epsilon}} \frac{\sqrt{\frac{\partial \bar{z}_0}{\partial \chi_1} \frac{\partial w_0}{\partial \chi_2}}}{\bar{z}_0 - w_0} \qquad (1.7.1)$$

$$+ e^{\frac{S(z_0)-S(\bar{w}_0)}{\epsilon}} \frac{\sqrt{\frac{\partial z_0}{\partial \chi_1} \frac{\partial \bar{w}_0}{\partial \chi_2}}}{z_0 - \bar{w}_0} + e^{\frac{S(\bar{z}_0)-S(\bar{w}_0)}{\epsilon}} \frac{\sqrt{\frac{\partial \bar{z}_0}{\partial \chi_1} \frac{\partial \bar{w}_0}{\partial \chi_2}}}{\bar{z}_0 - \bar{w}_0})(1 + O(\epsilon))$$

## Chapter 4

In Chapter 4 we first define lecture hall tableaux, focussing on bounded lecture hall tableaux. We detail their enumeration, their formulation in terms of lattice paths, as well as numerical experiments indicating the existence of a limit shape. We then give an in depth overview of tangent method. We apply this method to compute Arctic curves in the case of bounded lecture hall tableaux. A large emphasis is given to computing explicit examples.

The main result of this chapter is a parametrization of the Arctic curves arising from bounded lecture hall tableaux. Using the tangent method we are able to prove

**Theorem 1.7.3.** *For bounded LHT of shape $\lambda$ the arctic curve can be parametrized by*

$$X(x) = \frac{x^2 I'(x)}{I(x) + xI'(x)}$$
$$Y(x) = \tau \frac{1}{I(x) + xI'(x)} \qquad (1.7.2)$$

*for an appropriate range of $x$. Here $I(x) = e^{-\int_0^1 du \frac{1}{x-\alpha(u)}}$, $\tau = nt$, $n \to \infty$, and $\alpha(u)$, $u \in [0,1]$, is a piecewise differentiable function describing the limiting profile of $\lambda$.*

This work is very much in the spirit of [29, 30].

## Chapter 5

In Chapter 5 we discuss numeric simulations for several different lattice models using both a simple Metropolis-Hastings algorithm as well as coupling-from-the-past. Both of these algorithms rely on the fact that on a simply connected domain, the configuration space of each of these lattice models is connected under certain sets of local moves which we will define. This locality makes it possible to decompose the domain into subsets such that within each subset all the local moves are independent of one another. Such a division makes numerical simulations of lattice models perfect for parallelization.

The main results of this chapter are algorithms for numeric simulations of several lattice models which make use of the parallel capabilities provided by graphical processing units. As examples we show simulations for a variety of different models.

# Chapter 2

# Integrability of the inhomogeneous six vertex model

## 2.1 Introduction

In the thermodynamic limit, the height function of the homogeneous six vertex model develops a limit shape [96, 4, 22, 76]. Moreover, the limit shape height function can be derived from a variational principle similar to the one proven for bipartite dimer models [20]. For the homogeneous six vertex model on a cylinder the limit shape height function can also be interpreted as a Hamiltonian flow in Euclidean time along the cylinder. The Euler-Lagrange equations for this variational principle considered as an evolution equation in Euclidean time admit infinitely many conserved quantities [83]. The conservation laws are obtained by [83] in the Hamiltonian framework. The authors are able construct a Poisson commutative family of functionals, from this it is natural to expect that this Hamiltonian system is integrable.

In this chapter we extend the results of [83] to the case of the six vertex model with integrable inhomogeneities. We prove that Euler-Lagrange equations for critical points of the large deviation functional for this model on a cylinder also have infinitely many conserved quantities. As in the homogeneous case we use the Hamiltonian framework. These results are presented in [52].

One can argue that the existence of infinite number of conservation laws for the PDE defining the limit shape is related to the commutativity of transfer matrices of the six vertex model, and that the conservation laws are a semi-classical version of this property. The *integrable inhomogeneities* that we consider here correspond to shifts of the spectral parameters. As such, they do not change the commutativity of the transfer matrices. The ability to add inhomogeneities to the spectral parameters while preserving the commutativity of the transfer matrices was first observed by Baxter, see [5], and has been used many times in literature, for example [36].

Theorem 2.5.1 states the main result on the Poisson commutativity of an infinite family of integrals of motion. The theorem follows from analysis of bilinear differential identities for

the semi-canonical free energy function. These identities are proven in Theorem 2.5.3. The proof is based on properties of integral equations coming from the Bethe ansatz description of the ground state of the model. These properties are presented in Section 2.4. The analysis largely follows [72, 46]. The description of the free energy uses standard conjectures about the ground state of the six vertex model which are confirmed numerically in numerous cases and in some cases, such as a free-fermionic point, are proven.

The organization of the chapter is as follows: In Section 2.2, we briefly describe the transfer matrix and partition function of the six vertex model, including a review of the Bethe ansatz for determining the spectrum of the transfer matrix. In Section 2.3, we review the structure of the maximal eigenvalue in the thermodynamic limit. Integral equations describing the density of the free energy on a torus in the thermodynamic limit are analyzed in Section 2.4. In Section 2.5, we outline the variational principle and the Hamiltonian framework for the limit shape and prove the main theorem. In the last Section 2.6, we give concluding remarks and present some open problems.

## 2.2 The six vertex model on a cylinder

### The six vertex model

Here we recall some basic facts about the six vertex model (see [5], survey [82] and section 1 of [83] and references therein). Recall that the ice rule implies that the six vertex model can be seen as a set of path which do not cross, but may touch at vertex. Figure 2.1 show the possible states for a single vertex, note that we orient the path up and right.
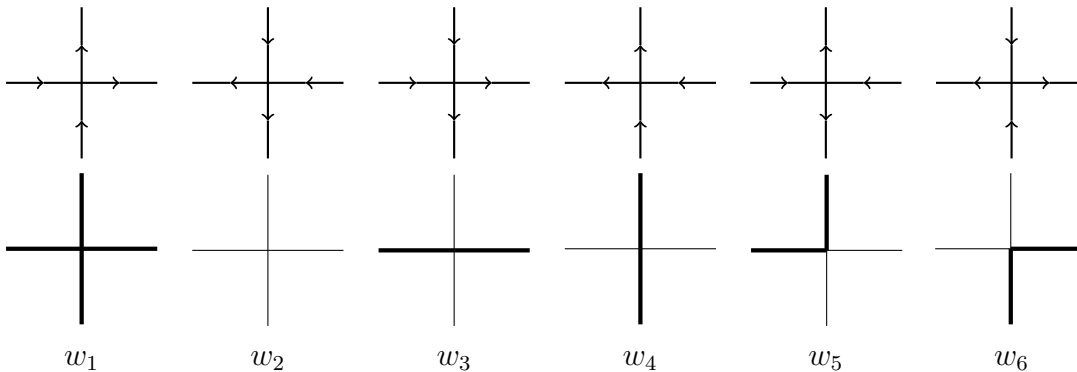


Figure 2.1: Six vertex configurations.

An important parameter of the six vertex model is

$$\Delta = \frac{w_1 w_2 + w_3 w_4 - w_5 w_6}{2\sqrt{w_1 w_2 w_3 w_4}}$$

Baxter gave the following important parameterizations of the weights for the symmetric six vertex model when $w_1 = w_2 = a$, $w_3 = w_4 = b$, and $w_5 = w_6 = c$.

1. When $\Delta > 1$:

   a) If $a > b + c$, let $(a, b, c) = (r \sinh(u + \eta), r \sinh u, r \sinh \eta)$, with $\eta > 0$.

   b) If $b > a + c$, let $(a, b, c) = (r \sinh(u - \eta), r \sinh u, r \sinh \eta)$, with $0 < \eta < u$.

   Here $\Delta = \cosh \eta$.

2. When $\Delta < -1$: let $(a, b, c) = (r \sinh(\eta - u), r \sinh u, r \sinh \eta)$ with $0 < u < \eta$. Here $\Delta = -\cosh \eta$.

3. When $-1 < \Delta < 1$:

   a) If $a > b + c$, let $(a, b, c) = (r \sin(u - \gamma), r \sin u, r \sin \gamma)$, with $0 < \gamma < u < \frac{\pi}{2}$. Here $\Delta = \cos \gamma$.

   b) If $b > a + c$, let $(a, b, c) = (r \sin(\gamma - u), r \sin u, r \sin \gamma)$, with $0 < u < \gamma < \frac{\pi}{2}$. Here $\Delta = -\cos \gamma$.

where $u$ is called the spectral parameter.

In the non-symmetric case the weights can be naturally parametrized as

$$
\begin{aligned}
w_1 &= ae^{H+V}, \; w_3 = be^{H-V}, & w_5 &= c\lambda \\
w_2 &= ae^{-H-V}, \; w_4 = be^{-H+V}, & w_6 &= c\lambda^{-1}
\end{aligned}
\tag{2.2.1}
$$

where $H$ and $V$ can be viewed as magnetic (or electric, depending on the interpretation) field. The magnetic fields can be introduced as edge weights in the symmetric model if we assign each occupied horizontal edge a weight of $e^{\frac{H}{2}}$ and each unoccupied $e^{-\frac{H}{2}}$. Similarly, each occupied vertical edge gets a weight of $e^{\frac{V}{2}}$ and each unoccupied $e^{-\frac{V}{2}}$.

Note that on the cylinder and torus the number of vertices with weight $w_5$ is equal to those with weight $w_6$, so we may set $\lambda = 1$ without loss of generality. As we are primarily concerned with these cases, we set $\lambda = 1$ for what follows.

## The Yang-Baxter equation

Let $e_1 = \begin{pmatrix} 1 \\ 0 \end{pmatrix}$ and $e_2 = \begin{pmatrix} 0 \\ 1 \end{pmatrix}$ be the standard basis of $\mathbb{C}^2$. To each edge we assign a vector in $\mathbb{C}^2$, with $e_1$ corresponding to an occupied edge, and $e_2$ to an unoccupied edge. Then, in the tensor product basis $e_1 \otimes e_1, e_1 \otimes e_2, e_2 \otimes e_1, e_2 \otimes e_2$, we can arrange the six vertex weights into the $4 \times 4$ matrix

$$
R(u, H, V) = \begin{pmatrix}
ae^{H+V} & 0 & 0 & 0 \\
0 & be^{H-V} & c & 0 \\
0 & c & be^{-H+V} & 0 \\
0 & 0 & 0 & ae^{-H-V}
\end{pmatrix}
\tag{2.2.2}
$$

Here we explicitly write the dependence on the spectral parameter and magnetic fields. Let $R(u) = R(u, 0, 0)$. We can write $R(u, H, V)$ as

$$R(u, H, V) = \left(D^H \otimes D^V\right) R(u) \left(D^H \otimes D^V\right) \tag{2.2.3}$$

where $D^H = \begin{pmatrix} e^{\frac{H}{2}} & 0 \\ 0 & e^{-\frac{H}{2}} \end{pmatrix}$. The ice rules imply the identity

$$\left(D \otimes D\right) R(u, H, V) = R(u, H, V) \left(D \otimes D\right) \tag{2.2.4}$$

for any diagonal matrix $D$.

In [5] Baxter showed that the R-matrix satisfies the Yang-Baxter equation

$$R_{12}(u) R_{13}(u + v) R_{23}(v) = R_{23}(v) R_{13}(u + v) R_{12}(u) \tag{2.2.5}$$

in $\mathbb{C}^2 \otimes \mathbb{C}^2 \otimes \mathbb{C}^2$, where the subscripts indicate which factors of the tensor product the matrix acts on and $R(u) = R(u, 0, 0)$. This along with equations (2.2.3) and (2.2.4) imply that

$$R_{12}(u) R_{13}(u + v, H, 0) R_{23}(v, H, 0) = R_{23}(v, H, 0) R_{13}(u + v, H, 0) R_{12}(u) \tag{2.2.6}$$

## The transfer matrix and partition function

Using the $R$-matrix above, we can construct the partition function for the six vertex model on a cylinder.

Consider the inhomogeneous 6-vertex model on a cylinder with inhomogeneity parameters $v_k, k = 1, \cdots, N$ corresponding to vertical lines of the lattice. That is, for a single row the spectral parameter at site $k$ is given by $u - v_k$. Construct that quantum monodromy matrix $T_a(u, \{v_k\}, H, 0) : \mathbb{C}^2 \otimes (\mathbb{C}^2)^{\otimes N} \to \mathbb{C}^2 \otimes (\mathbb{C}^2)^{\otimes N}$ by

$$\begin{aligned} T_a(u, \{v_k\}, H, 0) &= D_a^{2H} R_{1a}(u - v_1) D_a^{2H} R_{2a}(u - v_2) \cdots D_a^{2H} R_{Na}(u - v_N) \\ &= \begin{pmatrix} A(u) & B(u) \\ C(u) & D(u) \end{pmatrix}. \end{aligned} \tag{2.2.7}$$

Here, the first factor is enumerated by $a$, others by $1, \cdots, N$. The matrix elements of $T_a(u, H, 0)$ can be thought of as weight of the configuration on a single row with given boundary conditions. Taking the trace over the first factor and adding a vertical magnetic field we have the row-to-row transfer matrix $t(u, \{v_k\}, H, V) : (\mathbb{C}^2)^{\otimes N} \to (\mathbb{C}^2)^{\otimes N}$

$$t(u, \{v_k\}, H, V) = (D_1^{2V} \cdots D_N^{2V}) \text{Tr}_a\, T_a(u, \{v_k\}, H, 0). \tag{2.2.8}$$

The elements of this can be seen as the weight of a configuration of a single row on the cylinder with specified boundary conditions and magnetic fields $H$ and $V$. Finally, we can construct the partition function on a cylinder with $M$ row with free boundary conditions

and inhomogeneity parameters $u_i, i = 1, \cdots, M$ corresponding to the horizontal lines of the lattice

$$Z_{MN}^{cyl}(\{u_i\}, \{v_k\}, H, V) = t(u_1, \{v_k\}, H, V)t(u_2, \{v_k\}, H, V) \cdots t(u_M, \{v_k\}, H, V).$$

The partition function with boundary states $\xi_1$ and $\xi_2$ is

$$Z_{MN,\xi_1,\xi_2}^{cyl}(\{u_i\}, \{v_k\}, H, V) = (\xi_1, \ t(u_1, \{v_k\}, H, V)t(u_2, \{v_k\}, H, V) \cdots t(u_M, \{v_k\}, H, V)\xi_2).$$

where $(x, y)$ is the natural scalar product on $(\mathbb{C}^2)^{\otimes N}$. Note that equations (2.2.4) and (2.2.8) imply that in the case of the cylinder the vertical magnetic field only contributes an overall factor of $e^{M(N-2n)V}$ to the partition function, where $n$ is number of vertical edges occupied by paths in each row. Because of this we will focus on the partition function of a cylinder with $V = 0$.

If we then take the trace over $(\mathbb{C}^2)^{\otimes N}$, we get the partition function for the $M \times N$ torus

$$Z_{MN}^{torus}(\{u_i\}, \{v_k\}, H, V) = Tr\left(Z_{MN}^{cyl}(\{u_i\}, \{v_k\}, H, V)\right).$$

Note that

$$Z_{MN}^{torus}(\{u_i\}, \{v_k\}, H, V) = \sum_{n=0}^{N} e^{M(N-2n)V} Z_{MN}^{torus,n}(\{u_i\}, \{v_k\}, H).$$

According to the terminology in statistical mechanics, it is natural to call $Z_{MN}^{torus}(u, H, V)$ the grand canonical partition function, where we sum over all possible topological configurations of paths on the torus. The partition function $Z_{MN}^{torus,n}(u, H)$ in this sense should be called the semigrand canonical partition function, where the number of paths crossing a horizontal cycle is fixed by $n$.

## The spectrum of transfer-matrices for finite $N$

Here we assume $\Delta = \frac{(a^2+b^2-c^2)}{2ab} < -1$. In this region Baxter's parametrization is

$$a = \sinh(\eta - u), \quad b = \sinh u, \quad c = \sinh \eta.$$

In this parametrization $\Delta = -\cosh \eta$ and $0 < u < \eta$. Later we will comment on other values of $\Delta$.

The following construction is known as an algebraic Bethe ansatz[1]. It states that if $\{\alpha_j\}$ satisfy the Bethe equations

$$\prod_{k=1}^{N} \frac{\sinh(\frac{\eta}{2} + i\alpha_j - v_k)}{\sinh(\frac{\eta}{2} - i\alpha_j + v_k)} = e^{2HN} \prod_{m=1,m\neq j}^{n} \frac{\sinh(i(\alpha_j - \alpha_m) + \eta)}{\sinh(i(\alpha_j - \alpha_m) - \eta)} \tag{2.2.9}$$

[1] The idea of using a superposition of plane waves as an eigenfunction for the Heisenberg spin Hamiltonian (which is the the logarithmic derivative of the transfer-matrix of the homogeneous 6-vertex model at $u = 0$) goes back to H. Bethe [9]. It was first applied to the 6-vertex model by E. Lieb in [67] for zero magnetic fields. Shorty after C.P. Yang [94] applied it to the asymmetric 6-vertex model (with magnetic fields). The algebraic form we use is due to L. Faddeev and L. Takhtajan [38].

then the vector

$$B(\alpha_1)\dots B(\alpha_n)\,\Omega, \qquad \Omega = \begin{pmatrix} 0 \\ 1 \end{pmatrix} \otimes \cdots \otimes \begin{pmatrix} 0 \\ 1 \end{pmatrix} \tag{2.2.10}$$

is an eigenvector of the transfer-matrix (2.2.8) with the eigenvalue

$$\Lambda(u, \{v_k\}, H, 0) = e^{NH} \prod_{k=1}^{N} \sinh(\eta - u + v_k) \prod_{j=1}^{n} \frac{\sinh(\frac{\eta}{2} + u - i\alpha_j)}{\sinh(\frac{\eta}{2} - u + i\alpha_j)}$$

$$+ e^{-NH} \prod_{k=1}^{N} \sinh(u - v_k) \prod_{j=1}^{n} \frac{\sinh(\frac{3\eta}{2} - u + i\alpha_j)}{\sinh(u - \frac{\eta}{2} - i\alpha_j)}. \tag{2.2.11}$$

This is the description of the spectrum of the transfer-matrix for the model in the horizontal magnetic field $H$ with inhomogeneities $\{v_k\}$ for $\Delta < -1$.

Define functions $p$ and $\Theta$ defined by,

$$e^{ip(\alpha)} = \frac{e^{\eta + 2i\alpha} - 1}{e^{\eta} - e^{2i\alpha}}$$

$$= \frac{\sinh(\frac{\eta}{2} + i\alpha)}{\sinh(\frac{\eta}{2} - i\alpha)},$$

$$e^{i\Theta(\alpha - \beta)} = \frac{1 + e^{ip(\alpha) + ip(\beta)} - 2\Delta e^{ip(\alpha)}}{1 + e^{ip(\alpha) + ip(\beta)} - 2\Delta e^{ip(\beta)}}$$

$$= -\frac{\sinh(i\alpha - i\beta + \eta)}{\sinh(i\alpha - i\beta - \eta)}. \tag{2.2.12}$$

The following identities can be checked directly:

$$\begin{array}{ll} p(\alpha^*) = p(\alpha)^* & p(-\alpha) = -p(\alpha) \\ \Theta(\alpha^*) = \Theta(\alpha)^* & \Theta(-\alpha) = -\Theta(\alpha) \end{array} \tag{2.2.13}$$

Here $a^*$ is the complex conjugate of $a$. In terms of these functions, the Bethe equations can be conveniently written as

$$\prod_{k=1}^{N} e^{ip(\alpha_j + iv_k)} = e^{2HN} \prod_{m=1, m \neq j}^{n} \left( -e^{i\Theta(\alpha_j - \alpha_m)} \right).$$

*Remark* 2.2.1. The spectrum of the transfer-matix for other values of $\Delta$ can be obtained similarly, using the analytical continuation. In terms of functions $a(u), b(u), c(u)$ parametrizing weights of the model, the eigenvalues of the transfer matrix for all values of $\Delta$ can be written as

$$\Lambda(u, \{v_k\}, H, 0) = e^{NH} \prod_{k=1}^{N} a(u - v_k) \prod_{i=1}^{n} \frac{a(\lambda_i - u)}{b(\lambda_i - u)} + e^{-NH} \prod_{k=1}^{N} b(u - v_k) \prod_{i=1}^{n} \frac{a(u - \lambda_i)}{b(u - \lambda_i)}$$

encompassing any choice of parametrization, where the $\lambda_j$ solve the Bethe equations

$$\prod_{k=1}^{N} \frac{b(\lambda_j - v_k)}{a(\lambda_j - v_k)} = e^{2NH}(-1)^n \prod_{i=1, i \neq j}^{n} \frac{a(\lambda_i - \lambda_j)}{a(\lambda_j - \lambda_i)}.$$

Equations (2.2.11) and (2.2.9) follow from choosing the parametrization for $\Delta < -1$ and letting $\lambda_j = i\alpha_j + \frac{\eta}{2}$. For details, see, for example, [63].

Introduce notation

$$
\begin{aligned}
e^{\psi_+(\alpha+iu)} &= \frac{e^{\eta+2u} - e^{2i\alpha}}{e^{\eta-2i\alpha} - e^{2u}} = \frac{\sinh(\frac{\eta}{2} + u - i\alpha)}{\sinh(\frac{\eta}{2} - u + i\alpha)} \\
e^{\psi_-(\alpha+iu)} &= \frac{e^{2\eta+2i\alpha} - e^{2u-\eta}}{e^{2u} - e^{\eta+2i\alpha}} = \frac{\sinh(\frac{3\eta}{2} - u + i\alpha)}{\sinh(u - \frac{\eta}{2} - i\alpha)}.
\end{aligned}
\tag{2.2.14}
$$

Then the formula for eigenvalues of in terms of solutions to Bethe equations can be written as

$$
\begin{aligned}
\Lambda(u, \{v_k\}, H, 0) = e^{NH} \prod_{k=1}^{N} \sinh(\eta - u + v_k) \prod_{j=1}^{n} e^{\psi_+(\alpha_j+iu)} \\
+ e^{-NH} \prod_{k=1}^{N} \sinh(u - v_k) \prod_{j=1}^{n} e^{\psi_-(\alpha_j+iu)}.
\end{aligned}
\tag{2.2.15}
$$

## 2.3 The thermodynamic limit

In this section we will describe the asymptotic of the partition function when $N, M \to \infty$ using the analysis of the Bethe equations in the limit $N \to \infty$. We will first describe the case of homogeneous weights.

### The ground state for finite $N$

Recall the Bethe equations are

$$\prod_{k=1}^{N} e^{ip(\alpha_j+iv_k)} = e^{2HN}(-1)^{n-1} \prod_{m=1, m \neq j}^{n} e^{i\Theta(\alpha_j - \alpha_m)}.$$

Choosing branches of logarithms in the definition of $p(\alpha)$ and $\Theta(\alpha - \beta)$ we can write them as

$$\sum_{k=1}^{N} \frac{1}{N} p(\alpha_j + iv_k) = -2iH + \frac{2\pi I_j}{N} + \sum_{m=1, m \neq j}^{n} \frac{1}{N} \Theta(\alpha_j - \alpha_m)$$

where $I_j$ are integers for odd $n$ and half-integers for even $n$.

The first basic conjecture in the Bethe ansatz description of the largest eigenvalue of the transfer matrix, in the subspace with fixed $n$, states that

**Conjecture 2.3.1.** *When the inhomogeneities and $H$ are sufficiently small, or when the system is homogeneous, the maximal eigenvalue corresponds to solutions of Bethe equations with*

$$I_j = \frac{n+1-2j}{2}, \quad j = 1, \cdots, n$$

This conjecture has a long history. Perhaps, the first detailed study of this conjecture, applied to the Heisenberg XXZ spin chain was done in [95] where the authors also give an account of prior results. It was used to characterize the ground state when $N \to \infty$ and to compute the free energy in this limit in [94][89]. An account of this and other works on the 6-vertex model can be found in a survey [68] and in [5]. Among more recent results are: a detailed exposition of results from [94][89] was done in [73], for a rather detailed study of analytic properties of solutions to Bethe equations for SOS model with twisted boundary conditions see [7], an explicit description of the ground state energy and the free energy for the 5-vertex model was found in [42].

## The ground state in the limit $N \to \infty$, homogeneous case

The following conjecture describes the behavior of the solution to the Bethe equations corresponding to the maximal eigenvalue of the transfer-matrix in the limit when $N \to \infty$ and the ration $n/N$ is fixed.

**Conjecture 2.3.2.** *Fix the ratio $\frac{n}{N}$. As $N \to \infty$, the roots of Bethe equations corresponding to $I_j$ from conjecture 2.3.1 become distributed along a contour $C$ which is described below.*

To describe $C$, let us we introduce

$$2\pi t_j = 2\pi \frac{I_j}{N} \qquad -\frac{q}{2} \le t_j \le \frac{q}{2} \tag{2.3.1}$$

where $q = n/N$. We will write $\alpha(t_j)$ for $\alpha_j$.

As $N \to \infty$ with $q$ fixed, according to the conjecture 2.3.2, the roots $\alpha(t_j)$ of Bethe equations form a complex-valued function $\alpha(t)$, $t \in [-\frac{q}{2}, \frac{q}{2}]$. The Bethe equations become the non-linear integral equation for $\alpha(t)$

$$2\pi t = p(\alpha(t)) + 2Hi - \int_{-q/2}^{q/2} \Theta(\alpha(t) - \alpha(s)) \, ds. \tag{2.3.2}$$

The image of the function $\alpha$ is the contour $C$. This contour connects the endpoints $A = \alpha(-q/2)$ and $B = \alpha(q/2)$. Note that $A = A(q, H)$ depends on both the density and the magnetic field (and similarly for $B$).

Conversely, denote by $t(\alpha) : C \to [-\frac{q}{2}, \frac{q}{2}]$ the inverse of $\alpha(t)$. The function $t$ can be analytically continued off the contour, yielding a complex valued function $t(\alpha)$ which analytic away from singularities and branch cuts. Define $\rho$ to be the density of roots of Bethe equations along $C$. We have

$$\rho(z) = \frac{\partial t(z)}{\partial z}\Big|_{z \in C}. \tag{2.3.3}$$

Note that $\mathrm{Im}\big(\rho(z)\,dz|_C\big) = 0$ and

$$\int_A^B \rho(\alpha)\,d\alpha = q. \tag{2.3.4}$$

From the Bethe equations we obtain the equation for $t(\alpha)$ given by

$$2\pi t(\alpha) = p(\alpha) + 2iH - \int_A^B \Theta(\alpha - \beta)t'(\beta)d\beta. \tag{2.3.5}$$

Here $\alpha \in C$ and the integral is taken along $C$.

Note that $|\mathrm{Re}(t(\alpha))| \le \frac{q}{2}$ and $t(B) = \frac{q}{2}, t(A) = -\frac{q}{2}$.

Suppose $\alpha$ is on the contour so that $t(\alpha)$ is real. Conjugating equation (2.3.5), we have

$$\begin{aligned}
2\pi t(\alpha)^* &= p(\alpha)^* - 2iH + \int_C \Theta(\alpha - \gamma)^* t'(\gamma)^* d\gamma^* \\
&= p(\alpha^*) - 2iH + \int_C \Theta(\alpha^* - \gamma^*) t'(\gamma^*) d\gamma^* \\
&= -p(-\alpha^*) - 2iH + \int_{C^*} \Theta(\alpha^* - \gamma) t'(\gamma) d\gamma \\
&= -p(-\alpha^*) - 2iH - \int_C \Theta(\alpha^* + \gamma) t'(-\gamma) d\gamma \\
&= -p(-\alpha^*) - 2iH + \int_C \Theta(-\alpha^* - \gamma) t'(-\gamma) d\gamma \\
&= -2\pi t(-\alpha^*)
\end{aligned}$$

where we used the the fact that we extended $t$ analytically so that $t'(\gamma)^* = t'(\gamma^*)$. Thus we see that $-\alpha^*$ lies on the contour and $t(\alpha) = -t(-\alpha^*)$. It follows that the roots are distributed symmetrically with respect to reflecting across the imaginary axis. In particular, $B = -A^*$.

Differentiating equation (2.3.5) we obtain an integral equation for $\rho(\alpha)$ given by

$$2\pi\rho(\alpha) = p'(\alpha) - \int_C K(\alpha - \beta)\rho(\beta)d\beta \tag{2.3.6}$$

where $K = \Theta'$. Note that the kernel in the integral equation (2.3.6) is a meromorphic function of $\alpha$. This means that the contour can be deformed as long as it does not cross a pole of $K(\alpha - \beta)$. The condition (2.3.3) selects a representative of the equivalence class of continuous deformations of the contour, such that $\rho(\alpha)\,d\alpha$ is a positive density.

Given the solution to (2.3.6), the equation (2.3.5) defines $t(\alpha)$.

## Maximal eigenvalue in the thermodynamic limit

Recall the form of the eigenvalues (2.2.15) of the homogeneous transfer matrix

$$\Lambda(u, H, 0) = \Lambda_+(u, H, 0) + \Lambda_-(u, H, 0)$$

where

$$\Lambda_+(u, H, 0) = e^{NH} \sinh(\eta - u)^N \prod_{j=1}^{n} e^{\psi_+(\alpha_j + iu)}$$

and

$$\Lambda_-(u, H, 0) = e^{-NH} \sinh(u)^N \prod_{j=1}^{n} e^{\psi_-(\alpha_j + iu)}.$$

For generic values of $H$, only one of $\Lambda_\pm$ contributes in the thermodynamic limit.
Define

$$\psi_u^{(\pm)}(\alpha) = \psi_\pm(\alpha + iu)$$

where $\psi_\pm$ are defined by equation (2.2.14). These functions satisfy

$$\psi_u^{(\pm)}(\alpha)^* = \psi_u^{(\pm)}(-\alpha^*).$$

Define as well

$$l_+ = \ln \sinh(\eta - u), \quad l_- = \ln \sinh u, \tag{2.3.7}$$

where we recall that in our parametrization $0 < u < \eta$.

Fix $H$ and the ratio $q = \frac{n}{N}$. As $N \to \infty$, one of the two terms, $\Lambda_+$ or $\Lambda_-$ dominates and for the largest eigenvalue of the transfer matrix is

$$\Lambda_{\max}(u, q, H) = e^{N\mathcal{H}_u(q,H)}(1 + o(1)),$$

where the function $\mathcal{H}_u(q, H)$ is the semigrand canonical free energy of the six vertex model

$$\mathcal{H}_u(q, H) = \max_\pm \mathcal{H}_u^\pm(q, H) \tag{2.3.8}$$

where

$$\mathcal{H}_u^\pm(q, H) = \pm H + l_\pm + \int_C \psi_u^\pm(\alpha)\rho(\alpha)d\alpha \tag{2.3.9}$$

is the limit of $\frac{1}{N} \ln(\Lambda_\pm(u, q, H))$ when $q$ is fixed, and $\rho(\alpha)$ is the density of Bethe roots along the contour $C$ where they concentrate in the limit $N \to \infty$.

## The free energy of the six vertex model on a torus

Recall that grand canonical partition function of the six vertex model on a torus can be written as

$$Z_{MN}^{torus}(u, H, V) = \sum_{n=0}^{N} e^{M(N-2n)V} Z_{MN}^{torus,n}(u, H) \qquad (2.3.10)$$

where $Z_{MN}^{torus,n}(u, H)$ is the semigrand canonical partition function. The semigrand canonical partition function itself may be written as

$$Z_{MN}^{torus,n}(u, H) = \sum_{\{\alpha_i\}} (\Lambda_{\{\alpha_i\}}(u, H))^M$$

where the sum is over all collections $\{\alpha_1, \ldots, \alpha_n\}$ that solve the Bethe equations, and $\Lambda_{\{\alpha_i\}}$ is the eigenvalue of the transfer matrix $t(u, H, 0)$ corresponding to these Bethe roots.

Thus, when $N, M \to \infty$ with $q = \frac{n}{N}$ fixed, and $M >> N$, one expects the asymptotic of $Z_{MN}^{torus,n}(u, H)$ is determined by the contribution from the maximum eigenvalue. From this we have

$$Z_{MN}^{torus,n}(u, H) = e^{NM\mathcal{H}_u(q,H)}(1 + o(1)) \qquad (2.3.11)$$

with $\mathcal{H}_u(q, H)$ the semigrand free energy defined in (2.3.8). One can argue that this asymptotic is uniform in $\frac{N}{M}$ and is given by the same formula when $N, M \to \infty$ and the ratio $\frac{N}{M}$ is finite. Combining this asymptotic with (2.3.10) we obtain the following asymptotic of the grant canonical partition function as $N, M \to \infty$

$$Z_{MN}^{torus}(u, H, V) = e^{NMV} e^{NM f_u(H,V)}(1 + o(1)). \qquad (2.3.12)$$

Here the grand canonical free energy is the Legendre transform of the semigrand canonical free energy with the vertical magnetic field $V$ conjugate to $q$:

$$f_u(H, V) = \max_q (\mathcal{H}_u(q, H) - 2qV). \qquad (2.3.13)$$

## 2.4 Analysis of density integrals and integral equations

In this section we will study integral equations that appear from Bethe equations in the thermodynamic limit and prove the properties that we use in the proof of the Poisson commutativity of Hamiltonians. In Table 2.1, below, we summarize multiple notations that we use.

| Function | Definition | Location |
|---|---|---|
| $\Theta(\alpha - \beta)$ | $e^{i\Theta(\alpha-\beta)} = -\frac{\sinh(i(\alpha-\beta)+\eta)}{\sinh(i(\alpha-\beta)-\eta)}$ | Def. (2.2.12) |
| $K(\alpha - \beta)$ | $K(\alpha - \beta) = \frac{\partial}{\partial\alpha}\Theta(\alpha - \beta)$ | Eqn. (2.3.6) |
| $p(\alpha)$ | $e^{ip(\alpha)} = \frac{\sinh(\frac{\eta}{2}+i\alpha)}{\sinh(\frac{\eta}{2}-i\alpha)}$ | Def. (2.2.12) |
| $\psi_\pm(\alpha + iu)$ | $e^{\psi_\pm(\alpha+iu)} = \frac{\sinh(u-i\alpha-\frac{\eta}{2}\pm\eta)}{\sinh(\frac{\eta}{2}-u-i\alpha)}$ | Def. (2.2.14) |
| $\mathcal{H}_u^\pm(q, H)$ | $\mathcal{H}_u^\pm(q, H) = \pm H + \ln\,\sinh(\frac{\eta}{2} \pm (\frac{\eta}{2} - u)) + \int_C \psi_\pm(\alpha + iu)\rho(\alpha)d\alpha$ | Eqn. (2.3.9) |
| $F(\alpha, \gamma)$ | $\left(I + \frac{1}{2\pi}K\right) * F = \frac{1}{2\pi}\Theta$ | Eqn. (2.4.1) |
| $R(\alpha, \gamma)$ | $R(\alpha, \gamma) = \frac{\partial}{\partial\gamma}F(\alpha, \gamma)$ | Eqn. (2.4.2) |
| $D_+(\alpha)$ | $\left(I + \frac{1}{2\pi}K\right) * D_+(\alpha) = \frac{1}{2\pi}\left(\Theta(\alpha - B) + \Theta(\alpha - A)\right)$ | Eqn. (2.4.9) |
| $D_-(\alpha)$ | $\left(I + \frac{1}{2\pi}K\right) * D_-(\alpha) = \frac{1}{2\pi}$ | Eqn. (2.4.9) |
| $\xi$ | $\xi = 2\pi i\left(f'(B) + \int_C f'(\alpha)R(\alpha, B)d\alpha\right)$ | Eqn. (2.4.13) |
| $\widetilde{\xi}$ | $\widetilde{\xi} = 2\pi i\left(f'(A) + \int_C f'(\alpha)R(\alpha, A)d\alpha\right)$ | Eqn. (2.4.13) |

Table 2.1: The definitions of various important functions used in the chapter.

## Integrals kernels and integral equations

The integral equation (2.3.6) for $\rho$ can be written as

$$\rho + \left(\frac{1}{2\pi}K * \rho\right) = \frac{1}{2\pi}p'$$

or

$$\left(I + \frac{1}{2\pi}K\right) * \rho = \frac{1}{2\pi}p'$$

where $*$ is convolution, $I$ is the convolution identity, and we recall $K(\alpha) = \Theta'(\alpha)$.

Define $F$ by

$$F(\alpha, \gamma) + \frac{1}{2\pi}\int_C K(\alpha - \beta)F(\beta, \gamma)\,d\beta = \frac{1}{2\pi}\Theta(\alpha - \gamma). \tag{2.4.1}$$

Let $R(\alpha, \gamma) = \frac{\partial}{\partial \gamma} F(\alpha, \gamma)$. It satisfies

$$R(\alpha, \gamma) + \frac{1}{2\pi} \int_C K(\alpha - \beta) R(\beta, \gamma) d\beta = -\frac{1}{2\pi} K(\alpha - \gamma). \tag{2.4.2}$$

In other words,

$$R + \frac{1}{2\pi} K * R = -\frac{1}{2\pi} K$$
$$\Rightarrow \ (I + \frac{1}{2\pi} K) * R = -\frac{1}{2\pi} K$$
$$\Rightarrow \ (I + \frac{1}{2\pi} K) * R + (I + \frac{1}{2\pi} K) = I$$
$$\Rightarrow \ (I + \frac{1}{2\pi} K) * (I + R) = I$$

or as operators

$$I + R = \left( I + \frac{1}{2\pi} K \right)^{-1}.$$

We see that $F$ and $R$ satisfy

$$\left( I + \frac{1}{2\pi} K \right) * F = \frac{1}{2\pi} \Theta \tag{2.4.3}$$

$$\left( I + \frac{1}{2\pi} K \right) * (I + R) = I \tag{2.4.4}$$

**Lemma 2.4.1.** *The functions satisfy the following symmetries:*

*1.* $K(\alpha^*) = K(\alpha)$

*2.* $F(-\alpha^*, -\beta^*) = -F(\alpha, \beta)^*$

*3.* $\rho(\alpha)^* = \rho(-\alpha^*)$

*4.* $R(\alpha, \beta)^* = R(-\alpha^*, -\beta^*)$

**Lemma 2.4.2.**

$$\frac{\partial F(\alpha, \gamma)}{\partial \alpha} = -R(\alpha, \gamma) - R(\alpha, B) F(B, \gamma) + R(\alpha, A) F(A, \gamma)$$

*Proof.* Starting with the definition (2.4.1) of $F$ and taking the $\alpha$ derivative, we have

$$\frac{1}{2\pi}K(\alpha - \gamma) = \frac{\partial F}{\partial \alpha} + \frac{1}{2\pi}\int_C \frac{\partial}{\partial \alpha}K(\alpha - \beta)F(\beta,\gamma)d\beta$$

$$= \frac{\partial F}{\partial \alpha} - \frac{1}{2\pi}\int_C \frac{\partial}{\partial \beta}K(\alpha - \beta)F(\beta,\gamma)d\beta$$

$$= \frac{\partial F}{\partial \alpha} - \frac{1}{2\pi}\left(K(\alpha - B)F(B,\gamma) - K(\alpha - A)F(A,\gamma)\right)$$

$$+ \frac{1}{2\pi}\int_C K(\alpha - \beta)\frac{\partial F(\beta,\gamma)}{\partial \beta}d\beta.$$

Equivalently

$$\frac{1}{2\pi}\left(K(\alpha - \gamma) + K(\alpha - B)F(B,\gamma) - K(\alpha - A)F(A,\gamma)\right) = \left(I + \frac{1}{2\pi}K\right) * \frac{\partial F}{\partial \alpha}(\alpha,\gamma).$$

Multiplying by $(I + R)$ and using

$$\left((I + R) * \frac{1}{2\pi}K\right)(\alpha,\beta) = -R(\alpha,\beta) \tag{2.4.5}$$

we have the lemma. $\qquad\square$

## Analysis of density integrals

In the next section we will study integrals of the form

$$g(q, H) = \int_C f(\alpha)\, \rho(\alpha)\, d\alpha$$

for arbitrary functions $f$, where $\rho$ and $C$ are determined by Bethe integral equation (2.3.6), as well as conditions (2.3.3) and (2.3.4). We will also call these density integrals. Integrals of this type describe largest eigenvalue in the thermodynamic limit (see equations (2.3.8) and (2.3.9)). This section is a survey of [46] and [72].

**Lemma 2.4.3.** $g(q, H)$ *is real if* $f(\alpha)^* = f(-\alpha^*)$.

*Proof.* Since $-C^* = C$

$$g^* = \int_{C^*} f(\alpha)^* \rho(\alpha)^* d\alpha^*$$

$$= \int_{-C^*} f(\gamma) \rho(\gamma) d\gamma$$

$$= \int_C f(\gamma) \rho(\gamma) d\gamma = g$$

$$\square$$

We will assume $f(\alpha)^* = f(-\alpha^*)$ since the functions $\psi_\pm(\alpha)$ satisfy this assumption.

## First derivatives of $g(q, H)$

Here we will compute first derivatives of $g$ in $q$ and $H$. Recall that the endpoints of the contour also depend on $q$ and $H$. Let $dg(q, H) = \frac{\partial g}{\partial q} dq + \frac{\partial g}{\partial H} dH$ be the total derivative with respect to $q$ and $H$.

For the total derivative of $g(q, H)$ we have

$$
\begin{aligned}
dg(q, H) &= d \int_A^B f(\alpha) \rho(\alpha) d\alpha \\
&= dB \, f(B) \, \rho(B) - dA \, f(A) \, \rho(A) + \int_A^B f(\alpha) \, d\rho(\alpha) \, d\alpha
\end{aligned}
\tag{2.4.6}
$$

Recall from equation (2.3.3) that $\rho(\alpha)$ is the partial derivative of $t(\alpha)$ along the contour $C$. We can use this in the above and integrate by parts to obtain

$$
\begin{aligned}
dg(q, H) &= dB \, f(B) \, \rho(B) - dA \, f(A) \, \rho(A) + \int_A^B f(\alpha) \, \frac{\partial dt(\alpha)}{\partial \alpha} \, d\alpha \\
&= dB \, f(B) \, \rho(B) - dA \, f(A) \, \rho(A) + f(B) dt(B) - f(A) dt(A) \\
&\quad - \int_A^B \frac{\partial f(\alpha)}{\partial \alpha} \, dt(\alpha) \, d\alpha
\end{aligned}
\tag{2.4.7}
$$

We know that at the endpoints we have

$$
t(B) = \frac{1}{2} q
$$
$$
t(A) = -\frac{1}{2} q
$$

(see equation (2.3.5)). Varying these equations in $A$ and $B$ we obtain

$$
\begin{aligned}
dt(B) + \rho(B) \, dB &= \frac{1}{2} dq \\
dt(A) + \rho(A) \, dA &= -\frac{1}{2} dq
\end{aligned}
\tag{2.4.8}
$$

**Lemma 2.4.4.** *The variation of $t(\alpha)$ satisfies the following integral equation*

$$
\left( I + \frac{1}{2\pi} K \right) * dt(\alpha) = \frac{i}{\pi} dH - \frac{1}{4\pi} \left( \Theta(\alpha - B) + \Theta(\alpha - A) \right) dq
$$

*Proof.* Starting from equation (2.3.5) and using the previous calculation (2.4.7) with $f(\alpha) = \Theta(\alpha - \beta)$, we have

$$
\begin{aligned}
2\pi \, dt(\alpha) =& 2i \, dH - dB \, \Theta(\alpha - B) \, \rho(B) + dA \, \Theta(\alpha - A) \rho(A) \\
&- \Theta(\alpha - B) \, dt(B) + \Theta(\alpha - A) \, dt(A) - \int_C K(\alpha - \beta) \, dt(\beta) \, d\beta.
\end{aligned}
$$

Then substituting equations (2.4.8) for $\rho(A)dA$ and $\rho(B)dB$ gives

$$dt(\alpha) + \frac{1}{2\pi}K * dt(\alpha) = \frac{i}{\pi}dH - \frac{1}{4\pi}\Theta(\alpha - B)\, dq - \frac{1}{4\pi}\Theta(\alpha - A)\, dq$$

which can be rearranged to give the desired result. $\qquad\square$

Define functions $D_\pm(\alpha)$ as solutions to integral equations

$$\left(I + \frac{1}{2\pi}K\right) * D_-(\alpha) = \frac{1}{2\pi}$$

$$\left(I + \frac{1}{2\pi}K\right) * D_+(\alpha) = \frac{1}{2\pi}\Big(\Theta(\alpha - B) + \Theta(\alpha - A)\Big). \tag{2.4.9}$$

**Lemma 2.4.5.** *The functions $D_\pm$ satisfy*

1. $D_-(\alpha) = \frac{1}{2\pi}\left(1 + F(\alpha, B) - F(\alpha, A)\right)$

2. $D_+(\alpha) = F(\alpha, B) + F(\alpha, A).$

*Proof.*

1. By definition of $R$ we have

$$\left(I + \frac{1}{2\pi}K\right) * (I + R) = I, \quad (I + R) * \left(I + \frac{1}{2\pi}K\right) = I.$$

   Inverting $I + \frac{1}{2\pi}K$ in the definition of $D_-$ we obtain

$$\begin{aligned}
D_-(\alpha) &= \left((I + R) * \frac{1}{2\pi}\right)(\alpha) \\
&= \frac{1}{2\pi} + \frac{1}{2\pi}\int_A^B R(\alpha, \beta)\, d\beta \\
&= \frac{1}{2\pi} + \frac{1}{2\pi}\int_A^B \frac{\partial F(\alpha, \beta)}{\partial \beta}\, d\beta \\
&= \frac{1}{2\pi}\left(1 + F(\alpha, B) - F(\alpha, A)\right).
\end{aligned}$$

2. Similarly for $D_+$ we obtain

$$\begin{aligned}
D_+(\alpha) &= (I + R) * \frac{1}{2\pi}\left(\Theta(\alpha - B) + \Theta(\alpha - A)\right) \\
&= (I + R) * \left(\left(I + \frac{1}{2\pi}K\right) * F(\alpha, B) + \left(I + \frac{1}{2\pi}K\right) * F(\alpha, A)\right) \\
&= F(\alpha, B) + F(\alpha, A).
\end{aligned}$$

□

It is easy to see now that the variation of $t(\alpha)$ can be written as

**Lemma 2.4.6.**
$$dt(\alpha) = 2i \ D_-(\alpha) \ dH - \frac{1}{2} \ D_+(\alpha) \ dq. \tag{2.4.10}$$

Note the following properties of the functions $D_\pm$:

1. When we vary $q$ and $H$, $t(\alpha)$ remains real which implies that $dt(\alpha)$ is real. It follows then that

$$\text{Re } D_-(\alpha) = 0$$
$$\text{Im } D_+(\alpha) = 0.$$

2. The functions $D_\pm(\alpha)$ have the following symmetries with respect to the complex conjugation

$$D_-(\alpha)^* = 1 + F(-\alpha^*, -\beta^*) + F(-\alpha^*, -A^*) = D_-(-\alpha^*)$$
$$D_+(\alpha)^* = -F(-\alpha^*, A) - F(-\alpha^*, B) = -D_+(-\alpha^*).$$

In particular,
$$\begin{aligned} D_-(B) &= D_-(A) \\ D_+(B) &= -D_+(A). \end{aligned} \tag{2.4.11}$$

**Lemma 2.4.7.**

$$\frac{\partial D_+(\alpha)}{\partial \alpha} = -R(\alpha, B)(1 + D_+(B)) - R(\alpha, A)(1 - D_+(A))$$
$$\frac{\partial D_-(\alpha)}{\partial \alpha} = R(\alpha, A)D_-(A) - R(\alpha, B)D_-(B)$$

*Proof.* This follows from a simple computation using Lemmas 2.4.5 and 2.4.2. □

Now, using the variation of $t(\alpha)$, let us complete the first variation of $g(q, H)$.

**Proposition 2.4.8.** *Partial derivatives of $g(q, H)$ can be written as*

$$\frac{\partial g}{\partial H} = -2i \int_C f'(\alpha)D_-(\alpha) \ d\alpha$$
$$\frac{\partial g}{\partial q} = \frac{1}{2} \left( f(B) + f(A) \right) + \frac{1}{2} \int_C f'(\alpha)D_+(\alpha) \ d\alpha.$$

*Proof.* Using equation (2.4.8) and Lemma 2.4.6, we have

$$
\begin{aligned}
dg(q, H) &= dB\, f(B)\, \rho(B) - dA\, f(A)\, \rho(A) + \int_C f(\alpha)\, \partial_\alpha\big(dt(\alpha)\big)\, d\alpha \\
&= \big(dB\, \rho(B) + dt(B)\big)f(B) - \big(dA\, \rho(A) + dt(A)\big)f(A) - \int_C f'(\alpha)\, dt(\alpha)\, d\alpha \\
&= \frac{1}{2}(f(B) + f(A))\, dq - \int_C f'(\alpha)\Big(2i\, D_-(\alpha)\, dH - \frac{1}{2}\, D_+(\alpha)\, dq\Big)\, d\alpha \\
&= \frac{dq}{2}\Big((f(B) + f(A)) + \int_C f'(\alpha)D_+(\alpha)d\alpha\Big) - 2i\, dH \int_C f'(\alpha)D_-(\alpha)\, d\alpha
\end{aligned}
$$

from which the proposition follows. $\qquad\square$

## Second derivatives of $g(q, H)$

Next we turn to calculating the second derivatives of $g(q, H)$. To begin we prove several lemmas that will be useful for later computations.

**Lemma 2.4.9.**

$$
dF(\alpha, \gamma) = R(\alpha, B)\, F(B, \gamma)\, dB - R(\alpha, A)\, F(A, \gamma)\, dA
$$

*Proof.* Starting with the definition (2.4.1) and taking the total derivative we have

$$
\begin{aligned}
dF(\alpha, \gamma) &+ \frac{1}{2\pi} \int_A^B K(\alpha - \beta)\, dF(\beta, \gamma)\, d\beta \\
&+ \frac{1}{2\pi}\Big(K(\alpha - B)F(B, \gamma)\, dB - K(\alpha - A)F(A, \gamma)\, dA\Big) = 0
\end{aligned}
$$

So

$$
\Big(I + \frac{1}{2\pi}K\Big) * dF(\alpha, \gamma) = -\frac{1}{2\pi}\Big(K(\alpha - B)F(B, \gamma)\, dB - K(\alpha - A)F(A, \gamma)dA\Big) \qquad (2.4.12)
$$

Acting with $I + R$ on both sides and using equation (2.4.5) gives the lemma. $\qquad\square$

**Lemma 2.4.10.** *For the total derivative of $D_-(\alpha)$ we have*

$$
dD_-(\alpha) = R(\alpha, B)\, D_-(B)\, dB - R(\alpha, A)\, D_-(A)\, dA.
$$

*Proof.* From the formula for $D_-(\alpha)$ in Lemma 2.4.5 we get

$$
dD_-(\alpha) = \frac{1}{2\pi}\left(dF(\alpha, B) - dF(\alpha, A) + \frac{\partial F(\alpha, B)}{\partial B}dB - \frac{\partial F(\alpha, A)}{\partial A}dA\right).
$$

Substituting the result from Lemma 2.4.9 into the variation of $D_-(\alpha)$ we have

$$
\begin{aligned}
dD_-(\alpha) =& \frac{1}{2\pi} \Big( R(\alpha, B)\, F(B, B)\, dB - R(\alpha, A)\, F(A, B)\, dA \\
& -R(\alpha, B)\, F(B, A)\, dB + R(\alpha, A)\, F(A, A)\, dA + \frac{\partial F(\alpha, B)}{\partial B} dB - \frac{\partial F(\alpha, A)}{\partial A} dA \Big) \\
=& \frac{1}{2\pi} \big( R(\alpha, B)\big(F(B, B) - F(B, A) + 1\big)\, dB - R(\alpha, A)\big(F(A, B) - F(A, A) + 1\big)\, dA \big) \\
=& R(\alpha, B)\, D_-(B)\, dB - R(\alpha, A)\, D_-(A)\, dA
\end{aligned}
$$

as desired. $\qquad\square$

**Lemma 2.4.11.** *For the total derivative of $D_+(\alpha)$ we have*

$$
dD_+(\alpha) = R(\alpha, B) \big(1 + D_+(B)\big)\, dB + R(\alpha, A) \big(1 - D_+(A)\big)\, dA
$$

*Proof.* By straightforward computation starting from Lemma 2.4.5 we obtain

$$
\begin{aligned}
dD_+(\alpha) =& dF(\alpha, B) + dF(\alpha, A) + dB\, \frac{\partial F(\alpha, B)}{\partial B} + dA\, \frac{\partial F(\alpha, A)}{\partial A} \\
=& dF(\alpha, B) + dF(\alpha, A) + dB\, R(\alpha, B) + dA\, R(\alpha, A) \\
=& R(\alpha, B)\, dB + R(\alpha, A)dA + R(\alpha, B)F(B, B)\, dB - R(\alpha, A)F(A, B)\, dA \\
& + R(\alpha, B)F(B, A)\, dB - R(\alpha, A)F(A, B)\, dA \\
=& R(\alpha, B)\big(1 + F(B, B) + F(B, A)\big)\, dB + R(\alpha, A)\big(1 - F(A, B) - F(A, A)\big)\, dA.
\end{aligned}
$$

Using Lemma 2.4.5 again gives the desired result. $\qquad\square$

**Lemma 2.4.12.**

$$
(1 + D_+(B))\, D_-(B) = \frac{1}{2\pi}
$$

*Proof.* Let $J = (1 + D_+(B))\, D_-(B)$. It could be that $D_+, D_-$ depend on $A = -a + ib, B = a + ib$. Note, however, that $F(\alpha, \gamma)$ is invariant under a pure imaginary shift in $\alpha, \gamma$, and the contour, so $D_+(B), D_-(B)$ can only depend on $a$. When $a = 0$, we have $F(\alpha, \gamma) = \frac{1}{2\pi}\Theta(\alpha - \gamma)$ and it follows $J = \frac{1}{2\pi}$. It is left to show that the full derivative of $J$ with respect to $a$ is zero.

Taking derivatives we have

$$
\begin{aligned}
\frac{d}{da}D_-(B) &= \frac{\partial D_-(\alpha)}{\partial \alpha}\Big|_{\alpha=B} \frac{\partial B}{\partial a} + \frac{\partial D_-(\alpha)}{\partial A}\Big|_{\alpha=B} \frac{\partial A}{\partial a} + \frac{\partial D_-(\alpha)}{\partial B}\Big|_{\alpha=B} \frac{\partial B}{\partial a} \\
\frac{d}{da}D_+(B) &= \frac{\partial D_+(\alpha)}{\partial \alpha}\Big|_{\alpha=B} \frac{\partial B}{\partial a} + \frac{\partial D_+(\alpha)}{\partial A}\Big|_{\alpha=B} \frac{\partial A}{\partial a} + \frac{\partial D_+(\alpha)}{\partial B}\Big|_{\alpha=B} \frac{\partial B}{\partial a}.
\end{aligned}
$$

Using Lemmas 2.4.7, 2.4.10, and 2.4.11 for the derivatives and recalling $D_\pm(A) = \mp D_\pm(B) = \mp D_\pm$, these become

$$\frac{d}{da}D_-(B) = R(B,A)D_-(A) - R(B,B)D_-(B) + R(B,A)D_-(A) + R(B,B)D_-(B)$$
$$= 2R(B,A)D_-(B)$$

$$\frac{d}{da}D_+(B) = - R(B,B)(1 - D_+(A)) - R(B,A)(1 + D_+(B))$$
$$- R(B,A)(1 - D_+(A)) + R(B,B)(1 + D_+(B))$$
$$= - 2R(B,A)(1 + D_+(B)).$$

From which it follows

$$\frac{d}{da}J = D_-(B)\frac{d}{da}D_+(B) + (1 + D_+(B))\frac{d}{da}D_-(B)$$
$$= -2D_-(B)R(B,A)(1 + D_+(B)) + 2(1 + D_+(B))R(B,A)D_-(B)$$
$$= 0.$$

We see that $(1 + D_+(B))D_-(B) = \frac{1}{2\pi}$, independent of the endpoints of the contour. $\qquad\square$

Introduce

$$\xi = 2\pi i\Big(f'(B) + \int_C f'(\alpha)R(\alpha, B)\, d\alpha\Big),$$
$$\widetilde{\xi} = 2\pi i\Big(f'(A) + \int_C f'(\alpha)R(\alpha, A)\, d\alpha\Big).$$

(2.4.13)

Note that since $f(\alpha)^* = f(-\alpha^*)$ we have $\widetilde{\xi} = \xi^*$.

**Proposition 2.4.13.** *The following hold*

$$d\frac{\partial g}{\partial H} = -\frac{1}{\pi}D_-(B)\,\xi\, dB + \frac{1}{\pi}\,D_-(A)\,\widetilde{\xi}\, dA \qquad\qquad (2.4.14)$$

$$d\frac{\partial g}{\partial q} = -\frac{i}{4\pi}\big(1 + D_+(B)\big)\xi\, dB - \frac{i}{4\pi}\big(1 - D_+(A)\big)\widetilde{\xi}\, dA. \qquad (2.4.15)$$

*Proof.* We first prove (2.4.14). Starting from Prop. 2.4.8 we have

$$
\begin{aligned}
d\frac{\partial g}{\partial H} =& - 2i\, d \int_C f'(\alpha) D_-(\alpha) d\alpha \\
=& - 2i \left( dB\, f'(B)\, D_-(B) - dA\, f'(A)\, D_-(A) + \int_C f'(\alpha) dD_-(\alpha)\, d\alpha \right) \\
=& - 2i \Big( dB\, f'(B)\, D_-(B) - dA\, f'(A) D_-(A) \\
& + \int_C f'(\alpha) \left( R(\alpha, B)\, D_-(B)\, dB - R(\alpha, A)\, D_-(A)\, dA \right) d\alpha \Big) \\
=& - 2i \Big( dB\, D_-(B) \big( f'(B) + \int_C f'(\alpha) R(\alpha, B) d\alpha \big) \\
& - dA\, D_-(A) \big( f'(A) + \int_C f'(\alpha) R(\alpha, A)\, d\alpha \big) \Big)
\end{aligned}
$$

where we use Lemma 2.4.10. Now let us prove equation (2.4.15). From Prop. 2.4.8 we have

$$
\begin{aligned}
d\frac{\partial g}{\partial q} =& \frac{1}{2} (f'(B)\, dB + f'(A)\, dA) + \frac{1}{2} (f'(B) D_+(B)\, dB - f'(A) D_+(A)\, dA) \\
& + \frac{1}{2} \int_C f'(\alpha) \Big( R(\alpha, B)\, (1 + D_+(B))\, dB + R(\alpha, A)\, (1 - D_-(A))\, dA \Big) d\alpha \\
=& \frac{1}{2} \Big( f'(B) \big( 1 + D_+(B) \big) + (1 + D_+(B)) \int_C f'(\alpha) R(\alpha, B) d\alpha \Big)\, dB \\
& + \frac{1}{2} \Big( f'(A) \big( 1 - D_-(A) \big) + (1 - D_-(A)) \int_C f'(\alpha) R(\alpha, A) d\alpha \Big)\, dA
\end{aligned}
$$

where we use Lemma 2.4.11. $\qquad\square$

Now let us express $dA, dB$ in terms of $dH, dq$. Substituting the formula (2.4.10) for $dt(\alpha)$ into equation (2.4.8) we obtain

$$
2i\, D_-(B)\, dH - \frac{1}{2}\, D_+(B)\, dq + \rho(B) dB = \frac{1}{2} dq
$$
$$
2i\, D_-(A)\, dH - \frac{1}{2}\, D_+(A)\, dq + \rho(A) dA = -\frac{1}{2} dq
$$

or

$$
\begin{aligned}
dB &= \left( \frac{-2i D_-(B)}{\rho(B)} \right) dH + \left( \frac{1 + D_+(B)}{2\rho(B)} \right) dq \\
dA &= \left( \frac{-2i D_-(A)}{\rho(A)} \right) dH - \left( \frac{1 - D_+(A)}{2\rho(A)} \right) dq.
\end{aligned}
\qquad (2.4.16)
$$

**Proposition 2.4.14.** *The second derivatives of $g(q, H)$ are given by*

$$\frac{\partial^2 g}{\partial H^2} = \frac{2i}{\pi} \left( \frac{D_-(B)^2}{\rho(B)} \xi - \frac{D_-(A)^2}{\rho(A)} \widetilde{\xi} \right)$$

$$\frac{\partial^2 g}{\partial H \partial q} = -\frac{1}{2\pi} \left( \frac{1 + D_+(B)}{\rho(B)} D_-(B) \xi + \frac{1 - D_+(A)}{\rho(A)} D_-(A) \widetilde{\xi} \right)$$

$$\frac{\partial^2 g}{\partial q^2} = -\frac{i}{8\pi} \left( \frac{(1 + D_+(B))^2}{\rho(B)} \xi - \frac{(1 - D_+(A))^2}{\rho(A)} \widetilde{\xi} \right)$$

*Proof.* Combining (2.4.16) with formulas for the second variation, (2.4.14) and (2.4.15), we obtain

$$d\frac{\partial g}{\partial H} = -\frac{1}{\pi} \left( \left( \frac{-2iD_-(B)}{\rho(B)} \right) dH + \frac{1 + D_+(B)}{2\rho(B)} dq \right) D_-(B) \xi$$
$$+ \frac{1}{\pi} \left( \left( \frac{-2iD_-(A)}{\rho(A)} \right) dH - \frac{1 - D_+(A)}{2\rho(A)} dq \right) D_-(A) \widetilde{\xi}$$
$$= i \left( \frac{D_-(B)^2}{\rho(B)} \xi - \frac{D_-(A)^2}{\rho(A)} \widetilde{\xi} \right) dH$$
$$- \frac{1}{4} \left( \frac{1 + D_+(B)}{\rho(B)} D_-(B) \xi + \frac{1 - D_+(A)}{\rho(B)} D_-(A) \widetilde{\xi} \right) dq$$

and

$$d\frac{\partial g}{\partial q} = -\frac{i}{4\pi} (1 + D_+(B)) \xi \left( \left( \frac{-2iD_-(B)}{\rho(B)} \right) dH + \frac{1 + D_+(B)}{2\rho(B)} dq \right)$$
$$- \frac{i}{4\pi} (1 - D_+(A)) \widetilde{\xi} \left( \left( \frac{-2iD_-(A)}{\rho(A)} \right) dH - \frac{1 - D_+(A)}{2\rho(A)} dq \right)$$
$$= -\frac{1}{2\pi} \left( (1 + D_+(B)) \frac{D_-(B)}{\rho(B)} \xi + (1 - D_+(A)) \frac{D_-(A)}{\rho(A)} \widetilde{\xi} \right) dH$$
$$- \frac{i}{8\pi} \left( \frac{(1 + D_+(B))^2}{\rho(B)} \xi - \frac{(1 - D_+(A))^2}{\rho(A)} \widetilde{\xi} \right) dq.$$

$\square$

Recall that the quantity we are interested in is equation (2.3.9) in which the role of $f(\alpha)$ is played by $\psi_u^\pm(\alpha)$. The functions $\psi_u^\pm(\alpha)$ depend on the spectral parameter $u$ as $\psi^\pm(\alpha + iu)$. We will assume then that $f$ depends on the spectral parameter in the same way. In particular, $\frac{\partial f}{\partial u} = if'$.

**Proposition 2.4.15.**

$$\frac{\partial^2 g}{\partial H \partial u} = -\frac{i}{\pi}\left(D_-(B)\xi - D_-(A)\widetilde{\xi}\right)$$

$$\frac{\partial^2 g}{\partial q \partial u} = \frac{1}{4\pi}\left((1 + D_+(B))\,\xi + (1 - D_+(A))\,\widetilde{\xi}\right)$$

*Proof.* Starting with Proposition 2.4.8

$$\frac{\partial g}{\partial H} = -2i\int_C f'(\alpha)D_-(\alpha)\,d\alpha$$

$$= -2i\left(f(B)D_-(B) - f(A)D_-(A) - \int_C f(\alpha)D'_-(\alpha)\,d\alpha\right)$$

$$= -2i\left(f(B)D_-(B) - f(A)D_-(A) + \int_C f(\alpha)\big(R(\alpha,B)D_-(B) - R(\alpha,A)D_-(A)\big)\,d\alpha\right).$$

Differentiating with respect to $u$ gives

$$\frac{\partial^2 g}{\partial H \partial u} = 2\left(f'(B)D_-(B) - f'(A)D_-(A) + \int_C f'(\alpha)\big(R(\alpha,B)D_-(B) - R(\alpha,A)D_-(A)\big)\,d\alpha\right)$$

$$= 2D_-(B)\left(f'(B) + \int_C f'(\alpha)R(\alpha,B)\,d\alpha\right) - 2D_-(A)\left(f'(A) + \int_C f'(\alpha)R(\alpha,A)\,d\alpha\right)$$

$$= -\frac{i}{\pi}\left(D_-(B)\,\xi - D_-(A)\,\widetilde{\xi}\right).$$

Similarly

$$\frac{\partial g}{\partial q} = \frac{1}{2}\left(f(B) + f(A)\right) + \frac{1}{2}\int_C f'(\alpha)D_+(\alpha)\,d\alpha$$

$$= \frac{1}{2}f(B)(1 + D_+(B)) + \frac{1}{2}f(A)(1 - D_-(A)) - \frac{1}{2}\int_C f(\alpha)D'_+(\alpha)\,d\alpha$$

$$= \frac{1}{2}f(B)(1 + D_+(B)) + \frac{1}{2}f(A)(1 - D_-(A)) + \frac{1}{2}\int_C f(\alpha)R(\alpha,B)(1 + D_+(B))d\alpha$$

$$+ \frac{1}{2}\int_C f(\alpha)R(\alpha,A)(1 - D_+(A))d\alpha.$$

Differentiating with respect to $u$ gives

$$\frac{\partial^2 g}{\partial q \partial u} = \frac{1}{4\pi}\left((1 + D_+(B))\,\xi + (1 - D_+(A))\,\widetilde{\xi}\right).$$

$\square$

## 2.5  The limit shape and its integrability

### The variational principle

Using the same arguments as in the case of dimer models [20], and in the homogeneous six vertex model [96, 76, 83], one can formulate the variational principle for the six vertex model with inhomogeneous weights.

Introduce the height function for the six vertex model in the usual way, see for example [83]. It is an integer valued function $\theta_{n,m}$ defined on faces of the square grid. Its value on a face is determined by local rules shown in Fig. 2.2. After choosing the value $\theta_{a,b}$ at a single face, the local rules give a bijection between possible height functions and six vertex configurations on a planar simply connected domain.

However, local rules do not define a height function on a cylinder. In this case, the local definition of the height function may lead to a discontinuity along a non-contractible path. This simply means that the global object defined by these local rules is not a function but a section of the corresponding line bundle.

To have a height function be a true function we cut the cylinder at column $n = 0$ and fix its value at a face with the condition $\theta_{0,0} = 0$. Thus, the height function for us is a function $\theta_{n,m}$ with $n = 0, 1, \ldots, N, m = 0, 1, \ldots, M$. If a six vertex configuration has $n_0$ paths entering from the bottom and exiting from the top, the height function has monodromy

$$\theta_{N,m} - \theta_{0,m} = n_0.$$
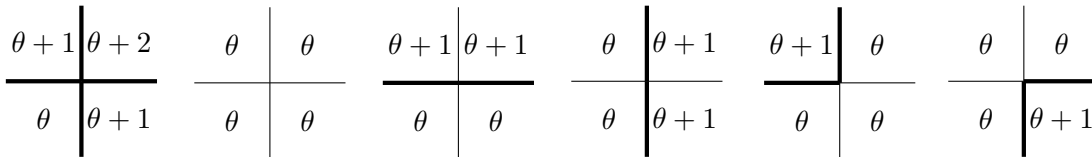


Figure 2.2: Local rules for the height function of the six vertex model.

Let us describe the thermodynamic limit for a torus and the formation of the limit shape.

Fix a sequence $\{\epsilon_k\}_{k=1}^{\infty}$ such that $\epsilon_k \to 0$ as $k \to \infty$ and $\epsilon_k > 0$. One should think of it as a sequence of mesh lengths. Consider a sequence of cylinders of size $N_k \times M_k$ such that $N_k \epsilon_k \to L$ and $M_k \epsilon_k \to T$ as $k \to \infty$. Fix two functions $\phi_1, \phi_2 : [0, L] \to \mathbb{R}$ satisfying conditions

$$|\phi_i(x) - \phi_i(x')| \leq |x - x'|$$

assuming that $\phi_i(L) = \phi_i(0) + q$ for some $0 < q < 1$.

Fix a sequence of non-negative integers $n_0^k$ such that $\epsilon_k n_0^k \to q$ as $k \to \infty$. For each $k$ fix functions $\theta^{k,1}, \theta^{k,2} : \{0, 1, \ldots, N_k\} \to \mathbb{Z}$ such that

$$|\theta_n^{k,i} - \theta_{n,}^{k,i}| \leq |n - n'|, \quad \theta_{N_k}^{k,i} - \theta_0^{k,i} = n_0^k$$

Assume that as $k \to \infty$, normalized boundary height functions $\epsilon_k \theta^{k,i}$, regarded as a piecewise linear function on $[0, L]$, converges to $\phi_i$ in $L_\infty$ topology. Also, assume that $u_i = u(\epsilon_k i)$ and $v_i = v(\epsilon_k i)$ where $u(x)$ and $v(y)$ are smooth functions.

Define the space $H_{L,T,q}^{\phi_1,\phi_2}$ of asymptotic height functions as the space of mappings $h : [0, L] \times [0, T] \to \mathbb{R}$ with the properties

$$|h(x,y) - h(x',y)| < |x - x'|, \quad |h(x,y) - h(x,y')| < |y - y'|$$

$$h(L,y) = h(0,y) + q, \quad h(x,0) = \phi_1(x), \quad h(x,T) = \phi_2(x)$$

where $0 \le q \le 1$.

Applying the same arguments as [20] we expect that the sequence of random variables $\theta_{n,m}^k$ (height functions for the six vertex model on $N_k \times M_k$ cylinders with boundary conditions $\theta^{k,1}$ and $\theta^{k,2}$) have the following asymptotic:

$$\epsilon_k \theta_{n,m} \to h_0(x,y) + \epsilon_k \phi(x,y) + \ldots$$

Here we assume that $\epsilon_k n \to x, \epsilon_k m \to y$. The deterministic functions $h_0(x,y)$ is the limit shape and the random variable $\phi(x,y)$ describes Gaussian fluctuations around the limit shape. The convergence is in probability, with respect to to the six vertex probability measures on $N_k \times M_k$ cylinders.

The limit shape $h_0$ in the inhomogeneous six vertex model is the minimizer of the functional

$$S[h] = \int_0^L \int_0^T \sigma_{u(y)-v(x)}(\partial_x h, \partial_y h) dy dx \tag{2.5.1}$$

in the space $H_{L,T,q}^{\phi_1,\phi_2}$.

## Hamiltonian formulation

As was done in the homogeneous case [83] let us reformulate the variational principle in the Hamiltonian framework. For the time being we will assume that the six vertex model is homogeneous in the vertical direction, i.e. $u(y) = u$.

Define the space of asymptotic height functions $\mathcal{H}_{L,q}$ in one horizontal layer as the space of mappings $h : [0, L] \to \mathbb{R}$ satisfying the Lipschitz and periodicity conditions

$$|h(x) - h(x')| < |x - x'|, \quad h(L,y) = h(0,y) + q,$$

where $0 < q < 1$ is fixed. Elements of the cotangent space $T^* \mathcal{H}_{L,q}$ can be identified with pairs of functions $(\pi(x), h(x))$ where $h(x)$ is as above and $\pi(x)$ is a function periodic in $x$. It is an infinite dimensional symplectic manifold with symplectic form

$$\omega = \int_0^L \delta \pi(x) \wedge \delta h(x) dx. \tag{2.5.2}$$

Now let us formulate the Hamiltonian version of the variational principal. It is an easy exercise to check that if $(\pi(x,y), h(x,y))$ is a flow line of the Hamiltonian vector field on $T^*\mathcal{H}_{L,q}$ generated by the Hamiltonian function

$$H_u(\pi, h) = \int_0^L \mathcal{H}_{u-v(x)}(\partial_x h(x), \pi(x))dx. \tag{2.5.3}$$

then $h(x,y)$ is a solution to the Euler-Lagrange equations. Here the function $\mathcal{H}_u(q, H)$ is the semigrand canonical free energy (2.3.8).

Moreover, there is unique flow line $(\pi_0, h_0)$ of this Hamiltonian vector field which connects Lagrangian subspaces $T^*_{\phi_1}\mathcal{H}_{q,L}$ and $T^*_{\phi_2}\mathcal{H}_{q,L}$ in Euclidian time $T$. And the component $h_0$ is the minimizer of 2.5.1. Also, the pair $(\pi_0, h_0)$ is the unique critical point in $T^*H^{\phi_1,\phi_2}_{L,T,q}$ of the Hamilton-Jacobi functional

$$S_{HJ}(\pi, h) = \int_0^L \int_0^T (\pi(x,y)\partial_y h(x,y) - \mathcal{H}_{u-v(x)}(\partial_x h(x,y), \pi(x,y)))dydx \tag{2.5.4}$$

Indeed, first minimizing in $\pi$ and evaluating this functional at the unique critical point we will arrive to the minimization problem for (2.5.1). The existence and uniqueness of the critical point follows from the convexity of $\mathcal{H}_u(s,t)$ in $t$.

## Poisson commutativity of the Hamiltonians

The main result of this chapter is the Poisson commutativity of the family $H_u(\pi, h)$ where $v(x)$ is an arbitrary smooth functions as described in 2.5. The first step is the following proposition that characterizes the commutativity of the Hamiltonians $H_u$ in terms of differential identities for the densities $\mathcal{H}_{u-v(x)}$.

**Theorem 2.5.1.** *The Hamiltonians 2.5.3 form Poisson commutative family*

$$\{H_u, H_w\} = 0$$

*for any $u$ and $w$ if the following identities hold for $\mathcal{H} = \mathcal{H}(\pi, h, u-v(x))$ and $\widetilde{\mathcal{H}} = \mathcal{H}(\pi, h, w-v(x))$:*

$$\begin{aligned}
\mathcal{H}_{11}\widetilde{\mathcal{H}}_{22} - \widetilde{\mathcal{H}}_{11}\mathcal{H}_{22} &= 0 \\
\mathcal{H}_{11}\widetilde{\mathcal{H}}_{23} + \mathcal{H}_{12}\widetilde{\mathcal{H}}_{13} - \mathcal{H}_{13}\widetilde{\mathcal{H}}_{12} - \mathcal{H}_{23}\widetilde{\mathcal{H}}_{11} &= 0 \\
\mathcal{H}_{12}\widetilde{\mathcal{H}}_{23} + \mathcal{H}_{22}\widetilde{\mathcal{H}}_{13} - \mathcal{H}_{13}\widetilde{\mathcal{H}}_{22} - \mathcal{H}_{23}\widetilde{\mathcal{H}}_{12} &= 0
\end{aligned} \tag{2.5.5}$$

*where $f_i$ means the derivative of $f$ with respect to the $i$-th argument.*

*Remark* 2.5.2. The assumption that $v(x)$ is smooth can be relaxed; for example, the computations are almost identical when $v(x)$ is piecewise smooth, but with some subtleties that we will not discuss here.

*Proof.* Straightforward computation gives

$$\{H_u, H_w\} = \int_0^L \left( A\, \partial_x \pi + B\, \partial_x^2 h + C\, \partial_x(u - v(x)) \right)\, dy \tag{2.5.6}$$

where

$$
\begin{aligned}
A &= \mathcal{H}_{11}\widetilde{\mathcal{H}}_2 - \widetilde{\mathcal{H}}_{11}\mathcal{H}_2 \\
B &= \mathcal{H}_{12}\widetilde{\mathcal{H}}_2 - \widetilde{\mathcal{H}}_{12}\mathcal{H}_2 \\
C &= \mathcal{H}_{13}\widetilde{\mathcal{H}}_2 - \widetilde{\mathcal{H}}_{13}\mathcal{H}_2.
\end{aligned}
\tag{2.5.7}
$$

The integrand in (2.5.6) will be a total derivative if all the mixed derivatives are zero (a closed one form), that is

$$
\begin{aligned}
\partial_2 A - \partial_1 B &= 0 \\
\partial_3 A - \partial_1 C &= 0 \\
\partial_3 B - \partial_2 C &= 0.
\end{aligned}
\tag{2.5.8}
$$

$\square$

In section 2.5 , we will prove that the identities (2.5.5) hold for the 6-vertex model.

## Proof of Commuting Hamiltonians

Let us apply the analysis of integral equations in the previous section to the case of interest eqn. (2.3.9), reproduced here

$$\mathcal{H}^{\pm}_{u-v(x)}(q, H) = \pm H + l_\pm + \int_C \psi_u^\pm(\alpha)\rho(\alpha)d\alpha$$

where $l_\pm$ depend only on the spectral parameter. Note that when we take second derivatives, only the contributions from the integral above will remain. This integral is precisely of the form of $g(q, H)$. Using Prop. 2.4.14 and 2.4.15 and Lemma 2.4.12, we have

$$
\begin{aligned}
\mathcal{H}_{11} &= -\frac{4D_-^2}{\pi}\; \mathrm{Im}(\xi/q) \\
\mathcal{H}_{12} &= -2 \qquad \mathrm{Re}(\xi/q) \\
\mathcal{H}_{22} &= \frac{\pi}{D_-^2} \qquad \mathrm{Im}(\xi/q) \\
\mathcal{H}_{13} &= \frac{2D_-}{\pi} \qquad \mathrm{Im}(\xi) \\
\mathcal{H}_{23} &= \frac{1}{D_-} \qquad \mathrm{Re}(\xi)
\end{aligned}
$$

where we write $D_\pm$ for $D_\pm(B)$. As these identities hold for both $\mathcal{H}^+$ and $\mathcal{H}^-$, they hold the max as well. Note that all these quantities depend on the spectral parameter.

**Theorem 2.5.3.** *The identities (2.5.5) hold for the 6-vertex model.*

*Proof.* Start with the second equation of (2.5.5). Substituting the above expressions for $\mathcal{H}$ give

$$\mathcal{H}_{11}\widetilde{\mathcal{H}}_{23} + \mathcal{H}_{12}\widetilde{\mathcal{H}}_{13} - \mathcal{H}_{13}\widetilde{\mathcal{H}}_{12} - \mathcal{H}_{23}\widetilde{\mathcal{H}}_{11}$$
$$= -\frac{4D_-}{\pi}\left(\text{Im}(\xi/q)\,\text{Re}(\widetilde{\xi}) + \text{Re}(\xi/q)\,\text{Im}(\widetilde{\xi}) - (\widetilde{\cdot} \leftrightarrow \cdot)\right)$$
$$= \frac{4D_-}{\pi}\left(\text{Im}(\xi\widetilde{\xi}/q) - \text{Im}(\widetilde{\xi}\xi/q)\right) = 0.$$

Here we used the fact that $q$ and $H$ are fixed (the same for $\mathcal{H}$ and $\widetilde{\mathcal{H}}$), and that the roots of the Bethe equations do not depend on the spectral parameter $u$ (so that $D_-$ does not depend on $u$).

Similarly, for the third equation

$$\mathcal{H}_{12}\widetilde{\mathcal{H}}_{23} + \mathcal{H}_{22}\widetilde{\mathcal{H}}_{13} - \mathcal{H}_{13}\widetilde{\mathcal{H}}_{22} - \mathcal{H}_{23}\widetilde{\mathcal{H}}_{12}$$
$$= -\frac{2}{D_-}\left(\text{Re}(\xi/q)\,\text{Re}(\widetilde{\xi}) - \text{Im}(\xi/q)\,\text{Im}(\widetilde{\xi}) - (\widetilde{\cdot} \leftrightarrow \cdot)\right)$$
$$= -\frac{2}{D_-}\left(\text{Re}(\xi\widetilde{\xi}/q) - \text{Re}(\xi\widetilde{\xi}/q)\right) = 0.$$

The first equation follows from commutativity of homogeneous Hamiltonians. Reproducing this for completeness, we have

$$\mathcal{H}_{11}\widetilde{\mathcal{H}}_{22} - \widetilde{\mathcal{H}}_{11}\mathcal{H}_{22}$$
$$= -\frac{4D_-^2}{\pi}\text{Im}(\xi/q)\frac{\pi}{D_-^2}\text{Im}(\widetilde{\xi}/q) + -\frac{4D_-^2}{\pi}\text{Im}(\widetilde{\xi}/q)\frac{\pi}{D_-^2}\text{Im}(\xi/q)$$
$$= -4\text{Im}(\xi/q)\text{Im}(\widetilde{\xi}/q) + 4\text{Im}(\widetilde{\xi}/q)\text{Im}(\xi/q)$$
$$= 0.$$

$\square$

## 2.6 Concluding remarks

We proved the Poisson commutativity of the family of Hamiltonians (2.5.3). It implies that the Euler-Lagrange equations, regarded as an evolution equation in Euclidean time, have infinitely many conservation laws. Thus, we can conjecture that the equations describing the 6-vertex model with integrable inhomogeneities in the horizontal direction, and which is homogeneous in the vertical direction, is integrable.

When the model is inhomogeneous in the vertical direction, i.e. when $u(y)$ is not a constant function of $y$, we have the same conservation laws for the time dependent Hamiltonian

$$H_{u(y)}(\pi, h) = \int_0^L \mathcal{H}_{u(y)-v(x)}(\partial_x h(x), \pi(x))dx.$$

This fact has a simple illustration in the finite dimensional case.

Assume $(M, \omega)$ is a symplectic manifold and and $H_1, \ldots, H_n$ are Poisson commuting functions on $M$. Consider a time dependent Hamiltonian

$$H_t(x) = f(H_1(x), \ldots, H_n(x), t)$$

where $f$ is a smooth function. It is easy to check that functions $H_1, \ldots, H_n$ remain constant along Hamiltonian flow lines generated by $H_t$, i.e. along solutions to differential equations

$$\frac{dx^i(t)}{dt} = \sum_j (\omega^{-1}(x(t))^{ij} \frac{\partial H_t}{\partial x^i}(x(t)$$

where this is written in local coordinates $x^i$ on $M$ and $\omega^{-1}(x)$ is the inverse matrix to the tensor $\omega_{ij}(x)$ representing $\omega(x) = \sum_{ij} \omega_{ij}(x)dx^i \wedge dx^j$, $\sum_j \omega^{-1}(x)^{ij}\omega_{jk}(x) = \delta_k^i$.

We were focusing on the case $\Delta < -1$ and small inhomogeneities. Extending these results to $-1 \le \Delta \le 1$ and to $\Delta > 1$ is straightforward. In the describing the Hamiltonian framework we were assuming smoothness of $\mathcal{H}_u(q, H)$ in $q$ and $H$ which is not alway true. However, this assumption is valid when the values of $(\partial_x h, \partial_y h)$ are in the disordered region. This can always be achieved by choosing appropriate initial and target values of the height function.

# Chapter 3

# Correlation for dimer models on the hexagonal lattice

## 3.1 Introduction

Dimer models on the hexagonal lattice can be seen as a five vertex limit of the six model studied in the previous chapter. Like the six vertex model, dimers on the hexagonal lattice develop a limit shape; that is, in the thermodynamic limit the height function as a random variable converges to a deterministic function. In this chapter we study the asymptotic of local correlation functions of this limiting height function for dimer models on special domains of the hexagonal lattices. These results are presented in [51].

Asymptotical formulae for local correlation functions of height functions in dimer models were computed in a number of papers for various regions and lattices, see for example [56, 17, 79]. Here we emphasize the relation to Dirac fermions, rather than to a Gaussian field. Dirac fermions can be written in terms of Gaussian field due to the Bose-Fermi correspondence in space one dimension, but the resulting expression is non-local. However, in many ways it is preferable to think that Dirac fermions are more fundamental objects.

In the first section we recall basic facts about dimer models on the hexagonal lattice. We compute the asymptotic of correlation functions using the integral representation in the second section. In Section 3 we compute the same asymptotic using the definition in terms of the difference equation.

## 3.2 Dimers on the hexagonal lattice and the Kasteleyn operator

### Dimer models on the hexagonal lattice

Let $H$ be the hexagonal lattice with the bipartite structure shown on Fig. 3.1 and $\Gamma \subset H$ be a finite subgraph which is a connected, simply-connected domain in $H$ without 1-

valent vertices. In other words $\Gamma$ is a connected, simply-connected domain assembled from elementary hexagons.
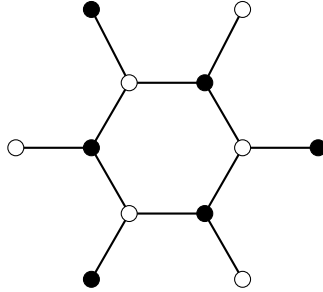


Figure 3.1: Hexagonal lattice with bipartite structure.

A dimer configuration on $D$ is a perfect matching on vertices connected by edges. In other words, it is a partition of edges into two groups, occupied by a dimer and not occupied, such that each vertex should be occupied by a dimer and two dimers never share a common vertex. The Boltzmann weight of a dimer configuration is

$$w(D) = \prod_{e \in D} w(e)$$

where the product is taken over edges occupied in the dimer configuration $D$, and $w(e) > 0$ are weights of edges which should be fixed in order to define the model.

Boltzmann weights define the probability distribution on dimer configurations on $\Gamma$ with

$$Prob(D) = \frac{w(D)}{Z}$$

where $Z$ is the partition function

$$Z = \sum_{D \subset \Gamma} w(D)$$

The characteristic function of an edge $e$ on the space of dimer configurations is the function $\sigma_e$ which has value on $D$ of 1 when the $e$ is occupied and 0 when $e$ is not occupied. Local correlation functions for dimer models are expectation values of products of characteristic functions

$$E(e_1, \ldots, e_n) = \sum_{D \subset \Gamma} Prob(D) \prod_{i=1}^{n} \sigma_{e_i}$$

It is clear that the dimer probability distribution and therefore local correlation functions are invariant with respect to transformations $w(e) \mapsto s(e_+)w(e)s(e_-)$ where $s$ is any function on vertices with positive values and $e_\pm$ are endpoints of $e$.

For the hexagonal lattice (our terminology will match Fig. 3.1) this means that we can choose weights of tilted NW-SE edges and of the horizontal edges to be 1. And we will denote remaining weights of SW-NE edges by $x(e)$.

# The Kasteleyn operator

As it was discovered in the 1960's the partition function and correlation functions of dimer models can be computed in terms of determinants. For details see original references [50][39] and an expository part of [18].

To define such determinantal solution we should choose a special orientation of edges, a Kasteleyn orientation. On the hexagonal lattice it can be chosen as it is shown on Fig. 3.2. In order to have determinants, not Pfaffians, one should choose an identification of black and white vertices. We assume that they are identified by horizontal edges.
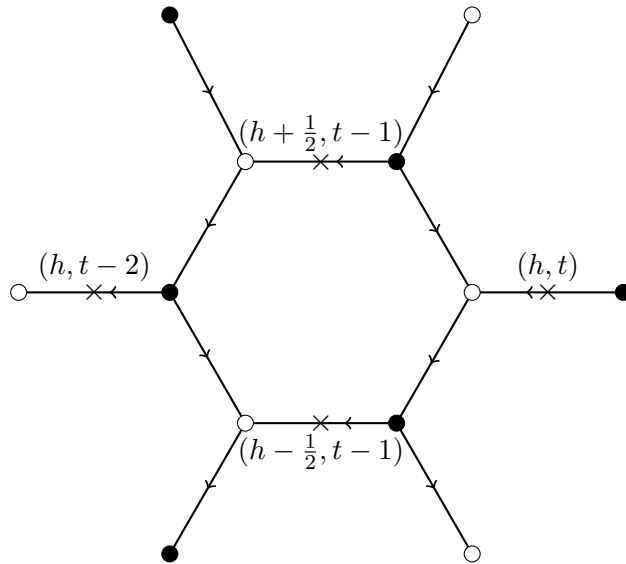


Figure 3.2: Hexagonal lattice with the Kasteleyn orientation which we use and with coordinates of horizontal edges which are identified with adjacent vertices.

Choose an embedding of the hexagonal lattice in a square grid as is shown on Fig. 3.2. We will denote coordinates of centers of horizontal edges as $(h, t)$. Here $h \in \frac{1}{2}\mathbb{Z}$ and $t \in \mathbb{Z}$. Let $\mathcal{D} \subset \frac{1}{2}\mathbb{Z}$ denote the embedded hexagonal lattice.

The Kasteleyn operator is a linear operator (a difference operator) acting on vertices of the graph. After the identification of black and white vertices by horizontal dimers it becomes a difference operator on a domain in a square grid with coordinates $(h, t) \in \mathcal{D}$ acting as

$$(Kf)(h,t) = f(t,h) - f(t-1, h + \frac{1}{2}) + x(h, t - \frac{1}{2})f(t-1, h - \frac{1}{2}) \qquad (3.2.1)$$

It is convenient to think about such functions as functions on an extended domain $\tilde{\mathcal{D}}$ where we add edges with 1-valent vertices to boundary vertices and define $f(v) = 0$ for each 1-valet vertex $v$. According to the Kasteleyn theorem, the partition function $Z$ is the absolute value of the determinant of $K$.

Local correlation functions can be computed in terms the inverse to $K$. We let $R(t, h|t', h')$ be kernel of the inverse to the Kasteleyn operator on $\mathcal{D} \subset \frac{1}{2}\mathbb{Z} \times \mathbb{Z}$. That is if

$$Kf = g$$

then

$$f(h, t) = \sum_{(h', t') \in \mathcal{D}} R(h, t|h', t')g(h', t')$$

We have

$$R(t, h|t', h') - R(t - 1, h + \frac{1}{2}|t', h') + x(t - \frac{1}{2})R(t - 1, h - \frac{1}{2}|t', h') = \delta(t, t')\delta(h, h') \quad (3.2.2)$$

with boundary conditions $R(t, h|t', h') = 0$ when $(h, t)$ correspond to a 1-valent vertex. When the domain $\mathcal{D}$ is non-compact one should impose boundary conditions when $(t, h) \to \infty$ but we will not focus on this here.

Consider horizontal edges with coordinates $x_k = (h_k, t_k)$. Then for the local correlation function we have the following formula

$$E(x_1, \ldots, x_n) = det(R(t_k, h_k|t_l, h_l))_{k,l=1}^n \quad (3.2.3)$$

Note that Kasteleyn operators can be defined for non-compact domains as well, but that should be supplemented by appropriate boundary conditions.

## Kasteleyn fermions

The Kasteleyn solution of dimer models (the determinant formulae above) can be written in terms of Grassman integral. Let $V_{\mathcal{D}}$ be the real vector space where the basis is enumerated by vertices in the region $\mathcal{D}$. Choose an element $I \in \wedge^N V_{\mathcal{D}}$. It defines the Grassman integral over $\wedge^\bullet V_{\mathcal{D}}$ as

$$\int f = f_I$$

where $f \in \wedge^\bullet V_{\mathcal{D}}$ and $f_I$ is its component in the basis $I \in \wedge^N V_{\mathcal{D}}$. Let $\psi(h, t)$ be elements of $\wedge^\bullet V_{\mathcal{D}}$ corresponding to the basis vectors in $V_{\mathcal{D}}$. Typically $I$ is chosen as a monomial in $\psi$ (longest ordered product with no repetitions). There are two choices of such integral $I$ and $-I$.

Elements $\psi$ are generators of the Grassman algebra $\wedge^\bullet V_{\mathcal{D}}$. In physics they are called fermions since

$$\psi(h', t')\psi(h, t) = -\psi(h, t)\psi(h', t')$$

In terms of generators we will write

$$\int f = \int f d\psi$$

Similarly the Grassman integral can be defined for the dual vector space $V_{\mathcal{D}}^*$. We will denote corresponding fermions as $\psi^*(h, t)$.

The Grassman algebra $\wedge^\bullet(V_{\mathcal{D}} \oplus V_{\mathcal{D}}^*)$ is naturally isomorphic to $\wedge^\bullet V_{\mathcal{D}} \otimes \wedge^\bullet V_{\mathcal{D}}^*$. The integral on this algebra can be identifies with the tensor product of integrals. We will write

$$\int F = \int F d\psi^* d\psi$$

for such integral where $F$ is a polynomial in anticommuting variables $\psi, \psi^*$, generators of $\wedge^\bullet(V_{\mathcal{D}} \oplus V_{\mathcal{D}}^*)$.

Define

$$A = \sum_{(h,t) \in \mathcal{D}} \psi^*(h, t)(K\psi)(h, t)$$

where $K\psi$ is defined as in (3.2.1).

Note that our Grassman algebra has a natural anti-involution $* : \psi_i \mapsto \psi_i^*, \psi_i^* \mapsto \psi_i$ and $A^* = A$.

The determinant formulae for the partition function and for correlation functions can be written in terms of fermions as

$$Z = |\int e^A d\psi^* d\psi|$$

and

$$E(x_1, \ldots, x_n) = \frac{\int e^A \psi(h_1, t_1)\psi^*(h_1, t_1) \ldots \psi(h_n, t_n)\psi^*(h_n, t_n) d\psi^* d\psi}{\int e^A d\psi^* d\psi}$$

Note that neither the formula for the partition function, nor the formula for local correlation functions depends on the choice of monomials defining the integrals.

Also, note that the inverse to the Kasteleyn matrix can be written as

$$R(t, h|t', h') = \frac{\int e^A \psi(h, t)\psi^*(h', t') d\psi^* d\psi}{\int e^A d\psi^* d\psi}$$

We will call $\psi, \psi^*$ Kasteleyn fermions.

## 3.3 Continuum limit from the integrals representation

### Continuum limit

Denote by $\varphi_\epsilon : \frac{1}{2}\mathbb{Z} \times \mathbb{Z} \to \mathbb{R}^2$ the embedding of the square grid into $\mathbb{R}^2$ such that $(h, t) \mapsto (\epsilon t, \epsilon h)$. We are interested in the asymptotic of local correlation functions in the limit $\epsilon \to 0$ when the lattice domain $D$ expands such that the image $\varphi_\epsilon(\mathcal{D})$ fills an $\mathbb{R}^2$ domain $\mathbb{D}$. Because of the determinantal formulae (3.2.3) it is enough to find the asymptotic of the kernel $R((t_1, h_1), (t_2, h_2))$ of the inverse Kasteleyn matrix.

We assume that as $\epsilon \to 0$ and the lattice region is expanding accordingly to fill the Euclidean domain $\mathbb{D}$, the coordinates $t_i$ and $h_i$ behaving as $t_i = \tau_i/\epsilon, h_i = \chi_i/\epsilon$ where $(\tau_i, \chi_i) \in \mathbb{D}$.

## The integral formula for inverse to the Kasteleyn operator

For special lattice domains $\mathcal{D} \in \mathbb{Z} \times \frac{1}{2}\mathbb{Z}$ the kernel of $R = K^{-1}$ has a convenient integral representation. For a semi-infinite domain shown on Fig. 3.3 such representation was found in [75]. Boundary conditions at infinity are determined by asymptotical configuration of dimers as it is shown on Fig. 3.3.
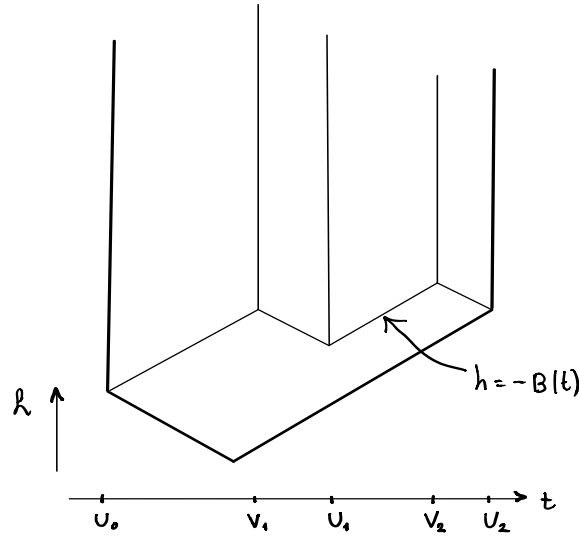


Figure 3.3: The lattice domain $\mathcal{D}$ with asymptotical boundary configuration of dimers. The function $B(t)$ is defined in (3.3.2). For details see [75].

Assume that the edge weights $x(t - \frac{1}{2}, h)$ in (3.2.1) are $x(m, h) = q^m$ when $V_i < m < U_i$ and $x(m, h) = q^{-m}$ when $U_i < m < V_{i+1}$. Define $\mathcal{D}_+$ to be the set of $m$ such that $V_i < m < U_i$ for some $i$, and $\mathcal{D}_-$ to be the set of $m$ such that $U_i < m < V_{i+1}$ for some $i$. Then formulae from [75] give the following integral representation of the inverse Kasteleyn operator:

$$R((t_1, h_1), (t_2, h_2)) = \left(\frac{1}{2\pi i}\right)^2 \int_{C_z} \int_{C_w} \frac{\Phi_-(z, t_1)\Phi_+(w, t_2)}{\Phi_+(z, t_1)\Phi_-(w, t_2)} z^{-h_1 - B(t_1)} w^{h_2 + B(t_2)}$$
$$\frac{\sqrt{zw}}{z - w} \frac{dz}{z} \frac{dw}{w} \qquad (3.3.1)$$

where

$$\Phi_+(z, t) = \prod_{m > t, m \in \mathcal{D}_+} (1 - zq^m), \quad \Phi_-(z, t) = \prod_{m < t, m \in \mathcal{D}_-} (1 - z^{-1}q^{-m})$$

$$B(t) = \frac{1}{2} \sum_{i=1}^{N} |t - V_i| - \frac{1}{2} \sum_{i=1}^{N-1} |t - U_i| \tag{3.3.2}$$

for $m \in \mathbb{Z} + \frac{1}{2}$ and $t \in \mathbb{Z}$. We assume $\sum_{i=1}^{N} V_i = \sum_{i=1}^{N-1} U_i$ and $U_0 + U_N = 0$.

From our set up we see that for the case when $t \in \mathcal{D}_+$, $V_i < t < U_i$, we have:

$$\Phi_+(z,t) = \prod_{m=t+\frac{1}{2}}^{U_i - \frac{1}{2}} (1 - zq^m) \prod_{m=V_{i+1}+\frac{1}{2}}^{U_{i+1} - \frac{1}{2}} (1 - zq^m) \prod_{m=V_{i+2}+\frac{1}{2}}^{U_{i+2} - \frac{1}{2}} \cdots$$

$$\Phi_-(z,t) = \prod_{m=U_{i-1}+\frac{1}{2}}^{V_i - \frac{1}{2}} (1 - z^{-1}q^{-m}) \prod_{m=U_{i-2}+\frac{1}{2}}^{V_{i-1} - \frac{1}{2}} \cdots$$

and for the case when $t \in \mathcal{D}_-$, $U_i < t < V_{i+1}$:

$$\Phi_+(z,t) = \prod_{m=V_{i+1}+\frac{1}{2}}^{U_{i+1} - \frac{1}{2}} (1 - zq^m) \prod_{m=V_{i+2}+\frac{1}{2}}^{U_{i+2} - \frac{1}{2}} \cdots$$

$$\Phi_-(z,t) = \prod_{m=U_i+\frac{1}{2}}^{t - \frac{1}{2}} (1 - z^{-1}q^{-m}) \prod_{m=U_{i-1}+\frac{1}{2}}^{V_i - \frac{1}{2}} (1 - z^{-1}q^{-m}) \prod_{m=U_{i-2}+\frac{1}{2}}^{V_{i-1} - \frac{1}{2}} \cdots$$

## Continuum limit

Now assume that $q = \exp(-\epsilon)$, $\epsilon \to 0$ and that $u_i = U_i\epsilon$, $v_i = V_i\epsilon$, $\tau_a = t_a\epsilon$, $\chi_a = h_a\epsilon$ are kept finite in this limit.

**Lemma on q-dilogarithms.**

The following lemma is known. We present it anyway for completeness .

**Lemma 3.3.1.**

$$\prod_{m=t_1+\frac{1}{2}}^{t_2-\frac{1}{2}} (1 - zq^m) = e^{\frac{1}{\epsilon} \int_{ze^{-\tau_2}}^{ze^{-\tau_1}} \frac{ln(1-t)}{t} dt} (1 + O(\epsilon))$$

*Proof.* Recall the $q$-Pochhammer symbol (q-dilogarithm) defined by $(z;q)_\infty = \prod_{k=0}^{\infty} (1 - zq^k)$. Suppose $(z;q)_\infty$ can be expanded as:

$$(z;q)_\infty = e^{\frac{S(z)}{\epsilon}} f(z)(1 + O(\epsilon))$$

as $\epsilon \to 0$. Then we have:

$$(zq;q)_\infty = \frac{1}{1-z}(z;q)_\infty = e^{\frac{S(z)}{\epsilon}} \frac{f(z)}{1-z}(1 + O(\epsilon))$$

as well as:

$$(zq; q)_\infty = e^{\frac{S(zq)}{\epsilon}} f(zq)(1 + O(\epsilon))$$

We now write $q = e^{-\epsilon}$ and expand the above in orders of $\epsilon$:

$$S(z - z\epsilon + z\frac{\epsilon^2}{2}) = S(z) + z(-\epsilon + \frac{\epsilon^2}{2})S'(z) + z^2\frac{\epsilon^2}{2}S''(z) + \ldots$$

$$= S(z) - \epsilon z S'(z) + \frac{\epsilon^2}{2}(zS'(z) + z^2 S''(z)) + O(\epsilon^3)$$

Equating the two expressions for $(zq; q)_\infty$ we have:

$$e^{-zS'(z)}(1 + \frac{\epsilon}{2}(zS'(z) + z^2 S''(z)) + \ldots)(f(z) - \epsilon z f'(z) + \ldots) = \frac{1}{1-z}f(z)$$

Now let's look at terms order-by-order. For the 0-order terms we have:

$$S'(z) = \frac{ln(1-z)}{z}$$

If $S$ is chosen such that $S(0) = 0$ then

$$S(z) = \int_0^z \frac{ln(1-t)}{t}dt$$

For the $\epsilon$-order terms we have:

$$\frac{1}{2}(zS'(z) + z^2 S''(z))f(z) - zf'(z) = \frac{1}{2}z(zS'(z))'f(z) - zf'(z) = 0$$

Using what we know about $S(z)$ this becomes :

$$f'(z) = -\frac{1}{2}\frac{f(z)}{1-z}$$

giving

$$f(z) = \sqrt{z-1}$$

Putting this all together we have:

$$(z, q)_\infty = exp\left(\frac{1}{\epsilon}\int_0^z \frac{ln(1-t)}{t}dt\right)\sqrt{z-1}(1 + O(\epsilon))$$

Now we write our finite product as a ratio of infinite products and use the above result:

$$\prod_{m=t_1+\frac{1}{2}}^{t_2-\frac{1}{2}} (1 - zq^m) = \frac{(zq^{t_1+\frac{1}{2}};q)_\infty}{(zq^{t_2+\frac{1}{2}};q)_\infty}$$

$$= exp\left(\frac{1}{\epsilon}\int_{zq^{t_2+\frac{1}{2}}}^{zq^{t_1+\frac{1}{2}}} \frac{ln(1-t)}{t}dt\right)\sqrt{\frac{zq^{-\tau_1}-1}{zq^{-\tau_2}-1}}(1+O(\epsilon))$$

$$= exp\left(\frac{1}{\epsilon}\int_{z_2(1-\frac{\epsilon}{2})}^{z_1(1-\frac{\epsilon}{2})} \frac{ln(1-t)}{t}dt\right)\sqrt{\frac{zq^{-\tau_1}-1}{zq^{-\tau_2}-1}}(1+O(\epsilon))$$

$$= exp\left(\frac{1}{\epsilon}\int_{z_2}^{z_1} \frac{ln(1-t)}{t}dt - \frac{1}{2}(ln(1-ze^{-\tau_1})+ln(1-ze^{-\tau_2}))\right)$$

$$\sqrt{\frac{zq^{-\tau_1}-1}{zq^{-\tau_2}-1}}(1+O(\epsilon)) = exp\left(\frac{1}{\epsilon}\int_{ze^{-\tau_2}}^{ze^{-\tau_1}} \frac{ln(1-t)}{t}dt\right)(1+O(\epsilon))$$

$$\square$$

Similarly we have:

$$\prod_{t_1+\frac{1}{2}}^{t_2-\frac{1}{2}} (1 - z^{-1}q^{-m}) = (-z)^{-(t_2-t_1)}\prod_{m=t_1+\frac{1}{2}}^{t_2-\frac{1}{2}} q^{-m}\prod_{t_1+\frac{1}{2}}^{t_2-\frac{1}{2}} (1-zq^m)$$

So as $\epsilon \to 0$ we have:

$$\prod_{t_1+\frac{1}{2}}^{t_2-\frac{1}{2}} (1 - z^{-1}q^{-m}) = (-1)^{t_2-t_1}z^{-\frac{\tau_2-\tau_1}{\epsilon}}e^{\frac{\tau_2^2-\tau_1^2}{2\epsilon}}exp\left(\frac{1}{\epsilon}\int_{ze^{-\tau_2}}^{ze^{-\tau_1}} \frac{ln(1-t)}{t}dt\right)(1+O(\epsilon))$$

Note that this asymptotic expansion is a meromorphic function of $z$ on the complex plane with branch cuts along $[e^{\tau_1}, e^{\tau_2}]$.

## Functions $\Phi_\pm$ in the continuum limit

Now we can use computations from the previous section to find the asymptotic of $\Phi_\pm(z,t)$.

Indeed for $t \in \mathcal{D}_+$, i.e $V_i < t < U_i$ we have

$$\Phi_+(z,t) = \prod_{m=t+\frac{1}{2}}^{U_i-\frac{1}{2}} (1 - zq^m) \prod_{m=V_{i+1}+\frac{1}{2}}^{U_{i+1}-\frac{1}{2}} (1 - zq^m) \prod_{m=V_{i+2}+\frac{1}{2}}^{U_{i+2}-\frac{1}{2}} \ldots$$

$$= exp\left(\frac{1}{\epsilon} \int_{ze^{-u_i}}^{ze^{-\tau}} \frac{ln(1-t)}{t} dt\right) exp\left(\frac{1}{\epsilon} \int_{ze^{-u_{i+1}}}^{ze^{-v_{i+1}}} \frac{ln(1-t)}{t} dt\right)$$

$$exp\left(\frac{1}{\epsilon} \int_{ze^{-u_{i+2}}}^{ze^{-v_{i+2}}} \frac{ln(1-t)}{t} dt\right) \ldots$$

$$= exp\left(\frac{1}{\epsilon} \int_{ze^{-u_i}}^{ze^{-\tau}} + \frac{1}{\epsilon} \int_{ze^{-u_{i+1}}}^{ze^{-v_{i+1}}} + \frac{1}{\epsilon} \int_{ze^{-u_{i+2}}}^{ze^{-v_{i+2}}} \frac{ln(1-t)}{t} dt + \ldots\right)$$

$$\Phi_-(z,t) = \prod_{m=U_{i-1}+\frac{1}{2}}^{V_i-\frac{1}{2}} (1 - z^{-1}q^{-m}) \prod_{m=U_{i-2}+\frac{1}{2}}^{V_{i-1}-\frac{1}{2}} \ldots$$

$$= (-z)^{-\frac{v_i-u_{i-1}}{\epsilon}} e^{\frac{v_i^2-u_{i-1}^2}{2\epsilon}} exp\left(\frac{1}{\epsilon} \int_{ze^{-v_i}}^{ze^{-u_{i-1}}} \frac{ln(1-t)}{t} dt\right)$$

$$(-z)^{\frac{v_{i-1}-u_{i-2}}{\epsilon}} e^{\frac{v_{i-1}^2-u_{i-2}^2}{2\epsilon}} exp\left(\frac{1}{\epsilon} \int_{ze^{-v_{i-1}}}^{ze^{-u_{i-2}}} \frac{ln(1-t)}{t} dt\right) \ldots$$

$$= (-z)^{-\frac{1}{\epsilon}\sum_{j\leq i} v_j-u_{j-1}} e^{\frac{1}{2\epsilon}\sum_{j\leq i} v_j^2-u_{j-1}^2}$$

$$exp\left(\frac{1}{\epsilon} \int_{ze^{-v_i}}^{ze^{-u_{i-1}}} + \frac{1}{\epsilon} \int_{ze^{-v_{i-1}}}^{ze^{-u_{i-2}}} \frac{ln(1-t)}{t} dt + \ldots\right)$$

Similarly, for $t \in \mathcal{D}_-$, i.e. $U_i < t < V_{i+1}$ we obtain:

$$\Phi_+(z,t) = exp\left(\frac{1}{\epsilon} \int_{ze^{-u_{i+1}}}^{ze^{-v_{i+1}}} + \frac{1}{\epsilon} \int_{ze^{-u_{i+2}}}^{ze^{-v_{i+2}}} \frac{ln(1-t)}{t} dt + \ldots\right)$$

$$\Phi_-(z,t) = (-z)^{-\frac{\tau-u_i}{\epsilon} - \frac{1}{\epsilon}\sum_{j<i} v_j-u_{j-1}} e^{\frac{1}{2\epsilon}(\tau^2-u_i^2+\sum_{j<i} v_j^2-u_{j-1}^2)}$$

$$exp\left(\frac{1}{\epsilon} \int_{ze^{-\tau}}^{ze^{-u_i}} + \frac{1}{\epsilon} \int_{ze^{-v_i}}^{ze^{-u_{i-1}}} \frac{ln(1-t)}{t} dt + \ldots\right)$$

Recall:

$$B(t) = \frac{1}{2} \sum_{i=1}^{N} |t - V_i| - \frac{1}{2} \sum_{i=1}^{N-1} |t - U_i|$$

Now define:

$$L(t) = \begin{cases} \sum_{j \le i} V_j - U_{j-1}, & \text{for } t \in \mathcal{D}_+, V_i < t < U_i \\ t - U_i + \sum_{j < i} V_j - U_{j-1}, & \text{for } t \in \mathcal{D}_-, U_i < t < V_{i+1} \end{cases}$$

For $t \in \mathcal{D}_+$, $V_i < t < U_i$:

$$B(t) + L(t) = \frac{1}{2} \sum_{j=1}^{N} |t - V_j| - \frac{1}{2} \sum_{j=1}^{N-1} |t - U_j| + \sum_{j \le i} (V_j - U_{j-1})$$

$$= \frac{1}{2} \left( \sum_{j=1}^{i} t - \sum_{j=i+1}^{N} t + \sum_{j=i}^{N-1} t - \sum_{j=1}^{i-1} t - \sum_{j=1}^{i} V_j + \sum_{j=i+1}^{N} V_j - \sum_{j=i}^{N-1} U_j + \sum_{j=1}^{i-1} U_j \right) +$$

$$\sum_{j=1}^{i} V_j - \sum_{j=1}^{i-1} U_j + U_0 = \frac{t}{2} + \frac{1}{2} \left( \sum_{j=1}^{N} V_j - \sum_{j=1}^{N-1} U_j \right) - U_0 = \frac{t}{2} - U_0$$

where we use that $\sum_{j=1}^{N} V_j = \sum_{j=1}^{N-1} U_j$. A similar calculation can be done for $t \in \mathcal{D}_-$, $U_i < t < V_{i+1}$.

Now for the ratio of the $\Phi$'s:

$$\frac{\Phi_-(z,t)}{\Phi_+(z,t)} z^{-h-B(t)} = C \exp\left( \frac{S(z)}{\epsilon} \right) (1 + O(\epsilon))$$

where $C$ is a constant. Its value is not important as it will cancel in the asymptotic of the integral. The function $S(z)$ is :

$$S(z) = \sum_{i=0}^{N} Li_2(ze^{-u_i}) - \sum_{i=1}^{N} Li_2(ze^{-v_i}) - Li_2(ze^{-\tau}) - \left( \frac{\tau}{2} - u_0 + \chi \right) \ln z$$

and $Li_2(z) = \int_0^z \frac{ln(1-x)}{x} dx$ is the dilogarithm.

Combining result from above we have the following asymptotical integral representation for $R$.

$$R((\tau_1, \chi_1), (\tau_2, \chi_2)) = \left( \frac{1}{2\pi i} \right)^2 \int_{C_z} \int_{C_w} e^{\frac{S(z,\tau_1,\chi_1) - S(w,\tau_2,\chi_2)}{\epsilon}}$$

$$\frac{\sqrt{zw}}{z - w} \frac{dz}{z} \frac{dw}{w} (1 + O(\epsilon)) \tag{3.3.3}$$

where the function $S(z)$ as above. The integration contours are shown on Fig. 3.4.

**The asymptotic of the integral (3.3.3).**

We will be computing the asymptotic using the method of steepest descent, so first we should study critical points of the function $S(z)$.
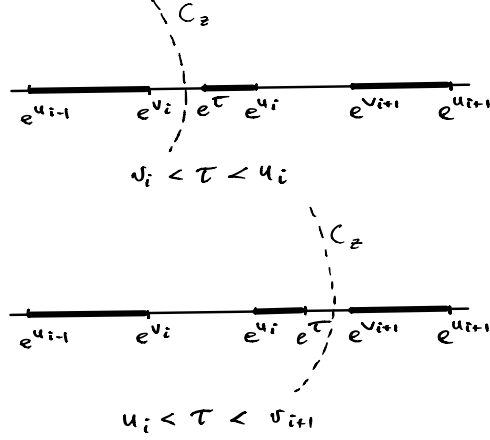
Figure 3.4: The integration contours in (3.3.3) are circles with $|z| < |w|$ when $\tau_1 < \tau_2$ and $|w| > |z|$ when $\tau_1 > \tau_2$ centered at the origin. They the contour $C_z$ intersect the positive part of the real line as it is shown above with $\tau = \tau_1$. The contour $C_w$ intersect the positive part of the real line similarly with $\tau = \tau_2$.

**Lemma 3.3.2.** *The following identity holds*

$$z_0^2 S''(z_0) = \left(\frac{\partial z_0}{\partial \chi}\right)^{-1}$$

*where $z_0$ is a critical point of $S(z)$.*

*Proof.* For the first derivative of $S$ in $z$ we have:

$$z\frac{\partial S(z)}{\partial z} = \sum_{i=0}^{N} ln(1 - ze^{-u_i}) - \sum_{i=1}^{N} ln(1 - ze^{-v_i}) - ln(1 - ze^{-\tau}) -$$

$$\left(\frac{\tau}{2} - u_0 + \chi\right) = ln\left(\frac{\prod_{i=0}^{N}(1 - ze^{-u_i})}{\prod_{i=1}^{N}(1 - ze^{-v_i})} \frac{1}{(1 - ze^{-\tau})}\right) -$$

$$\left(\frac{\tau}{2} - u_0 + \chi\right) = ln\left(\frac{f(z)}{(1 - ze^{-\tau})}\right) - \left(\frac{\tau}{2} + \chi\right)$$

where $f(z) = \frac{\prod_{i=0}^{N}(1-ze^{-u_i})}{\prod_{i=1}^{N}(1-ze^{-v_i})}e^{u_0}$.

From this we see that if $z_0$ is a critical point of $S$, i.e. $S'(z_0) = 0$ we have:

$$e^{\chi + \frac{\tau}{2}} = \frac{f(z_0)}{1 - z_0 e^{-\tau}}$$

This defines $z_0$ as an implicit function of $\chi$ and $\tau$. Taking a derivative we have:

$$1 = \frac{\partial z_0}{\partial \chi}\left(ln\left(\frac{f(z_0)}{1 - z_0 e^{-\tau}}\right)\right)'$$

For the second derivative of $S(z)$ we have

$$\left(z\frac{\partial}{\partial z}\right)^2 S(z) = z\left(ln\left(\frac{f(z_0)}{1 - z_0 e^{-\tau}}\right)\right)'$$

Taking into account the equation for the derivative of the critical point in $\chi$ and that

$$\left(z\frac{\partial}{\partial z}\right)^2 S(z) = zS'(z) + z^2 S''(z)$$

we obtain the value of the second derivative of $S(z)$ at the critical point $z_0$ and the desired identity. $\qquad\square$

Before we will compute the asymptotic of (3.3.3), we need one more lemma.

**Lemma 3.3.3.** *The following identities hold:*

$$e^{-S_\tau} = \frac{\sqrt{z_0}}{1 - z_0 e^{-\tau}} \quad e^{-\frac{1}{2}S_\chi} = \sqrt{z_0}$$

Indeed, we have the following identities which imply the lemma.

$$\frac{d}{d\tau}S(z_0) = \frac{\partial z_0}{\partial \tau}S'(z_0) + \frac{\partial S}{\partial \tau}|_{z_0} = -\frac{1}{2}ln(z_0) + ln(1 - z_0 e^{-\tau})$$
$$\frac{d}{d\chi}S(z_0) = \frac{\partial z_0}{\partial \chi}S'(z_0) + \frac{\partial S}{\partial \chi}|_{z_0} = -ln(z_0)$$

**Theorem 3.3.4.** *The integral (3.3.3) has the following asymptotic when $\epsilon \to 0$ and all parameters are scaling as before*

$$R(h,t|h't') = (e^{\frac{S(z_0)-S(w_0)}{\epsilon}}\frac{\sqrt{\frac{\partial z_0}{\partial \chi_1}\frac{\partial w_0}{\partial \chi_2}}}{z_0 - w_0} + e^{\frac{S(\bar{z}_0)-S(w_0)}{\epsilon}}\frac{\sqrt{\frac{\partial \bar{z}_0}{\partial \chi_1}\frac{\partial w_0}{\partial \chi_2}}}{\bar{z}_0 - w_0} \qquad (3.3.4)$$

$$e^{\frac{S(z_0)-S(\bar{w}_0)}{\epsilon}}\frac{\sqrt{\frac{\partial z_0}{\partial \chi_1}\frac{\partial \bar{w}_0}{\partial \chi_2}}}{z_0 - \bar{w}_0} + e^{\frac{S(\bar{z}_0)-S(\bar{w}_0)}{\epsilon}}\frac{\sqrt{\frac{\partial \bar{z}_0}{\partial \chi_1}\frac{\partial \bar{w}_0}{\partial \chi_2}}}{\bar{z}_0 - \bar{w}_0})(1 + O(\epsilon))$$

*Proof.* As it is shown in [75] for $(\tau, \chi)$ inside the discriminant curve there are two complex conjugate critical points of $S(z)$. The discriminant curve also know as the arctic circle is

$$S'(z) = S''(z) = 0$$

Deforming integration contours to the contours which pass critical points in the steepest descent direction and computing corresponding Gaussian integrals we arrive at (3.3.4). $\quad\square$

## 3.4 Asymptotical solutions to Kasteleyn difference equation

### Formal asymptotical solutions to the Kasteleyn equations

Here we will study the difference equation

$$f(t, h) - f(t - 1, h + \frac{1}{2}) + x(t - \frac{1}{2}, h)f(t - 1, h - \frac{1}{2}) = 0 \tag{3.4.1}$$

in the continuum limit when $\epsilon \to 0$ and $\tau = \epsilon t$, $\chi = \epsilon h$ are fixed. It is convenient to change of coordinates:

$$\xi_+ = \chi + \frac{\tau}{2}, \quad \xi_- = \chi - \frac{\tau}{2}$$
$$\partial_+ = \partial_\tau + \frac{1}{2}\partial_\chi, \quad \partial_- = -\partial_\tau + \frac{1}{2}\partial_\chi$$

Let us look for asymptotic solutions to the difference equation (3.4.1) of the form $f(t, h) = e^{\frac{1}{\epsilon}S(\xi_+, \xi_-)}\phi(\xi_+, \xi_-)$. The equation (3.4.1) gives:

$$e^{\frac{1}{\epsilon}S(\xi_+, \xi_-)}\phi(\xi_+, \xi_-) - e^{\frac{1}{\epsilon}S(\xi_+, \xi_- + \epsilon)}\phi(\xi_+, \xi_- + \epsilon)+$$
$$v(\xi_+ - \xi_- - \frac{\epsilon}{2})e^{\frac{1}{\epsilon}S(\xi_+ - \epsilon, \xi_-)}\phi(\xi_+ - \epsilon, \xi_-) = 0$$

Taking the limit $\epsilon \to 0$, we get the following non-linear differential equation for $S$ at 0-th order in $\epsilon$:

$$1 - e^{\partial_- S} + ve^{-\partial_+ S} = 0 \tag{3.4.2}$$

The first order terms 1-order terms give linear differential equation for $\phi$:

$$-\frac{1}{2}\partial_-^2 Se^{\partial_- S} - \frac{\partial_- \phi}{\phi}e^{\partial_- S} + \frac{1}{2}v\partial_+^2 Se^{-\partial_+ S} - v\frac{\partial_+ \phi}{\phi}e^{-\partial_+ S} - \frac{1}{2}v'e^{-\partial_+ S} = 0 \tag{3.4.3}$$

### The function $S$

Taking into account equation (3.4.2) we can write:

$$e^{\partial_- S} = \frac{1}{1 - z_0 v}, \quad e^{-\partial_+ S} = \frac{z_0}{1 - z_0 v}$$

for some function $z_0(\xi_+, \xi_-)$.

**Lemma 3.4.1.** *The function $z_0(\xi_+, \xi_-)$ satisfies differential equation*

$$\partial_- z_0(\xi_+, \xi_-) + z_0(\xi_+, \xi_-)v(\xi_+ - \xi_-)\partial_+ z_0(\xi_+, \xi_-) = 0$$

*Proof.* Indeed, differentiating (3.4.2) we obtain:

$$\partial_+(\partial_- S) = -\partial_+ ln(1 - z_0 v) = \frac{\partial_+(z_0 v)}{1 - z_0 v}$$

$$\partial_-(\partial_+ S) = \partial_-(ln(1 - z_0 v) - ln(z_0)) = -\frac{\partial_-(z_0 v)}{(1 - z_0 v)z_0 v} + \frac{\partial_- v}{v}$$

These two identities imply

$$\partial_-(z_0 v) + (z_0 v)\partial_+(z_0 v) = (1 - z_0 v)z_0 \partial_- v$$

Because $v = v(\xi_+ - \xi_-)$ we can rewrite this as:

$$(\partial_- z_0)v - z_0 v' + z_0 v(\partial_+ z_0)v + z_0^2 vv' = -z_0 v' + z_0^2 vv'$$

this gives the desired identity. $\qquad\qquad\square$

Note that when $v$ is constant the equation for $z_0$ is exactly the complex Burgers equation from [60].

**The function $\phi$**

Here we will describe general solution to the differential equation for $\phi$.

**Theorem 3.4.2.** *Let $z_0(\xi_+, \xi_-)$ be as above, define the function*

$$\phi = \psi \frac{\sqrt{(\partial_+ + \partial_-)z_0}}{z_0 - w_0} \tag{3.4.4}$$

*where $w_0$ does not depend on $\xi_\pm$. $\phi$ is a solution to (3.4.3) if and only if $\psi$ satisfies the equation*

$$(\partial_- + z_0 v\partial_+)\psi = 0$$

*Proof.* First, let us now look at the the terms in equation (3.4.3) not containing $\phi$. We have:

$$
\frac{1}{2}\frac{\partial_- ln(1-z_0v)}{1-z_0v} + \frac{1}{2}v\partial_+(ln(z_0)-ln(1-z_0v))\frac{z_0}{1-z_0v} - \frac{1}{2}v'\frac{z_0}{1-z_0v}
$$

$$
= -\frac{1}{2}\frac{\partial_-(z_0v)}{(1-z_0v)^2} - \frac{1}{2}v\left(\frac{\partial_+ z_0}{z_0} + \frac{\partial_+(z_0v)}{1-z_0v}\right)\frac{z_0}{1-z_0v} - \frac{1}{2}v'\frac{z_0}{1-z_0v}
$$

$$
= -\frac{1}{2}\frac{\partial_-(z_0v)+vz_0\partial_+(z_0v)}{(1-z_0v)^2} - \frac{1}{2}v\frac{\partial_+ z_0}{1-z_0v} - \frac{1}{2}v'\frac{z_0}{1-z_0v}
$$

$$
= -\frac{1}{2}\frac{v(\partial_-(z_0)+vz_0\partial_+(z_0))+z_0(\partial_-v+vz_0\partial_+v)}{(1-z_0v)^2} - \frac{1}{2}v\frac{\partial_+ z_0}{1-z_0v} - \frac{1}{2}\frac{v'z_0}{1-z_0v}
$$

$$
= \frac{1}{2}\frac{z_0v'}{1-z_0v} - \frac{1}{2}\frac{v\partial_+ z_0}{1-z_0v} - \frac{1}{2}\frac{v'z_0}{1-z_0v}
$$

$$
= -\frac{1}{2}\frac{v\partial_+ z_0}{1-z_0v}
$$

where in the fourth line we use the lemma from above.

Now the terms containing $\phi$ after the substitution (3.4.4) can be transformed as

$$
\frac{1}{1-z_0v}\frac{\partial_-\phi}{\phi} + \frac{vz_0}{1-z_0v}\frac{\partial_+\phi}{\phi}
$$

$$
= \frac{\partial_-\psi+z_0v\partial_+\psi}{\psi(1-z_0v)} + \frac{1}{2}\frac{(\partial_-+vz_0\partial_+)(\partial_+ z_0+\partial_- z_0)}{(\partial_+ z_0+\partial_- z_0)(1-z_0v)} - \frac{(\partial_-+z_0v\partial_+)z_0}{(1-z_0v)(z_0-\tilde{z}_0)}
$$

$$
= \frac{\partial_-\psi+z_0v\partial_+\psi}{\psi(1-z_0v)} + \frac{1}{2}\frac{(\partial_-+vz_0\partial_+)(\partial_+ z_0+\partial_- z_0)}{(\partial_+ z_0+\partial_- z_0)(1-z_0v)}
$$

where we again use the lemma from above. The denominator of the second term we can write as

$$
(\partial_-+z_0v\partial_+)(\partial_+ z_0+\partial_- z_0)
$$

$$
= (\partial_++\partial_-)(\partial_-+z_0v\partial_+)z_0 + (\partial_++\partial_-)(z_0v)\partial_+ z_0
$$

$$
= (\partial_++\partial_-)(z_0v)\partial_+ z_0
$$

$$
= v(\partial_++\partial_-)(z_0)\partial_+ z_0
$$

Here we use the lemma and the fact that $(\partial_++\partial_-)v = 0$. Combining expressions above, we have the following expression for terms in (3.4.3)

$$
\frac{1}{1-z_0v}\frac{\partial_-\phi}{\phi} + \frac{vz_0}{1-z_0v}\frac{\partial_+\phi}{\phi} = \frac{\partial_-\psi+z_0v\partial_+\psi}{\psi(1-z_0v)} + \frac{1}{2}\frac{v\partial_+ z_0}{1-z_0v}
$$

Putting everything together, the equation for $\phi$ becomes

$$
-\frac{1}{2}\frac{v\partial_+ z_0}{1-z_0v} + \frac{\partial_-\psi+z_0v\partial_+\psi}{\psi(1-z_0v)} + \frac{1}{2}\frac{v\partial_+ z_0}{1-z_0v} = \frac{\partial_-\psi+z_0v\partial_+\psi}{\psi(1-z_0v)}
$$

The theorem follows. $\qquad\square$

## The asymptotical behavior of the inverse to the Kasteleyn operator in the continuum limit

Now let us find the asymptotic of the inverse to the Kasteleyn operator from the difference equation.

Let $z_0(\tau.\chi)$ be a complex critical point of $S(z, \chi, \tau)$ and $w_0(\tau', \chi')$ be a complex critical point of $S(z, \chi', \tau')$. Combining the previous results of this section we arrive to the following asymptotic of $R(h, t|h't')$:

$$R(h, t|h't') = (e^{\frac{S(z_0)-S(w_0)}{\epsilon}} \frac{\sqrt{\frac{\partial z_0}{\partial \chi_1} \frac{\partial w_0}{\partial \chi_2}}}{z_0 - w_0} + e^{\frac{S(\bar{z}_0)-S(w_0)}{\epsilon}} \frac{\sqrt{\frac{\partial \bar{z}_0}{\partial \chi_1} \frac{\partial w_0}{\partial \chi_2}}}{\bar{z}_0 - w_0} \qquad (3.4.5)$$

$$e^{\frac{S(z_0)-S(\bar{w}_0)}{\epsilon}} \frac{\sqrt{\frac{\partial z_0}{\partial \chi_1} \frac{\partial \bar{w}_0}{\partial \chi_2}}}{z_0 - \bar{w}_0} + e^{\frac{S(\bar{z}_0)-S(\bar{w}_0)}{\epsilon}} \frac{\sqrt{\frac{\partial \bar{z}_0}{\partial \chi_1} \frac{\partial \bar{w}_0}{\partial \chi_2}}}{\bar{z}_0 - \bar{w}_0})(1 + O(\epsilon))$$

Which agrees with (3.3.4) when $v(x) = e^{-x}$.

## 3.5 Conformal correlation functions

Note that the asymptotical formula for the inverse to the Kasteleyn operator can be interpreted in terms of Kasteleyn fermions in the following way. In the appropriate sense one can say that as $\epsilon \to 0$

$$\psi(t, h) \to a(z_0(\tau, \chi))e^{\frac{S(z_0(\tau, \chi))}{\epsilon}} + a(\overline{z_0(\tau, \chi)})e^{\frac{\overline{S(z_0(\tau, \chi))}}{\epsilon}}$$

$$\psi^*(t, h) \to b(z_0(\tau, \chi))e^{\frac{S(z_0(\tau, \chi))}{\epsilon}} + b(\overline{z_0(\tau, \chi)})e^{\frac{\overline{S(z_0(\tau, \chi))}}{\epsilon}}$$

where $a(z)$ and $b(z)$ are components of the Dirac fermionic field with correlation functions

$$< a(z)b(w) >= \frac{1}{z - w}$$

The square roots in the formulae (3.4.5) appear from the spinor nature of conformal fields $a$ and $b$.

## 3.6 Conclusion

In this chapter, we compute the dimer correlation functions for dimers on certain domains of the hexagonal lattice. We compute these correlation functions using two different methods. First, from the asymptotic analysis of the contour integral formula for the inverse Kasteleyn matrix and, second, from the definition of the Kasteleyn matrix as a difference equation. We relate our results to description of the dimer model in terms of Kasteleyn fermions and the

Dirac field. It would be interesting to generalize these results to more boundary conditions and to study how the effects of the boundary conditions affect the formulation in terms of the difference equation.

# Chapter 4

# Arctic curves for bounded lecture hall tableaux

## 4.1 Introduction

In this chapter, we study limit shape formation in a model known as bounded lecture hall tableaux. Unlike the six vertex and dimer models which were originally motivated by physical phenomenon, the lecture hall tableaux are combinatorial object arising from the study of symmetric polynomials. We will show that in fact these tableaux can also be seen as a collection of non-intersecting lattice paths. Moreover, they can be seen as a dimer model that is very closely related to the hexagonal lattice dimers studied in the previous chapter. We will show numerical evidence that the bounded lecture hall tableaux, like the six vertex model and $\mathbb{Z}^2$-periodic dimer models, exhibit the limit shape phenomenon. Then, assuming that this is the case, we study the resulting Arctic curves. These results are presented in [27].

Sylvie Corteel and Jang Soo Kim introduced lecture hall tableaux in their study of multivariate little $q$-Jacobi polynomials [26]. They then enumerated bounded lecture hall tableaux and showed that their enumeration is closely related to standard and semistandard Young tableaux [25].
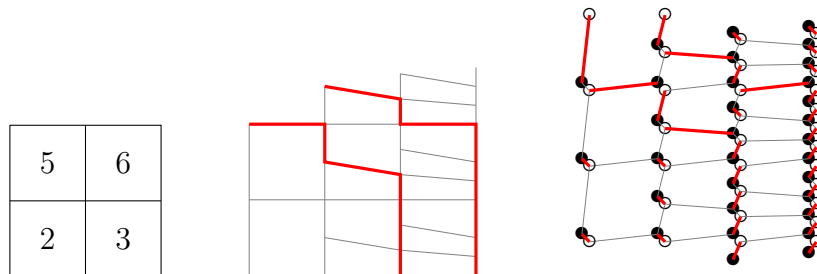


Figure 4.1: Tableau, non-intersecting paths, and dimers

Given a positive integer $t$ and a partition $\lambda = (\lambda_1, \ldots, \lambda_n)$ with $\lambda_1 \geq \ldots \geq \lambda_n \geq 0$, the bounded lecture hall tableaux are fillings of the diagram of $\lambda$ with integers $T_{i,j}$ such that

1. $T_{i,j} < t(n - i + j)$

2. $T_{i,j}/(n - i + j) \geq T_{i,j+1}/(n - i + j + 1)$

3. $T_{i,j}/(n - i + j) \geq T_{i+1,j}/(n - i - 1 + j)$

We call them bounded lecture hall tableaux (BLHT) of shape $\lambda$, bounded by $t$. On the left of Figure 4.1, we give an example of such a tableau for $t = 2$ and $\lambda = (2, 2)$. In this chapter we study the asymptotic behavior of these bounded tableaux thanks by mapping them to collections of non-intersecting lattice paths. An example of the path model is given on the middle of Figure 4.1. The right on Figure 4.1 shows how it is also possible to map the bounded lecture hall tableaux to a dimer model in which the faces of the underlying graph consist of hexagons and octogons. While we will we not need this mapping in what follows, we include its description as it shows how the BLHT an interesting class of dimer models distinct form the well-studied $\mathbb{Z}^2$ invariant dimer models. Detailed definitions will be given in Section 4.2.

The first special quality of this model is that the number of configurations is easy to compute [25]. Given $t, n$ and $\lambda = (\lambda_1, \ldots, \lambda_n)$, the number of bounded lecture hall tableaux of shape $\lambda$ and bounded by $t$ is

$$Z_\lambda(t) = t^{|\lambda|} \prod_{1 \leq i < j \leq n} \frac{\lambda_i - i - \lambda_j + j}{j - i},$$

where $|\lambda| = \lambda_1 + \ldots + \lambda_n$.

Our main interest here is to compute their asymptotic behavior. Given $n \gg 0$ and a piecewise differentiable function $\alpha : [0, 1] \to [0, k]$ with $k \in \mathbb{R}$ and $\tau \in \mathbb{R}$, our main question is to understand the asymptotic behavior of bounded lecture hall tableaux of shape $\lambda = (\lambda_1, \ldots, \lambda_n)$ with $\lambda_i + n - i = \lfloor n\alpha(i/n) \rfloor$ bounded by $t = \tau n$. The function $\alpha$ describes the limiting profile of $\lambda$.

In this chapter, we will detail two examples

- The staircase: $\lambda = (n, n - 1, \ldots, 2, 1)$. In this case $\alpha(u) = 2 - 2u$.

- The square: $\lambda = (n, n, \ldots, n)$. In this case $\alpha(u) = 2 - u$.

We will also present a general result that computes a parametrization of the Arctic curve in the general case.

**Theorem 4.1.1.** *As $n \to \infty$, lecture hall tableaux of shape $\lambda = (\lambda_1, \ldots, \lambda_n)$ bounded by $\tau n$ exhibit the Arctic curve phenomena. The Arctic curve can be parametrized by*

$$X(x) = \frac{x^2 I'(x)}{I(x) + x I'(x)}$$

$$Y(x) = \tau \frac{1}{I(x) + x I'(x)}$$

$$(4.1.1)$$

*for an appropriate range of $x$. Here $I(x) = e^{-\int_0^1 du \frac{1}{x-\alpha(u)}}$ and $\lambda_i + n - i = \lfloor n\alpha(i/n) \rfloor$.*

Even though this model seems more complicated than the typical systems coming from the square grid graphs [30], we will discover that they have some surprising properties and many of similarities with non-intersecting paths on the grid (or equivalently dimer models on the hexagonal lattice, semistandard Young tableaux or lozenge tilings). Numerous asymptotic results exists for non-intersecting paths, or equivalently tilings models or dimer models on graphs that are regular and $\mathbb{Z}^2$ invariant [58]. The Arctic curve phenomenon was named about twenty years ago when Cohn, Elkies and Propp studied the tilings of a large Aztec diamond with dominoes [19, 48]. Indeed the "typical" tiling of the Aztec diamond with dominoes is known to display an Arctic circle separating frozen phases in the corners which are regularly tiled from a liquid phase in the center which is disordered. Many tiling problems of finite plane domains of large size are known to exhibit the same phenomenon. Typically, one studies the asymptotics of tilings of scaled domains whose limits can be nicely characterized. Dimer models on regular graphs, which are the dual version of tiling problems, exhibit the same phenomenon [59, 60]. The general method to obtain the Arctic curve location is the asymptotic study of bulk expectation values, which requires the computation of the inverse of the Kasteleyn matrix or at least its asymptotics. Other rigorous methods use, for example, the machinery of cluster integrable systems of dimers [34, 62, 78]. Recently several papers use the recent method of Colomo and Sportiello [21, 23] called the tangent method to compute (non-rigorously) the Arctic curves [30, 31, 32, 33, 29]. A very recent preprint of Aggarwal builds a method to make this heuristic rigorous in the case of the 6-vertex model [1].

As our model is not $\mathbb{Z}^2$ invariant we can not apply directly all the methods elaborated for the $\mathbb{Z}^2$ invariant models. In Section 4.2 we will define the path model, the dimer model and explain the connections between these models and bounded lecture hall tableaux. In Section 4.3 we explain how we randomly generate the tableaux and present some simulations. In Section 4.4 we use the tangent method to compute the Arctic curve for any function $\alpha$. We end this chapter in Section 4.5 with open questions and concluding remarks.

## 4.2 Combinatorics and counting

In this section , we give definitions and basic properties of our three combinatorial models: the tableaux, the path model and the dimer model.

Figure 4.2: On the left is a lecture hall tableau $T$ for $n = 5$ and $\lambda = (4, 3, 1, 0, 0)$. The diagram on the right shows the number $T(i, j)/(n - i + j)$.

## Lecture hall tableaux

Lecture hall partitions were studied by Bousquet-Mélou and Eriksson [13, 14, 15] in the context of the combinatorics of affine Coxeter groups. They are sequences $(T_1, \ldots, T_n)$ such that

$$\frac{T_1}{n} \geq \frac{T_2}{n-1} \geq \ldots \geq \frac{T_n}{1} \geq 0.$$

They have been studied extensively in the last two decades. See the recent survey written by Savage [85]. In [26] the first author and Jang Soo Kim showed that these objects are closely related to the little $q$-Jacobi polynomials. Thanks to this approach they defined lecture hall tableaux related to the multivariate little $q$-Jacobi polynomials.

Given a partition $\lambda = (\lambda_1, \ldots, \lambda_n)$ such that $\lambda_1 \geq \ldots \geq \lambda_n \geq 0$, the Young diagram of $\lambda$ is a left justified union of cells such that the $i^{th}$ row contains $\lambda_i$ cells. The cell in row $i$ and column $j$ is denoted by $(i, j)$.

**Definition 4.2.1.** [26] For an integer $n$ and a partition $\lambda = (\lambda_1, \ldots, \lambda_n)$ with $n$ non-negative parts, a *lecture hall tableau* of shape $\lambda$ is a filling $T$ of the cells in the Young diagram of $\lambda$ with non-negative integers satisfying the following conditions:

$$\frac{T(i, j)}{n - i + j} \geq \frac{T(i, j + 1)}{n - i + j + 1}, \qquad \frac{T(i, j)}{n - i + j} > \frac{T(i + 1, j)}{n - i - 1 + j}.$$

where $T(i, j)$ is the filling of the cell in row $i$ and column $j$.

See Figure 4.2 for an example of a lecture hall tableau on the left of the Figure. On the right of the Figure, we show that this tableau is "lecture hall" by exhibiting $T_{i,j}/(n - i + j)$ for all $i, j$.

In this chapter we study lecture hall tableaux with an extra condition. We impose that each entry $T(i, j)$ is striclty less then $t(n + j - i)$. We say that the tableau are bounded by $t$. These tableaux are called *bounded* lecture hall tableaux and were enumerated in [25].

**Proposition 4.2.2.** *[25] Given $t, n$ and $\lambda$, the number of bounded lecture hall tableaux is*

$$Z_\lambda(t) = t^{|\lambda|} \prod_{1 \leq i < j \leq n} \frac{\lambda_i - i - \lambda_j + j}{j - i}, \tag{4.2.1}$$

*where $|\lambda| = \lambda_1 + \ldots + \lambda_n$.*
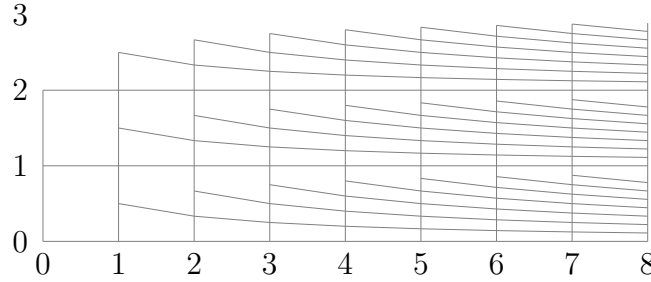
Figure 4.3: The graph $\mathcal{G}_t$ for $t = 3$

## Paths on the lecture hall graph and the dual graph

In this Section we give a bijection between bounded lecture hall tableaux and non-intersecting paths on a graph. Let us give a detailed definition of our graph.

**Definition 4.2.3.** Given a positive integer $t$, the *lecture hall graph* is a graph $\mathcal{G}_t = (V_t, E_t)$. This graph is conveniently described through an embedding in the plane, in which the vertices are:

- $(i, j/(i+1))$ for $i \geq 0$ and $0 \leq j < t(i+1)$.

and the directed edges are

- from $(i, k + r/(i+1))$ to $(i+1, k + r/(i+2))$ for $i \geq 0$ and $0 \leq r \leq i$ and $0 \leq k < t$.

- from $(i, k + (r+1)/(i+1))$ to $(i, k + r/(i+1))$ for $i \geq 0$ and $0 \leq r \leq i$ and $0 \leq k < t-1$ or for $i \geq 0$ and $0 \leq r < i$ and $k = t - 1$.

This graph was defined in [25]. An example of the graph $\mathcal{G}_3$ is given on Figure 4.3.

Given a positive integer $t$ and a partition $\lambda = (\lambda_1, \dots, \lambda_n)$ with $\lambda_1 \geq \dots \geq \lambda_n \geq 0$, the non-intersecting path system is a system of $n$ paths on the graph $\mathcal{G}_t$. The $i^{th}$ path starts at $(n - i, t - 1/(n - i + 1))$ and ends at $(\lambda_i + n - i, 0)$. The paths are said to be not intersecting if they do not share a vertex. On Figure 4.4 we give an example of non-intersecting paths on $\mathcal{G}_4$ for $n = 5$ and $\lambda = (4, 3, 1, 0, 0)$. Note that the paths are on a finite portion of $\mathcal{G}_t$ and we can delete all the vertices $(x, y)$ with $x > \lambda_1 + n - 1$.

We give a sketch of the proof of their enumeration:

**Theorem 4.2.4.** *[25] Given $t, n$ and $\lambda$, the number $Z_\lambda(t)$ of non-intersecting path configurations that start at $(n - i, t - 1/(n - i + 1))$ and end at $(\lambda_i + n - i, 0)$ for $i = 1, \dots, n$ is*

$$t^{|\lambda|} \prod_{1 \leq i < j \leq n} \frac{\lambda_i - i - \lambda_j + j}{j - i},$$

*where $|\lambda| = \lambda_1 + \dots + \lambda_n$.*
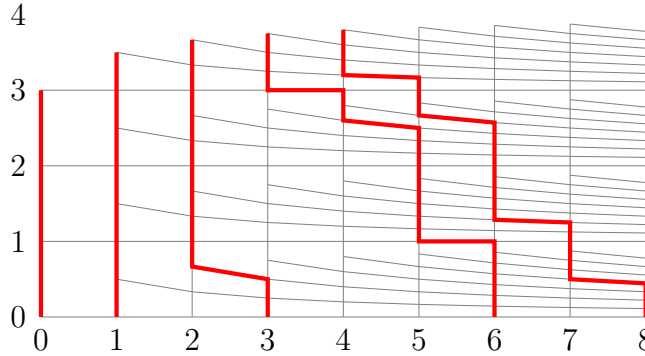
Figure 4.4: non-intersecting lattice paths on $\mathcal{G}_4$ for $n = 5$ and $\lambda = (4, 3, 1, 0, 0)$.

*Proof.* Using the Lindström-Gessel-Viennot Lemma [40], we know that the number of configurations is equal to

$$\det(P(u_i, v_j))_{1 \leq i, j \leq n}$$

where $P(u_i, v_j)$ is the number of paths from $(n - i, t - 1/(n - i + 1))$ $(\lambda_j + n - j, 0)$. It is easy to prove that if $t = 1$ the number of paths is $\binom{\lambda_j + n - j}{n - i}$. Using induction on $t$ one can easily check that

$$P(u_i, v_j) = \binom{\lambda_j + n - j}{n - i} t^{\lambda_j - j + i}.$$

The result follows. Indeed computing the determinant can be done using induction on $n$ and the fact that

$$t^{\lambda_j - j + i} \binom{\lambda_j + n - j}{n - i} = \frac{t^{\lambda_j - j}(\lambda_j + n - j)}{t^{-i}(n - i)} \binom{\lambda_j + n - j - 1}{n - i - 1}.$$

Details and generalizations can be found in [25]. $\qquad\square$

In the case $t = 1$, we get back a very classical result [88, Chapter 7]. The Schur polynomial $s_\lambda(x_1, \ldots, x_n)$ specialized at $x_i = 1$ for all $i$ is equal to

$$s_\lambda(1, \ldots, 1) = \prod_{1 \leq i < j \leq n} \frac{\lambda_i - i - \lambda_j + j}{j - i}.$$

Now let us present the link between the paths and the tableaux:

**Theorem 4.2.5.** *[25] There exists a bijection between the bounded lecture tableaux of shape $\lambda$ and bounded by $t$ and non-intersecting paths on $\mathcal{G}_t$ starting at $(n - i, t - 1/(n - i + 1)$ and ending at $(n - i + \lambda_i, 0)$ for $i = 1, \ldots, n$.*

*Proof.* The $i^{th}$ path starts at $(n - i, t - 1/(n - i + 1)$ and ends at $(\lambda_i + n - i, 0)$. It is in bijection with the $i^{th}$ row of the tableau. The number of cells under the $j^{th}$ horizontal step of the $i^{th}$ path is exactly $T_{i,j}$. $\qquad\square$
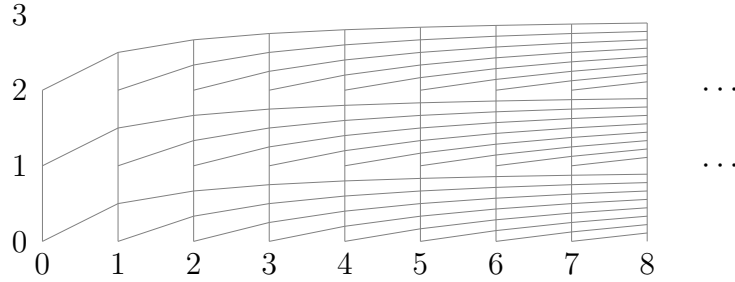
Figure 4.5: The graph $\mathcal{D}_t$ for $t = 3$

The tableau on the left of Figure 4.2 is in bijection with the paths on Figure 4.4.

The graph $\mathcal{G}_t$ has a dual graph that we denote by $\mathcal{D}_t$. The duality here is *not* the duality of planar graphs but the duality of paths on these graphs. The concept of dual paths is an idea due to Gessel and Viennot [41, Section 4] which we generalize to our context.

**Definition 4.2.6.** Given a positive integer $t$, the *dual lecture hall graph* is a graph $\mathcal{D}_t = (V_t, E_t)$. The vertices of the $\mathcal{D}_t$ are:

- $(i, j/(i + 1))$ for $i \geq 0$ and $0 \leq j < t(i + 1)$.

and the directed edges are

- from $(i, k+r/(i+1))$ to $(i+1, k+(r+1)/(i+2))$ for $i \geq 0$ and $0 \leq r \leq i$ and $0 \leq k < t$.

- from $(i, k+r/(i+1))$ to $(i, k+(r+1)/(i+1))$ for $i \geq 0$ and $0 \leq r \leq i$ and $0 \leq k < t-1$ or for $i \geq 0$ and $0 \leq r \leq i$ and $k = t - 1$.

Note that the vertices of $\mathcal{G}_t$ and $\mathcal{D}_t$ are embedded in the plane in the same way. The only difference is that the edges $(i, k + r/(i + 1))$ to $(i + 1, k + r/(i + 2))$ in $\mathcal{G}_t$ are replaced by $(i, k + r/(i + 1))$ to $(i + 1, k + (r + 1)/(i + 2))$ in $\mathcal{D}_t$ and the direction of the vertical edges is reversed.

An example of the graph $\mathcal{D}_3$ is given on Figure 4.5.

Let us now explain why the paths on the graphs $\mathcal{D}_t$ and $\mathcal{G}_t$ are dual. Given $\lambda = (\lambda_1, \ldots, \lambda_n)$ with $\lambda_1 \leq m$, let $\lambda' = (\lambda'_1, \ldots \lambda'_m)$ be such that

$$\lambda'_i = \#\{j \mid \lambda_j \geq i\}.$$

We call $\lambda'$ the conjugate of $\lambda$.

**Proposition 4.2.7.** *There exists a bijection between*

- *Systems of $n$ non-intersecting paths on $\mathcal{G}_t$ that start at $(n - i, t - 1/(n - i + 1))$ and end at $(\lambda_i + n - i, 0)$ for $i = 1, \ldots, n$. and*
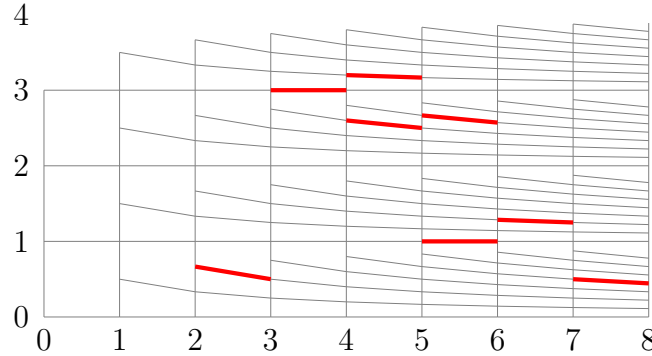
Figure 4.6: Horizontal steps of the non-intersecting lattice paths on Figure 4.4
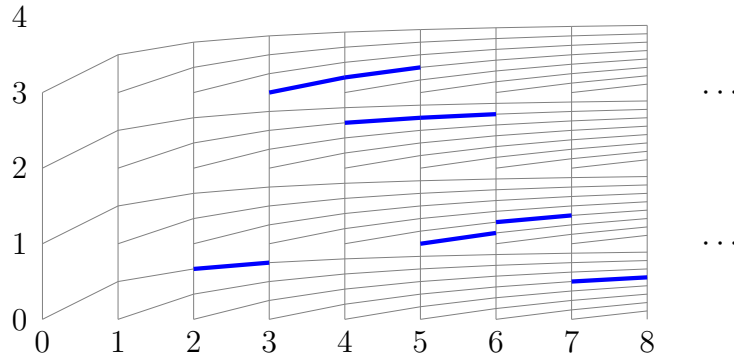


Figure 4.7: Horizontal steps of the dual graph

- *Systems of $m$ non-intersecting paths on $\mathcal{D}_t$ that start at $(n + i - 1 - \lambda'_i, 0)$ and end at $(n + i - 1, t - 1/(n + i))$ for $i = 1, \ldots, m$.*

*Proof.* Starting from a system of $n$ non-intersecting paths on $\mathcal{G}_t$ (see Figure 4.4), we delete all the vertical steps on $\mathcal{G}_t$. See Figure 4.6. We then replace each horizontal step of the form $(i, k + r/(i + 1))$ to $(i + 1, k + r/(i + 2))$ on $\mathcal{G}_t$ by a step $(i, k + r/(i + 1))$ to $(i + 1, k + (r + 1)/(i + 2))$ on $\mathcal{D}_t$. See Figure 4.7. We add the vertical steps on $\mathcal{D}_t$ so that the paths start at $(\lambda_1 + i + 1 - \lambda'_i, 0)$ and ending at $(\lambda_1 + i + 1, t - 1/(\lambda_1 + i + 2))$. See Figure 4.8. This is easily reversible. $\qquad\square$

An example is given on Figures 4.6 and 4.7. We start from the paths from Figure 4.4 for $\lambda = (4, 3, 1, 0, 0)$ and $n = 5$ and end with the paths on Figure 4.8 for $\lambda' = (3, 2, 2, 1)$ and $m = 4$. We draw the horizontal edges in blue and the vertical edges in red to illustrate the construction.
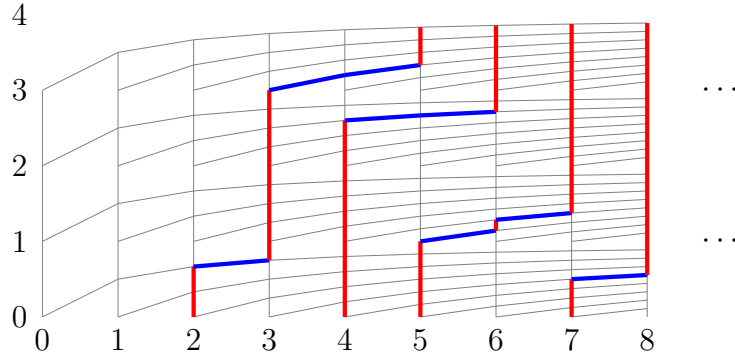
Figure 4.8: Non-intersecting lattice paths on $\mathcal{D}_4$ for $m = 4$ and $\lambda' = (3, 2, 2, 1)$.
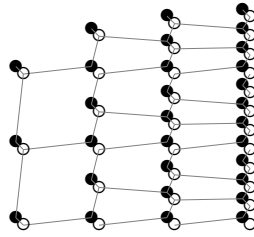


Figure 4.9: The lecture hall lattice $\mathcal{H}_3$

## Dimer models

In this section we give a bijection between lecture hall tableaux of shape $\lambda$ bounded by $t$ and the dimer model on an embedded bipartite graph whose faces are hexagons and octagons. To do so we first replace each vertex $(i, k + r/(i+1))$ of the lecture Hall graph $\mathcal{G}_t$ by a white vertex $w(i, k + r/(i + 1))$ and a black vertex $b(i, k + r/(i + 1))$ joined by an edge. Then we replace

- the edge from $(i, k + r/(i + 1))$ to $(i + 1, k + r/(i + 2))$ for $i \geq 0$ and $0 \leq r \leq i$ and $0 \leq k < t$; by the edge from the black vertex $b(i + 1, k + r/(i + 2))$ to the white vertex $w(i, k + r/(i + 1))$.

- the edge from $(i, k + (r + 1)/(i + 1))$ to $(i, k + r/(i + 1))$ for $i \geq 1$ and $0 \leq r \leq i$ and $0 \leq k < t$; by the edge from the weight vertex $w(i, k + (r + 1)/(i + 1))$ to the black vertex $b(i, k + r/(i + 1))$.

We call this new graph the *lecture hall lattice* and denote it by $\mathcal{H}_t$. An example for $t = 3$ is given on Figure 4.9. To simplify the notation, we now write the black vertex $(i, k + r(i+1))$ for the black vertex $b(i, k + r(i + 1))$.

Now to build a bijection from lecture Hall tableaux of shape $\lambda$ bounded by $t$ and dimer models on $\mathcal{H}_t$, we look at dimer configurations where
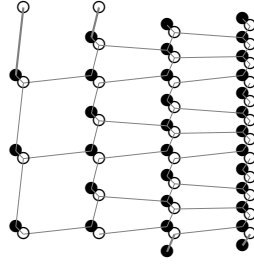
Figure 4.10: The decorated lecture hall lattice $\mathcal{H}_3(2,2)$
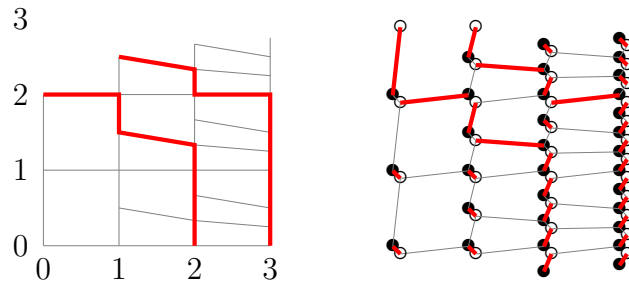


Figure 4.11: From paths on the lecture hall graph $\mathcal{G}_3$ to dimers on the lecture hall lattice $\mathcal{H}_3(2,2)$

- we add a white vertex $(n-i,t)$ and an edge from this vertex to the black vertex $(n-i,t-1/(n-i+j)$;

- we add a black vertex $(n-i+\lambda_i, -1/(n-i+\lambda_i+1))$ and an edge from the white vertex $(n-i+\lambda_i, 0)$ to this vertex;

for $1 \leq i \leq n$. We call this graph the decorated lecture hall lattice $\mathcal{H}_t(\lambda)$. On Figure 4.10 we give an example of $\mathcal{H}_3(2,2)$.

We now give the bijection from the non-intersecting paths to the dimer model. The bijection is a specialization to our graphs of a classical technique in non-intersecting lattice paths and dimer models. Whenever a path uses an edge from vertex $(x,y)$ to vertex $(w,z)$ on the lecture hall graph, we put a dimer on the edge from the white vertex $(x,y)$ to the black vertex $(w,z)$ on the lecture hall lattice. Whenever a vertex $(x,y)$ is not used by any path, we put a dimer on the edge from the black vertex $(x,y)$ to the white vertex $(x,y)$. Then we add dimers on the edge from the white vertex $(n-i,t)$ to the black vertex $(n-i,t-1/(n-i+j)$ and on the edge from the white vertex $(n-i+\lambda_i, 0)$ to the black vertex $(n-i+\lambda_i, -1/(n-i+\lambda_i+1))$ for $1 \leq i \leq n$. An example is given on Figure 4.11. Here $n=2$ and $\lambda = (2,2)$.

## 4.3   Simulations

In order to validate numerically our findings on the Arctic Curve of the model, we have performed the uniform sampling of large bounded lecture hall tableaux. In this section we explain the algorithm by which we randomly generated the bounded lecture hall tableaux. We use an algorithm called "coupling from the past" [81]. We adapted a parallel implementation of coupling from the past due to the second author and Sridhar that generates random tilings using GPU [53].

Given a partition $\lambda = (\lambda_1, \ldots, \lambda_n)$ and an integer $t$ we define a partial order on the bounded lecture hall tableaux of shape $\lambda$.

**Definition 4.3.1.** Given two lecture hall tableau $T$ and $U$ of shape $\lambda$ bounded by $t$ then $T \leq U$ if and only if

$$T(i,j) \leq U(i,j) \ \text{ for all } i,j.$$

This partial order has a unique minimum $T_{min}$ and maximum $T_{max}$ where

$$
\begin{aligned}
T_{min}(i,j) &= n-i; \\
T_{max}(i,j) &= t(n-i+j)-j; \ \text{ for all } i,j.
\end{aligned}
$$

We build the Markov chain $MLHT$ on the set of lecture hall tableaux of shape $\lambda$ bounded by $t$. The vertices of the chain are all the tableaux counted by $Z_\lambda(t)$ and there is a transition from a tableau $T$ to a tableau $U$ with transition probability $\pi(T,U) = 1/|\lambda|$ with $|\lambda| = \lambda_1 + \ldots + \lambda_n$; if

$$T \leq U; \ \text{ and } 1 + \sum_{i,j} T(i,j) = \sum_{i,j} U(i,j);$$

or

$$U \leq T; \ \text{ and } 1 + \sum_{i,j} U(i,j) = \sum_{i,j} T(i,j).$$

Then we add the transitions $\pi(T,T) = 1 - \sum_{U \neq T} \pi(T,U)$ for all tableaux $T$. This Markov chain is reversible and symmetric. Thus its stationary distribution is uniform.

To sample a random bounded lecture hall tableau, we would like to perform a random walk on $MLHT$. Nevertheless we do not know the mixing time of this Markov chain. So we use a celebrated technique due to Propp and Wilson [81] called coupling from the past. The coupling-from-the-past algorithm effectively simulates running the Markov chain for an infinite time. It works as follows: we will run two backward walks one starting at $T_{min}$ and the other one at $T_{max}$. Let $T_{min}^m$ and $T_{max}^m$ be the tableaux after $m$ steps. These walks will be such that for each $m$, $T_{min}^m \leq T_{max}^m$. The algorithm stops when $T_{min}^m = T_{max}^m$.

Let us now explain how one step of the algorithm is performed. We change slightly the Markov chain to speed up the generation. We number the cells of $\lambda$ from 1 to $|\lambda|$. Given two tableaux $T_{min}^m$ and $T_{max}^m$. We pick two numbers uniformly in the interval $[0,1]$. Let us call then $k$ and $\ell$. Then we pick the cell $\lfloor k|\lambda| \rfloor$ of the diagram of $\lambda$. Let us call this cell $(x,y)$. If the cell $(x,y)$ of $T_{min}^m$ could contain the integers $\{a, a+1, \ldots, b\}$ without
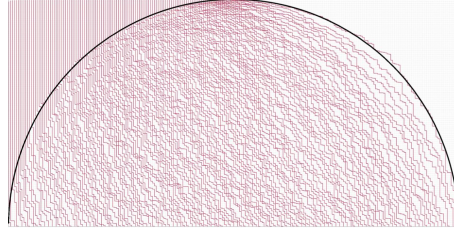
Figure 4.12: Simulation for $\lambda = (n, n-1, \ldots, 2, 1)$, $t = n = 120$

violating the condition for $T_{min}^m$ to be lecture hall then we change the cell $(x, y)$ to the value $\lfloor a + (b - a + 1)\ell \rfloor$. If the cell $(x, y)$ of $T_{max}^m$ could contain the integers $\{c, c+1, \ldots, d\}$ without violating the condition for $T_{max}^m$ to be lecture hall then we change the cell $(x, y)$ to the value $\lfloor c + (d - c + 1)\ell \rfloor$. We do not change the value of the other cells. The result is a pair of tableaux $T_{min}^{m+1}, T_{max}^{m+1}$ and we denote this by $(T_{min}^{m+1}, T_{max}^{m+1}) = R_{k,\ell}(T_{min}^m, T_{max}^m)$. As $a \leq c$ and $b \leq d$, then $a + (b - a + 1)\ell \leq c + (d - c + 1)\ell$ and $T_{min}^{m+1} \leq T_{max}^{m+1}$.

To get to $T_{min}^m$ and $T_{max}^m$, from $T_{min}$ and $T_{max}$ we need to pick $k_1, \ldots, k_m$ and $\ell_1, \ldots, \ell_m$ and as we run the walks backwards, then

$$(T_{min}^m, T_{max}^m) = R_{k_1,\ell_1}(R_{k_2,\ell_2}(\ldots (R_{k_m,\ell_m}(T_{min}, T_{max}) \ldots).$$

In practice we stop when $T_{min}^m$ and $T_{max}^m$ are "close". This is very similar to what was done for lozenge and domino tilings. See [53] for example.

Here we present the simulations for our two running examples. We will always present the non-intersecting paths on the lecture hall graph starting at $(n - i, t - 1/(n - i + 1))$ and ending at $(\lambda_i + n - i, 0)$ or on the dual lecture hall graph. We give the example for $\lambda = (n, n-1, \ldots, 2, 1)$ on Figure 4.12 and for $\lambda = (n, \ldots, n)$ on Figure 4.13. Here we set $t = n$. As we can see on these figures, we have several types of behavior: some regions are *frozen*, i.e. are empty or are filled with vertical paths and some regions are *liquid*, i.e. seem random. Some other things that we can see is that the separation from the liquid to the the frozen region is always sharp and the shape of this separation is always given by the trajectory of one of the paths on the lecture hall graph or on the dual lecture hall graph. We will use this observation to compute the curves separating the regions in Section 4.4. On Figures 4.12 and 4.13 we draw the conjectural curve that separates the frozen and liquid regions. As one can guess, these seem to be a semicircle and an ellipse. In Sections 4.4 we will explain how to compute these curves.

## 4.4   Tangent Method

Developed in [21] the tangent method provides a simple way to compute Arctic curves for models that can be described as a configuration of non-intersecting paths. Rather than computing bulk correlation functions to determine the boundary between the ordered and
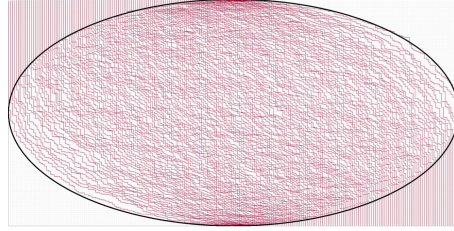
Figure 4.13: Simulation for $\lambda = (n, n, \ldots, n, n)$, $t = n = 120$

disordered phases, the tangent method requires only the computation of a boundary one-point function.

We will explain the procedure in the framework of lecture hall tableaux. Consider a lecture hall tableaux configuration drawn as a set of non-intersecting paths. Suppose that the boundary between the frozen and liquid regions is given by the trajectory of one of the paths. That is, in the thermodynamic limit a portion of the Arctic curve follows the expected value of the position of this boundary path. Call the endpoint of this path along the bottom boundary $p_0$. The assumption behind the tangent method states that as we vary $p_0$, the path will follow its original trajectory, along the Arctic curve, until it can travel in a straight line to its endpoint. Moreover, this line will be tangent to the Arctic curve. Together these are known as the *tangency assumption* of the tangent method.

In practice, we extend our domain to allow our path to end at a new point shifted horizontally by $q$ and lowered by $s$ from its original endpoint. We then calculate the expected location at which the path exited the original domain. Between these two points (the end point and the exit location) the path travels in a region empty of all other paths and its most probable free trajectory (or "geodesic") is determined by the underlying graph. If the underlying graph is translationally invariant, the geodesics are straight lines. As a potentially surprising further analogy between lecture-hall tableaux and ordinary SSYT, and a justification *a posteriori* of our choice of embedding of the graph, it turns out that the geodesics are straight lines also in our setting. The tangency assumption then states that the path will continue along this geodesic until meeting the Arctic curve, and that the geodesic will in fact be tangent to the Arctic curve.

If the tangent method holds (that is, the tangency assumption is true), then as we vary $q$ we obtain a family of lines forming an envelope of the Arctic curve. From this envelope one can obtain a parameterization of the Arctic curve itself. In what follows, we will employ this method to derive parameterizations for the Arctic curve for BLHT.

In this section, we first compute the asymptotic shape of a single path as a warm-up (and justification of the claim above). We then compute a parameterization the Arctic curve determined by the outer most paths. Finally, we consider the Arctic curve at a so called "freezing boundary". The main result of this section is equation (4.1.1).

## Single Path

Suppose we have a single path starting at $(n - 1, t - \frac{1}{n})$ and ending at $(n + k - 1, 0)$, corresponding to a single lecture hall partition. Recall that $Z_{n,k}(t) = \binom{n+k-1}{k}t^k$ gives the number of paths with the given starting point and ending point. We want to know where the path crosses a horizontal slice at height $s$. To this end we divide the full path into two paths, one starting at $(n - 1, t - \frac{1}{n})$ and ending at $(n + l - 1, s)$ and the other one starting at $(n + l - 1, s - \frac{1}{n+l})$ and ending at $(n + k - 1, 0)$. We rewrite the partition function for the full path as the product of the partition functions for the two partial paths, summing over all possible intermediate points $l$. We have

$$
\begin{aligned}
Z_{n,k}(t) &= \sum_{l=0}^{k} Z_{n,l}(t - s)\, Z_{n+l,k-l}(s) \\
&= \sum_{l=0}^{k} \binom{n + l - 1}{l}(t - s)^l \binom{n + k - 1}{k - l} s^{k-l}.
\end{aligned}
\tag{4.4.1}
$$

As an exercise in the type of calculations that will follow we prove the following:

**Proposition 4.4.1.** *Consider the limit $N \to \infty$, for parameters scaling as $n = N\nu$, $k = N\kappa$, $t = N\tau$, $s = N\sigma$, $l = N\lambda$, in which all Greek letters are $O(1)$. Asymptotically the single path travels in a straight line between its starting and ending points.*

*Proof.* Recall Stirling's approximation for the factorial gives

$$
x! = \sqrt{2\pi x}\, x^x e^{-x}\left(1 + O\left(\frac{1}{x}\right)\right)
$$

as $x \to \infty$. We can use this to approximate the binomial coefficients in equation (4.4.1) in the large $N$ limit. Doing so, we have asymptotically

$$
Z_{N\nu, N\kappa}(N\tau) \sim \frac{1}{2\pi} e^{N\kappa \ln(N)} \int_0^\kappa d\lambda \sqrt{\frac{\nu + \kappa}{\lambda\nu(\kappa - \lambda)}} e^{N\, S(\lambda)}
\tag{4.4.2}
$$

where

$$
S(\lambda) = \lambda \ln(\tau - \sigma) + (\kappa - \lambda)\ln(\sigma) + (\nu + \kappa)\ln(\nu + \kappa) - \lambda \ln(\lambda) - \nu \ln(\nu) - (\kappa - \lambda)\ln(\kappa - \lambda).
$$

This integral can be approximated via Laplace's method. Note that $S$ has its only critical point at

$$
\frac{(\tau - \sigma)(\kappa - \lambda^*)}{\sigma \lambda^*} = 1
$$

or, rearranging,

$$
\lambda^* = \kappa\left(1 - \frac{\sigma}{\tau}\right).
\tag{4.4.3}
$$

It is easy to check that this is a maximum.

Let $X, Y$ be coordinates on the rescaled domain $[0, \nu + \kappa] \times [0, \tau]$. Since the integrand is exponentially suppressed away from $\lambda^*$, the most likely position at which our path crosses the slice $Y = \sigma$ is at $X = \nu + \lambda^*$. Equation (4.4.3) then says that most likely path connecting the points $(\nu, \tau)$ to $(\nu + \kappa, 0)$, follows the straight line

$$Y = -\frac{\tau}{\kappa} X + \frac{\tau}{\kappa} (\nu + \kappa).$$

$\square$

## Outer Boundary

Here let us consider the outer boundary of the Arctic curve; that is, a section where the boundary between the frozen and disordered region is given by the trajectory of the first or the last path (in either path description). The following analysis is very similar to that of [30].

Let $\lambda = (\lambda_1, \ldots, \lambda_n)$, and consider the bounded lecture hall tableaux of shape $\lambda$ and height $t$. Recall that there is a bijection between the number of BLHT and configurations of non-intersecting, down-right paths with starting points $(n - i, t - \frac{1}{n+1-i})$ and ending points $(n + \lambda_j - j, 0)$.

In what follows, by the $k^{th}$ path we mean the path starting at $(n - k, t - \frac{1}{n+1-k})$ and ending at $(n + \lambda_k - k, 0)$. Equivalently, this is the path corresponding to $k^{th}$ row of $\lambda$.

Recall

$$Z_\lambda(t) = t^{|\lambda|} \prod_{1 \leq i < j \leq n} \frac{\lambda_i - \lambda_j + j - i}{j - i}. \tag{4.4.4}$$

To shorten the notation we write $Z = Z_\lambda(t)$.

### First Path

In order to use the tangent method we consider the possible configurations of paths in which the first path ends at the point $(n + \lambda_1 + q, -s)$. Let the partition function for this model be called $Z_{qs}$. Define $Z_r$ to be the partition function for BLHT of shape $\mu = (\lambda_1 + r, \lambda_2, \ldots, \lambda_n)$. In terms of non-intersecting paths, $Z_r$ is the partition function for configurations in which we have shifted the end point of the first path to the right by $r$. See Figure 4.14 for a diagram. With this $Z_{qs}$ can be written as the sum over $r$ of $Z_r$ times the partition function of a single path starting at $(n + \lambda_1 + r - 1, -\frac{1}{n+\lambda_1+r})$ and ending at $(n + \lambda_1 + q - 1, -s)$. We normalize by $Z$ (see eqn. (4.4.4)) to get

$$\frac{Z_{qs}}{Z} = \sum_{r=0}^{q} \frac{Z_r}{Z} s^{q-r} \binom{n + \lambda_1 - 1 + q}{q - r}. \tag{4.4.5}$$
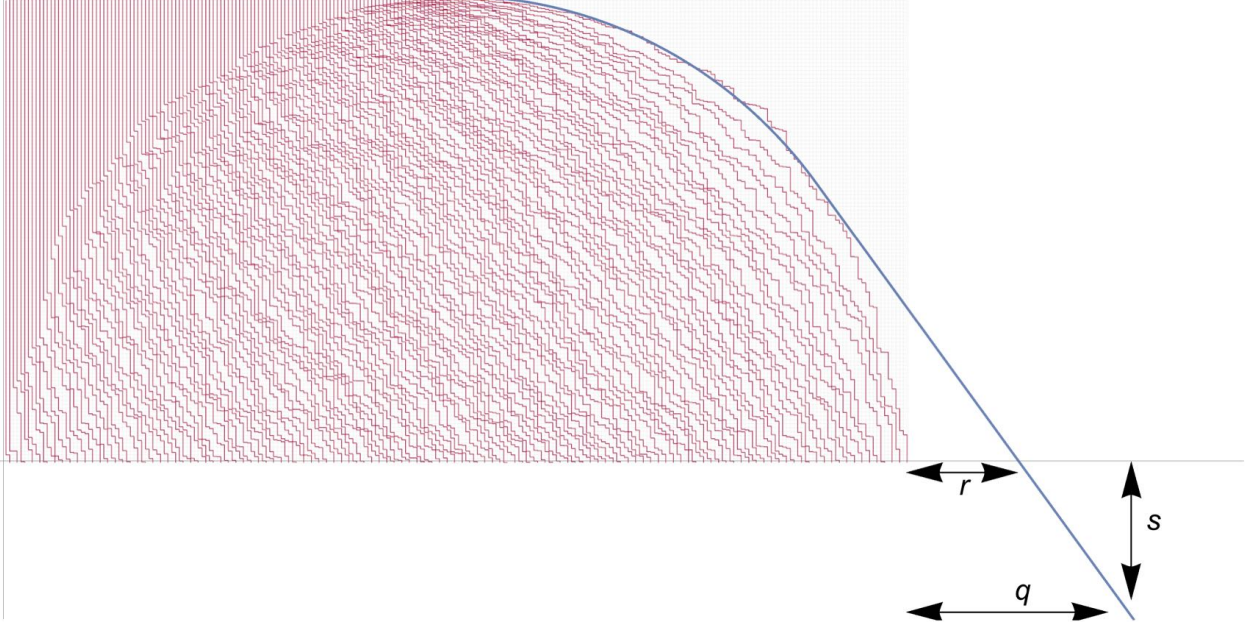
Figure 4.14: A configuration of paths corresponding to a BLHT of shape $\lambda = (n, n-1, \ldots, 1)$. The blue curve schematically shows the extended first path ending at $(n + \lambda_1 + q - 1, -s)$ and passing through $(n + \lambda_1 + r - 1, 0)$.

From the product formula (4.4.4), the ratio of $Z_r$ and $Z$ takes the simple form

$$
\begin{aligned}
\frac{Z_r}{Z} &= t^{|\mu| - |\lambda|} \prod_{1 \leq i < j \leq n} \frac{\mu_i - \mu_j + j - i}{\lambda_i - \lambda_j + j - i} \\
&= t^r \prod_{i=1, 2 \leq j \leq n} \frac{\lambda_1 + r - \lambda_j + j - 1}{\lambda_1 - \lambda_j + j - 1} \prod_{2 \leq i < j \leq n} \frac{\lambda_i - \lambda_j + j - i}{\lambda_i - \lambda_j + j - i} \\
&= t^r \prod_{j=2}^{n} \frac{\lambda_1 + r - \lambda_j + j - 1}{\lambda_1 - \lambda_j + j - 1}.
\end{aligned}
\tag{4.4.6}
$$

Using equation (4.4.6) we can rewrite equation (4.4.5) as

$$
\begin{aligned}
\frac{Z_{qs}}{Z} &= \sum_{r=0}^{q} \frac{Z_r}{Z} s^{q-r} \binom{n + \lambda_1 - 1 + q}{q - r} \\
&= \sum_{r=0}^{q} t^r s^{q-r} \prod_{j=2}^{n} \frac{\lambda_1 + r - \lambda_j + j - 1}{\lambda_1 - \lambda_j + j - 1} \binom{n + \lambda_1 - 1 + q}{q - r} \\
&= \sum_{r=0}^{q} t^r s^{q-r} \prod_{j=2}^{n} \frac{a_1 - a_j + r}{a_1 - a_j} \binom{a_1 + q}{q - r}.
\end{aligned}
\tag{4.4.7}
$$

where $a_i = n + \lambda_i - i$.

Note that what we have done is write $Z_{qs}$ as a sum over the possible ways the first path can cross the horizontal slice $y = 0$. The following lemma describes the most likely location the path will cross this slice as a function of the limiting ratios of $q$ and $s$ to $n$.

**Lemma 4.4.2.** *Consider the limit $n \to \infty$, for parameters scaling as $t = n\tau$, $s = n\sigma$, $r = n\rho$, $q = nz$, and $a_i = \lfloor n\alpha\left(\frac{i}{n}\right) \rfloor$. In this limit, the first path passes through the point $(\alpha(0) + \rho, 0)$, where $\rho$ is related to $z$ by*

$$z = \frac{\sigma}{\tau}(\alpha(0) + \rho)e^{-\int_0^1 du\, \frac{1}{\alpha(0)-\alpha(u)+\rho}} + \rho.$$

*Proof.* Taking the above limit in equation (4.4.7), the binomial coefficient can be approximated using Stirling's approximation giving

$$\binom{a_1 + q}{q - r} \sim \frac{1}{\sqrt{2\pi n}} \sqrt{\frac{\alpha(0) + z}{(\alpha(0) + \rho)(z - \rho)}} e^{n((\alpha(0)+z)\ln(\alpha(0)+z)-(\alpha(0)+\rho)\ln(\alpha(0)+\rho)-(z-\rho)\ln(z-\rho))},$$

while the product term can be written

$$\prod_{j=2}^{n} \frac{a_1 - a_j + r}{a_1 - a_j} = e^{n\left(\frac{1}{n}\sum_{j=2}^{n} \ln\left(\frac{a_1-a_j+r}{a_1-a_j}\right)\right)} \sim e^{n\int_0^1 du\, \ln\left(\frac{\alpha(0)-\alpha(u)+\rho}{\alpha(0)-\alpha(u)}\right)}.$$

All together equation (4.4.7) becomes

$$\frac{Z_{qs}}{Z} \sim \sqrt{\frac{n}{2\pi}} e^{nz\, \ln(n)} \int_0^z d\rho \sqrt{\frac{\alpha(0) + z}{(\alpha(0) + \rho)(z - \rho)}} e^{nS(\rho)} \qquad (4.4.8)$$

where

$$S(\rho) = \rho\, \ln(\tau) + (z - \rho)\ln(\sigma) - (\alpha(0) + \rho)\ln(\alpha(0) + \rho) - (z - \rho)\ln(z - \rho)$$
$$+ \int_0^1 du\, \ln\left(\frac{\alpha(0) - \alpha(u) + \rho}{\alpha(0) - \alpha(u)}\right).$$

As in Section (4.4), the integral is dominated by the contributions from the maximum of $S(\rho)$. This critical point occurs when

$$\frac{\tau(z - \rho)}{\sigma(\alpha(0) + \rho)} e^{\int_0^1 du\, \frac{1}{\alpha(0)-\alpha(u)+\rho}} = 1$$

or rearranging

$$z = \frac{\sigma}{\tau}(\alpha(0) + \rho)e^{-\int_0^1 du\, \frac{1}{\alpha(0)-\alpha(u)+\rho}} + \rho.$$

$\square$

Asymptotically the first path passes through the points $(\alpha(0) + \rho, 0)$ and $(\alpha(0) + z, -\sigma)$, where we know $\rho$ in terms of $z$ (and vice versa) from Lemma 4.4.2. By varying $z$ (or more conveniently $\rho$), we obtain a family of lines which, according to the tangent method, form an envelope of the Arctic curve. From these lines we will construct a parameterization of the curve. Let $X$ and $Y$ be continuum coordinates on the domain $[0, \alpha(0)] \times [0, \tau]$ into which we embed our collection of paths. We show

**Theorem 4.4.3.** *Assuming the tangent method holds, the portion of the Arctic curve following the first path can be parameterized by*

$$X(x) = \frac{x^2 I'(x)}{I(x) + xI'(x)}$$
$$Y(x) = \tau \frac{1}{I(x) + xI'(x)}$$

(4.4.9)

*with* $x \in [\alpha(0), \infty)$.

*Proof.* From the two points $(\alpha(0) + \rho, 0)$ and $(\alpha(0) + z, -\sigma)$ we have the line

$$Y = -\frac{\sigma}{z - \rho}(X - \alpha(0) - \rho).$$

Using Lemma 4.4.2 to eliminate $z$, this becomes

$$Y = -\frac{\tau}{\alpha(0) + \rho} e^{\int_0^1 du \, \frac{1}{\alpha(0) + \rho - \alpha(u)}} (X - \alpha(0) - \rho)$$

Rearranging, and letting $x = \alpha(0) + \rho$, we have

$$\frac{x}{\tau} I(x) Y + X - x = 0$$

(4.4.10)

where $I(x) = e^{-\int_0^1 du \, \frac{1}{x - \alpha(u)}}$. Note that $\rho \in [0, \infty)$ implies $x = \alpha(0) + \rho \in [\alpha(0), \infty)$.

Taking the derivative of equation (4.4.10) with respect to $x$ gives the system of equations for $(X, Y)$

$$\frac{x}{\tau} I(x) Y + X - x = 0$$
$$\frac{1}{\tau}(I(x) + xI'(x)) Y - 1 = 0$$

which can be solved to yield the desired parameterization. $\square$

In what follows, we reuse much of the notation from the preceding section.

**Last Path**

We can consider the same calculation as above on a portion of the Arctic curve which follows the last path in the thermodynamic limit. For such a section of the Arctic curve to exist, we must have that $\lambda_n$ is of size proportional to $n$. This means that the limiting profile must satisfy $\alpha(1) > 0$.

Suppose $\lambda$ is such a partition. We first consider the case when the endpoint of the last path is shifted to the left by $r$, that is, the path ends at $(\lambda_n - r, 0)$, with $r \in [0, \lambda_n]$. In the same manner as the previous section we have

$$\frac{Z_r}{Z} = t^{-r} \prod_{i=1}^{n-1} \frac{\lambda_i - \lambda_n + r + n - i}{\lambda_i - \lambda_n + n - i}. \tag{4.4.11}$$

Now suppose the last path ends at a point $(\lambda_n + q, -s)$, for $q \geq -\lambda_n$. Write the total number of configurations as $Z_{qs}$. As in the previous section, using equation (4.4.11), we write this partition function as

$$\frac{Z_{qs}}{Z} = \sum_{r=0}^{\lambda_n} \frac{Z_r}{Z} s^{q+r} \binom{\lambda_n + q}{q + r}$$

$$= \sum_{r=0}^{\lambda_n} t^{-r} s^{q+r} \prod_{i=1}^{n-1} \frac{a_i - a_n - r}{a_i - a_n} \binom{a_n + q}{q + r}. \tag{4.4.12}$$

See Figure 4.15.

**Lemma 4.4.4.** *Consider the limit $n \to \infty$, for parameters scaling as $t = N\tau$, $s = n\sigma$, $r = n\rho$, $q = nz$, and $a_i = \lfloor n\alpha \left(\frac{i}{n}\right) \rfloor$. In this limit, the last path passes through the point $(\alpha(1) - \rho, 0)$, where $\rho$ is related to $z$ by*

$$z = \frac{\sigma}{\tau}(\alpha(1) - \rho)e^{-\int_0^1 du \frac{1}{\alpha(1)-\rho-\alpha(u)}} - \rho. \tag{4.4.13}$$

*Proof.* In the above limit, we have

$$\frac{Z_{qs}}{Z} \sim \sqrt{\frac{n}{2\pi}} e^{nz \ln(n)} \int_0^{\alpha(1)} d\rho \sqrt{\frac{\alpha(1) + z}{(\alpha(1) - \rho)(z + \rho)}} e^{n S(\rho)}$$

where

$$S(\rho) = -\rho \ln(\tau) + (z + \rho) \ln(\sigma) - (\alpha(1) - \rho) \ln(\alpha(1) - \rho) - (z + \rho) \ln(z + \rho)$$

$$+ \int_0^1 du \ln \left( \frac{\alpha(u) - \alpha(1) + \rho}{\alpha(u) - \alpha(1)} \right)$$

The critical point occurs when

$$\frac{\tau}{\sigma} \frac{z + \rho}{\alpha(1) - \rho} e^{\int_0^1 du \frac{1}{\alpha(1)-\rho-\alpha(u)}} = 1.$$

Rearranging gives the desired result. $\qquad \square$
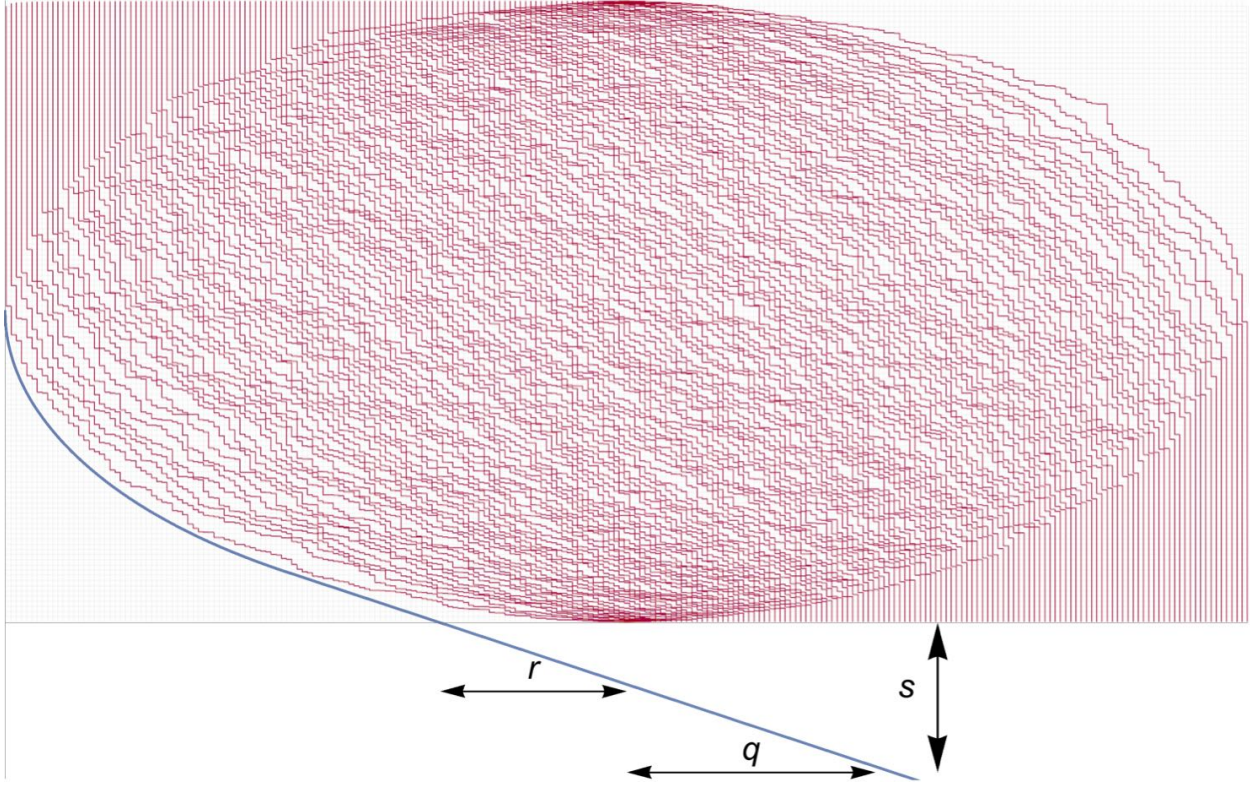
Figure 4.15: A configuration of paths corresponding to a BLHT of shape $\lambda = (n, \ldots, n)$. The blue curve schematically shows the trajectory of the extended last path which ends at $(\lambda_n + q, -s)$ and passes through $(\lambda_n - r, 0)$.

Using this we get a parameterization of this section of the Arctic curve.

**Theorem 4.4.5.** *Assuming the tangent method holds, the portion of the Arctic curve following the last path is parameterized by*

$$X(x) = \frac{x^2 I'(x)}{I(x) + x I'(x)}$$
$$Y(x) = \tau \frac{1}{I(x) + x I'(x)} \tag{4.4.14}$$

*with $x \in [0, \alpha(1)]$.*

*Remark* 4.4.6. Note this is the same parameterization as Theorem 4.4.3 for a different range of parameter, as is normally the case for dimer models (and *not* the case for models which are not free-fermionic). For $\mathbb{Z}^2$ invariant graphs, this is a theorem of Kenyon and Okounkov [59]. We will see that we the same parameterization works for all portions of the Arctic curve of the BLHT, despite the fact that the lecture hall graph is not $\mathbb{Z}^2$ invariant.

*Proof.* From the points $(\alpha(1) + z, -\sigma)$, $(\alpha(1) - \rho, 0)$, and equation (4.4.13) we have a family of lines

$$x\, I(x)Y + X - x = 0$$

with $x = \alpha(1) - \rho$ and $I(x) = \frac{1}{\tau} e^{-\int_0^1 du \frac{1}{x - \alpha(u)}}$. Taking the derivative with respect to $x$, we get the system of equations

$$xI(x)Y + X - x = 0$$
$$(I(x) + xI'(x))Y - 1 = 0$$

which can be solved to yield the desired parameterization. Note that since $\rho \in [0, \alpha(1)]$, the range of $x$ is $[0, \alpha(1)]$ as well. $\qquad\square$

Before moving on, we prove the following proposition. Recall the quantities $T_{ij}/(n+j-i)$ in the definition of a lecture hall tableaux depend on $n$, so apriori the lecture hall tableaux of shape $(\lambda_1, \ldots, \lambda_n)$ and $(\lambda_1, \ldots, \lambda_n, 0, \ldots, 0)$ are not the same.

**Proposition 4.4.7.** *Assuming the tangent method holds, the Arctic curve is unchanged when we extend the partition $\lambda = (\lambda_1, \ldots, \lambda_n)$ to $(\lambda_1, \ldots, \lambda_n, 0, \ldots, 0)$, where we add $m$ parts of size zero and $m$ scales as $m = nM$ in the thermodynamic limit.*

*Proof.* We'll show this for the portion of the Arctic curve following the first path. After extending $\lambda$, equation (4.4.6) becomes

$$\frac{Z_r}{Z} = t^r \prod_{j=2}^{n+m} \frac{\lambda_1 - \lambda_j + j - 1 + r}{\lambda_1 - \lambda_j + j - 1}$$

$$= t^r \prod_{j=2}^{n+m} \frac{a_1 - a_j + r}{a_1 - a_j} \tag{4.4.15}$$

where now the products range from 2 to $n + m$. With this equation (4.4.5) becomes

$$\frac{Z_{qs}}{Z} = \sum_{r=0}^{q} t^r s^{q-r} \prod_{j=2}^{n+m} \frac{a_1 - a_j + r}{a_1 - a_j} \binom{m + a_1 + q}{q - r}. \tag{4.4.16}$$

In the thermodynamic limit (with $m = nM$, and the rest as before), this is dominated by the maximum of

$$S(\rho) = \rho \, \ln(\tau) + (z - \rho) \, \ln(\sigma) - (z - \rho) \, \ln(z - \rho) - (M + \alpha(0) + \rho) \ln(M + \alpha(0) + \rho)$$
$$+ \int_0^1 du \, \ln\left(\frac{\alpha(0) + \rho - \alpha(u)}{\alpha(0) - \alpha(u)}\right) + \int_1^{1+M} du \, \ln\left(\frac{\alpha(0) + \rho + u - 1}{\alpha(0) + u - 1}\right)$$

This is given when

$$\frac{\tau(z - \rho)}{\sigma(M + \alpha(0) + \rho)} e^{\int_0^1 du \frac{1}{\alpha(0) + \rho - \alpha(u)}} \frac{M + \alpha(0) + \rho}{\alpha(0) + \rho} = 1.$$

Letting $x = \alpha(0) + \rho$, this results in the same parameterization.

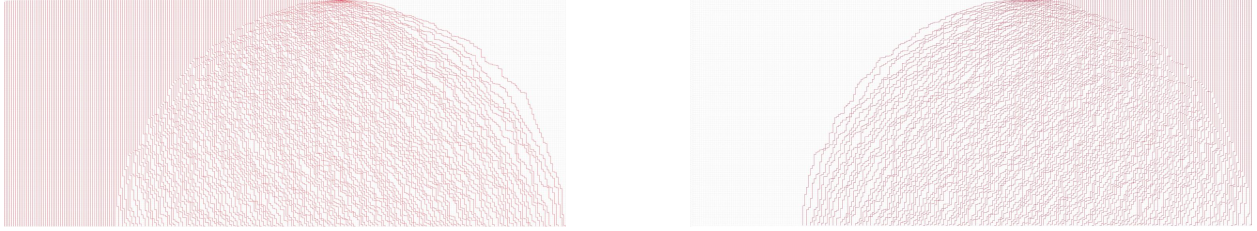The other portion can be done similarly. See Figure 4.16. $\qquad\square$

Figure 4.16: On the left, a configuration of paths for $\lambda = (n, n-1, \ldots, 1, 0, \ldots, 0)$, where there are $n/2$ parts of size 0. On the right, the corresponding dual paths.

## Dual Path Formulation

Let's consider the analogous calculation in the dual path formulation. In the case, the paths begin at $u_i = (n - 1 + i - \lambda'_i, -\frac{1}{(n+i-\lambda'_i)^2})$ and end at $v_j = (n + j - 1, t - \frac{1}{n+j-1})$. See Figure 4.16. Recall that vertical edges that were previously empty now have a path, while vertical edges that previously had a path are now empty. This means that switching to the dual path formulations swaps frozen regions of no paths and frozen regions of vertical paths. In particular, the Arctic curve remains the same. From this perspective, portions of the Arctic curve on the boundary between an area of frozen vertical paths and a disordered region in the original formulation now follow the trajectory of one of the dual paths. For what follows below we assume $\lambda$ has $n$ parts all greater than zero. In particular, $\lambda'_1 = n$.

By the $k^{th}$ dual path we mean the path beginning at $(n - 1 + k - \lambda'_k, -\frac{1}{(n+k-\lambda'_k)^2})$ and ending at $(n + k - 1, t - \frac{1}{n+k-1})$. Equivalently, this is the path corresponding to $k^{th}$ column of $\lambda$.

### First Dual Path

To calculate a parameterization for the portion of the Arctic curve following the first dual path we must first extend $\lambda$ to $(\lambda_1, \ldots, \lambda_n, 0, \ldots, 0)$ where we've added $m$ parts of length zero.

Let the number of BLHT with this shape be $Z$. In the dual paths picture, moving the start point of the first dual path to the left by $r$ corresponds to changing the first of the $r$ zeros in the extension of our partition to ones; that is, the partition becomes

$$\mu := (\lambda_1, \ldots, \lambda_n, \underbrace{1, \ldots, 1}_{r}, \underbrace{0, \ldots, 0}_{m-r}).$$

We call this partition $\mu$ and the corresponding partition function $Z_r$. Using the product formula for the partition function of the BLHT, we have

$$\frac{Z_r}{Z} = t^r \prod_{1 \leq i < j \leq n+m} \frac{\mu_i - \mu_j + j - 1}{\lambda_i - \lambda_j + j - i}.$$

Note that the only terms in the product that are not one come from $1 \leq i \leq n, n < j \leq n+r$ and $n < i \leq n+r, n+r < j \leq n+m$, and the product can be simplified to

$$\frac{Z_r}{Z} = t^r \prod_{1 \leq i \leq n < j \leq n+r} \frac{\lambda_i - 1 + j - i}{\lambda_i + j - i} \prod_{n < i \leq n+r < j \leq n+m} \frac{1 + j - i}{j - i}.$$

Fixing $i$, both products are telescoping, giving

$$\prod_{n < j \leq n+r} \frac{\lambda_i - 1 + j - i}{\lambda_i + j - i} = \frac{\lambda_i + n - i}{\lambda_i + n + r - i},$$

$$\prod_{n+r < j \leq n+m} \frac{1 + j - i}{j - i} = \frac{n + m - 1 + i}{n + r + 1 - i}$$

from which we have

$$\frac{Z_r}{Z} = t^r \prod_{i=1}^{n} \frac{\lambda_i + n - i}{\lambda_i + n + r - i} \prod_{i=n+1}^{n+r} \frac{n + m + 1 - i}{n + r + 1 - i}. \tag{4.4.17}$$

Now consider the possible configuration with the first dual path starting at $(-q, -s - \frac{1}{(m-q+1)^2})$, for some $q$ and $s$ such that $m > q \geq 0$ and $s > 0$. See Figure 4.17. Call the partition function $Z_{qs}$. Summing over the possible ways the path can cross the $y = 0$ slice, we have

$$\frac{Z_{qs}}{Z} = \sum_{r=0}^{q} \frac{Z_r}{Z} \binom{m-r}{m-q} s^{q-r}$$

$$= \sum_{r=0}^{q} t^r s^{q-r} \prod_{i=1}^{n} \frac{\lambda_i + n - i}{\lambda_i + n + r - i} \prod_{i=n+1}^{n+r} \frac{n + m + 1 - i}{n + r + 1 - i} \binom{m-r}{m-q}$$

$$= \sum_{r=0}^{q} t^r s^{q-r} \prod_{i=1}^{n} \frac{a_i}{a_i + r} \prod_{i=n+1}^{n+r} \frac{a_i + m}{a_i + r} \binom{m-r}{m-q} \tag{4.4.18}$$

where $\binom{m-r}{q-r} s^{q-r}$ counts the number of configurations of a single path from $(-q, -s - \frac{1}{(m-q+1)^2})$ to $(-r, -\frac{1}{m-r})$.

**Lemma 4.4.8.** *Consider the limit $n \to \infty$, for parameters scaling as $t = n\tau$, $s = n\sigma$, $r = n\rho$, $q = nz$, $m = nM$, and $a_i = \lfloor n\alpha\left(\frac{i}{n}\right) \rfloor$. In this limit, the first dual path passes through the point $(-\rho, 0)$, where $\rho$ is related to $z$ by*

$$z = \rho \frac{\sigma}{\tau} e^{\int_0^1 du \frac{1}{\alpha(u) + \rho}} + \rho \tag{4.4.19}$$
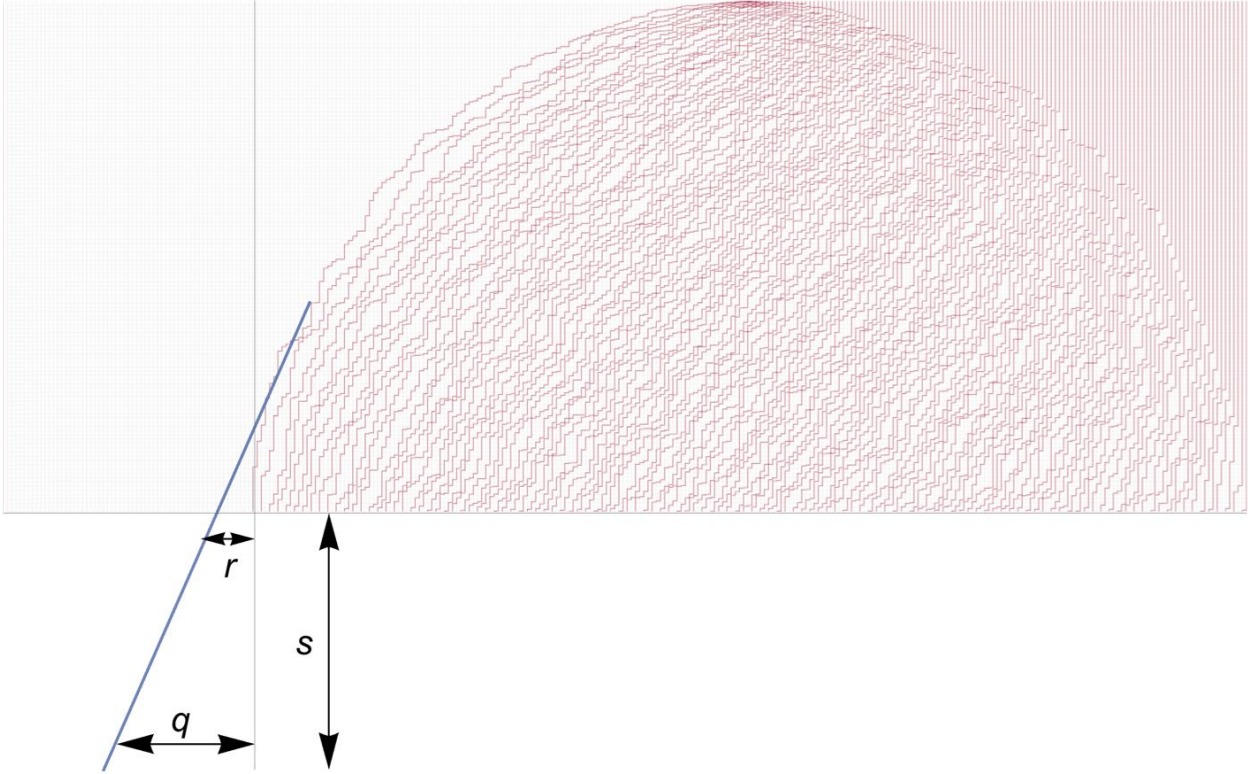
Figure 4.17: A configuration of dual paths corresponding to a BLHT of shape $\lambda = (n, n - 1, \ldots, 1, 0, \ldots, 0)$ with $n/2$ parts of size 0. The blue curve represents the trajectory of the extended first dual path, which starts at $(-q, -s - \frac{1}{(n-q+1)^2})$ and passes through $(-r, 0)$.

*Proof.* Taking the limit $n \to \infty$, the sum in equation (4.4.18) above becomes an integral which is dominated by the maximum of

$$S(\rho) = \rho \, \ln(\tau) + (z - \rho) \ln(\sigma) + (M - \rho) \ln(M - \rho) - (z - \rho) \ln(z - \rho)$$
$$+ \int_0^1 du \, \ln\left(\frac{\alpha(u)}{\alpha(u) + \rho}\right) + \int_1^{1+\rho} du \, \ln\left(\frac{\alpha(u) + M}{\alpha(u) + \rho}\right)$$

Note that for $u \in (1, 1 + \rho]$, $\alpha(u) = 1 - u$. Using this, we compute

$$\int_1^{1+\rho} du \, \ln\left(\frac{\alpha(u) + M}{\alpha(u) + \rho}\right) = \int_1^{1+\rho} du \, \ln\left(\frac{1 - u + M}{1 - u + \rho}\right)$$
$$= M \, \ln(M) - (M - \rho) \ln(M - \rho) - \rho \, \ln(\rho)$$

The maximum of $S$ occurs when

$$\frac{\tau(z - \rho)}{\sigma \, \rho} e^{-\int_0^1 du \, \frac{1}{\alpha(u) + \rho}} = 1$$

Rearranging gives the desired result. $\qquad\square$

Finally we have

**Theorem 4.4.9.** *Assuming the tangent method holds, the portion of the Arctic curve following the first dual path is parameterized by*

$$X(x) = \frac{x^2 I'(x)}{I(x) + xI'(x)}$$

$$Y(x) = \tau \frac{1}{I(x) + xI'(x)}$$

(4.4.20)

*with* $x \in (-\infty, 0]$.

*Proof.* In the large $n$ limit, the shifted first path passes through the point $(-z, -\sigma)$ and $(-\rho, 0)$. These define the family of lines

$$Y = \frac{\sigma}{z - \rho}(X + \rho)$$

Using equation (4.4.19), and rearranging the above, we have

$$\frac{x}{\tau} I(x)Y + X - x = 0$$

where $x = -\rho \in (-\infty, 0]$. Taking the derivative with respect to $x$, we get the system of equations for $(X, Y)$

$$\frac{x}{\tau} I(x)Y + X - x = 0$$

$$\frac{1}{\tau}(I(x) + xI'(x))Y - 1 = 0$$

which can be solved to yield the desired parameterization. □

**Last Dual Path**

In the case that $\lambda'_n$ is of size proportional to $n$, then this last dual path will be the boundary of a frozen region. In terms of the original partition, $\lambda'_n$ being macroscopically large means that the first $\lambda'_n$ parts of $\lambda$ are equal to $\lambda_1$. Here, for simplicity, we assume $\lambda_1 = n$, so that $\alpha(0) = \lim_{n \to \infty} 1 + \frac{\lambda_1}{n} - \frac{1}{n} = 2$.

We can repeat the above process varying the starting point of the last dual path instead of the first. We extend $\lambda$ to $(\lambda_1, \ldots, \lambda_n, 0, \ldots, 0)$. Call the partition function $Z$. Next we decrease $\lambda'_n$ by $r < \lambda'_n$. This varies the starting point of the $n^{th}$ dual path to the right by $r$. Call the partition function $Z_r$. In terms of the original partition, this means taking $\lambda_i$ to $\lambda_i - 1$ for each $i = \lambda'_n, \ldots, \lambda'_n - r + 1$. Call this new partition $\mu$. From the product formula (4.4.4) we have

$$\frac{Z_r}{Z} = t^{|\mu| - |\lambda|} \prod_{1 \le i < j \le n+m} \frac{\mu_i - \mu_j + j - i}{\lambda_i - \lambda_j + j - i}$$

(4.4.21)

The product can be simplified giving

$$\frac{Z_r}{Z} = t^{-r} \binom{\lambda'_n}{r} \prod_{\lambda'_n + 1 \leq j \leq n+m} \frac{(\lambda_{\lambda'_n} - 1) - \lambda_j + j - \lambda'_n}{\lambda_{\lambda'_n - r + 1} - \lambda_j + j - (\lambda'_n - r + 1)}.$$

Now extend the first path to start at $(2n - 1 - \lambda'_n - q, -s - \frac{1}{(2n - \lambda'_n - q)^2})$, with $q \in (-\lambda'_n, \infty)$. See Figure 4.18 for a diagram. Call the resulting partition function $Z_{qs}$. This can be written

$$\frac{Z_{qs}}{Z} = \sum_{r = \max(0,q)}^{\lambda'_n} \frac{Z_r}{Z} s^{q+r} \binom{m + 2n - 1 - \lambda'_n + r}{m + 2n - 1 - \lambda'_n - q}$$

$$= \sum_{r = \max(q,0)}^{\lambda'_n} t^{-r} s^{q+r} \binom{\lambda'_n}{r} \prod_{\lambda'_n + 1 \leq j \leq n+m} \frac{a_{\lambda'_n} - a_j - 1}{a_{\lambda'_n - r + 1} - a_j} \binom{m + 2n - 1 - \lambda'_n + r}{m + 2n - 1 - \lambda'_n - q} \quad (4.4.22)$$
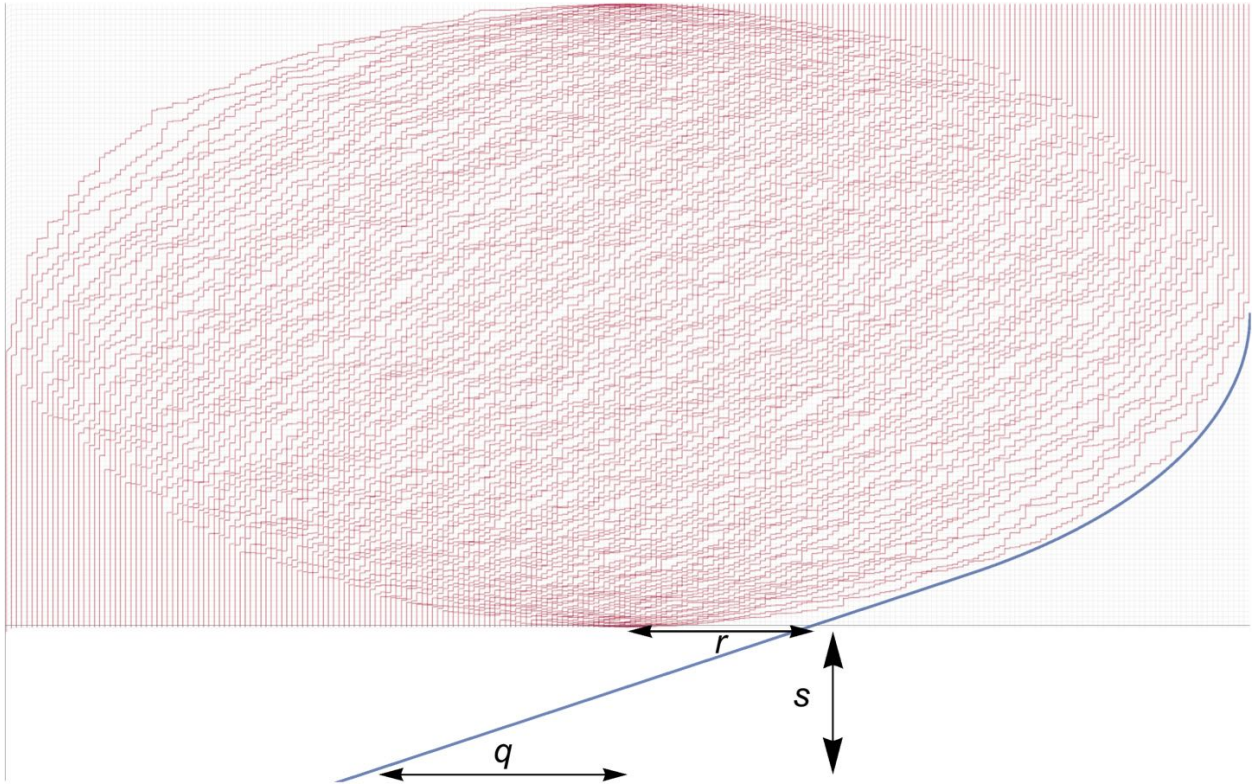


Figure 4.18: A configuration of dual paths corresponding to a BLHT of shape $\lambda = (n, \ldots, n)$. The blue curve represents the trajectory of the extended last dual path, which starts at $(2n - \lambda'_n + q - 1, -s - \frac{1}{(2n - \lambda'_n - q)^2})$ and passes through $(2n - \lambda'_n + r - 1, 0)$.

**Lemma 4.4.10.** *Consider the limit $n \to \infty$, for parameters scaling as $t = n\tau$, $s = n\sigma$, $r = n\rho$, $q = nz$, $m = nM$, $\lambda'_n = n\Lambda$, and $a_i = \lfloor n\alpha(\frac{i}{n}) \rfloor$. In this limit, the last dual path passes through the point $(\alpha(\Lambda) + \rho, 0)$ where $\rho$ is related to $z$ by*

$$z = \frac{\sigma}{\tau}(\alpha(\Lambda) + \rho)e^{-\int_0^1 du \, \frac{1}{\alpha(\Lambda)+\rho-\alpha(u)}} + \rho \qquad (4.4.23)$$

*Proof.* Taking the limit $n \to \infty$, the sum (4.4.22) is dominated at the maximum of

$$S(\rho) = -\rho \, \ln(\tau) + (z + \rho) \ln(\sigma) + (M + 2 - \Lambda + \rho) \ln(M + 2 - \Lambda + \rho) - (z + \rho) \ln(z + \rho)$$
$$- (\Lambda - \rho) \ln(\Lambda - \rho) - \rho \, \ln(\rho) + \int_\Lambda^{1+M} du \, \ln\left(\frac{\alpha(\Lambda) - \alpha(u)}{\alpha(\Lambda - \rho) - \alpha(u)}\right)$$

$$(4.4.24)$$

where we have neglected the terms not depending on $\rho$ as they do not effect the location of the critical point.

We note that $\alpha(u) = 2 - u$ when $u \in [0, \Lambda]$ and $\alpha(u) = 1 - u$ for $u \in [1, M]$. It follows that $\alpha(\Lambda) = 2 - \Lambda$ and $\alpha(\Lambda - \rho) = \alpha(\Lambda) + \rho$ for $\rho \geq 0$. Using these observations we can simplify (4.4.24). The portion of the integral in equation (4.4.24) over $u \in [1, 1 + M]$ can be expressed as

$$\int_1^{1+M} du \, \ln\left(\frac{\alpha(\Lambda) - \alpha(u)}{\alpha(\Lambda - \rho) - \alpha(u)}\right) = \int_1^{1+M} du \, \ln\left(\frac{1 + u - \Lambda}{1 + u - \Lambda + \rho}\right)$$
$$= (2 - \Lambda + M)\ln(2 - \Lambda + M) + (2 - \Lambda + \rho)\ln(2 - \Lambda + \rho) - (M + 2 - \Lambda + \rho)\ln(M + 2 - \Lambda + \rho) - (2 - \Lambda)\ln(2 - \Lambda).$$

With this equation (4.4.24) becomes

$$S(\rho) = -\rho \, \ln(\tau) + (z + \rho) \ln(\sigma) + (2 - \Lambda + \rho) \ln(M + 2 - \Lambda + \rho) - (z + \rho) \ln(z + \rho)$$
$$- (\Lambda - \rho) \ln(\Lambda - \rho) - \rho \, \ln(\rho) + \int_\Lambda^1 du \, \ln\left(\frac{\alpha(\Lambda) - \alpha(u)}{\alpha(\Lambda - \rho) - \alpha(u)}\right)$$

$$(4.4.25)$$

where we have again dropped terms not depending on $\rho$. Note we are left with only the integral over $u \in [\Lambda, 1]$. The critical point of (4.4.25) is given by

$$\frac{\sigma}{\tau} \frac{\alpha(\Lambda) + \rho}{z + \rho} \frac{\Lambda - \rho}{\rho} e^{-\int_\Lambda^1 du \, \frac{1}{\alpha(\Lambda)+\rho-\alpha(u)}} = 1.$$

Rearranging this gives

$$z = \frac{\sigma}{\tau}(\alpha(\Lambda) + \rho)\frac{\Lambda - \rho}{\rho} e^{-\int_\Lambda^1 du \, \frac{1}{\alpha(\Lambda)+\rho-\alpha(u)}} + \rho.$$

Finally we note that

$$e^{-\int_0^\Lambda du \, \frac{1}{\alpha(\Lambda)+\rho-\alpha(u)}} = e^{-\int_0^\Lambda du \, \frac{1}{u-\Lambda+\rho}} = e^{\ln\left(\frac{\rho-\Lambda}{\rho}\right)}.$$

Recall that $\rho < \Lambda$. Choosing the branch of the logarithm along the positive real axis we are left with

$$e^{-\int_0^\Lambda du \, \frac{1}{\alpha(\Lambda)+\rho-\alpha(u)}} = -\frac{\Lambda - \rho}{\rho}.$$

All together we have

$$z = -\frac{\sigma}{\tau}(\alpha(\Lambda) + \rho)e^{-\int_0^1 du \, \frac{1}{\alpha(\Lambda)+\rho-\alpha(u)}} + \rho$$

as desired. $\qquad\square$

**Theorem 4.4.11.** *Assuming the tangent method holds, the portion of the Arctic curve following the last dual path is parameterized by*

$$
\begin{aligned}
X(x) &= \frac{x^2 I'(x)}{I(x) + xI'(x)} \\
Y(x) &= \tau \frac{1}{I(x) + xI'(x)}
\end{aligned}
\tag{4.4.26}
$$

*with $x \in [\alpha(\Lambda), 2]$.*

*Proof.* In the large $n$ limit, the last dual path passes through $(\alpha(\Lambda)-z, -\sigma)$ and $(\alpha(\Lambda)+\rho, 0)$. This defines the line

$$Y = \frac{\sigma}{z + \rho}(X - \alpha(\Lambda) - \rho).$$

Using equation (4.4.23) and letting $x = \alpha(\Lambda) + \rho$, the above simplifies to

$$\frac{x}{\tau}I(x)Y + X - x = 0.$$

As $\rho \in [0, \Lambda]$ we see $x \in [\alpha(\Lambda), 2]$. Taking the derivative with respect to $x$, we get the system of equations

$$
\begin{aligned}
&\frac{x}{\tau}I(x)Y + X - x = 0 \\
&\frac{1}{\tau}(I(x) + xI'(x))Y - 1 = 0
\end{aligned}
$$

which can be solved to yield the desired parameterization. $\qquad\square$

## Examples

$\lambda = (n, \ldots, n)$

As an example of computing the outer boundary Arctic curve consider the case of $\lambda = (n, \ldots, n)$, where $\lambda$ has $n$ parts. In this case, $\alpha(u) = 2 - u$, $u \in [0, 1]$. We have

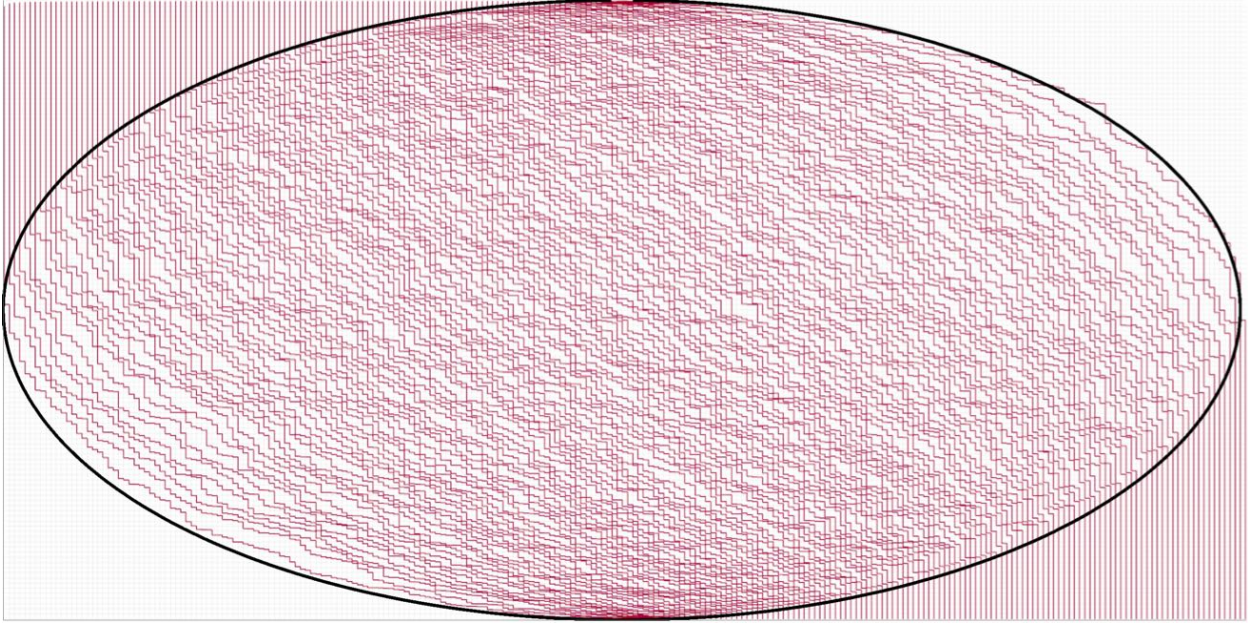$$I(x) = e^{-\int_0^1 du \, \frac{1}{x-2+u}} = \frac{x - 2}{x - 1}$$

Figure 4.19: A uniformly sampled configuration of paths corresponding to a BLHT of shape $\lambda = (n, \ldots, n)$, with $n = t = 120$. In black is the computed Arctic curve.

and

$$I'(x) = \frac{1}{(x-1)^2}.$$

Plugging this into our parameterization (equation (4.1.1)) we have

$$\begin{aligned} X(x) &= \frac{x^2}{x^2 - 2x + 2} \\ Y(x) &= \frac{\tau(x-1)^2}{x^2 - 2x + 2} \end{aligned} \tag{4.4.27}$$

for $x \in \mathbb{R}$. Eliminating the parameter we get a formula for the Arctic curve

$$(X-1)^2 + \left(\frac{2Y - \tau}{\tau}\right)^2 = 1.$$

See Figures 4.19 and 4.20 for $\tau = 1$ and $\tau = 4$ respectively.

$\lambda = (n, n-1, \ldots, 1)$

As a second example consider $\lambda = (n, n-1, \ldots, 1)$. Here $\alpha(u) = 2 - 2u$, $u \in [0, 1]$. We have

$$I(x) = e^{-\int_0^1 du \frac{1}{x-2+2u}} = \sqrt{\frac{x-2}{x}}$$

Figure 4.20: A uniformly sampled configuration of paths corresponding to a BLHT of shape $\lambda = (n, \ldots, n)$, with $n = 120$ and $t = 480$. In black is the computed Arctic curve.

and

$$I'(x) = \frac{1}{x^2}\sqrt{\frac{x}{x-2}}.$$

This results in the parameterization

$$X(x) = \frac{x}{x-1}$$
$$Y(x) = \frac{\tau\sqrt{x(x-2)}}{|x-1|}$$

(4.4.28)

for $x \in (-\infty, 0] \cup [2, \infty)$. This results in the Arctic curve

$$(X-1)^2 + \left(\frac{Y}{\tau}\right)^2 = 1, \qquad Y \geq 0.$$

See Figure 4.21.

$\lambda = ((p-1)n, \ldots, (p-1)n)$

As a generalization of the first example above, we consider $\lambda$ of the form $\lambda = ((p-1)n, \ldots, (p-1)n)$ where $p \in \mathbb{N}$, $p > 1$, is fixed. The limiting profile is $\alpha(u) = p - u$.
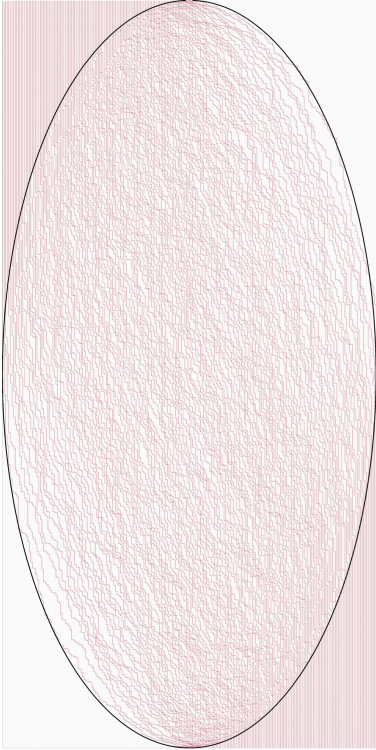
Figure 4.21: A uniformly sampled configuration of paths corresponding to a BLHT of shape $\lambda = (n, n-1, \ldots, 1)$, with $n = t = 120$. In black is the computed Arctic curve.

We see that

$$I(x) = e^{-\int_0^1 du \frac{1}{x-p+u}} = \frac{x-p}{x-p+1}$$

and

$$I'(x) = \frac{1}{(x-p+1)^2}$$

with $x \in \mathbb{R}$. This gives the parameterization

$$
\begin{aligned}
X(x) &= \frac{x^2}{x^2 - 2(p-1)x + p(p-1)} \\
Y(x) &= \tau \frac{(x+p-1)^2}{x^2 - 2(p-1)x + p(p-1)}
\end{aligned}
\tag{4.4.29}
$$

which gives the Arctic curve

$$(X - p + 1)^2 + \left(\frac{p}{\tau}Y - p + 1\right)^2 + \frac{2p-4}{\tau}XY = p^2 - 2p + 1.$$

See Figure 4.22.

$\lambda = ((p-1)n, (p-1)(n-1), \ldots, p-1)$

As a generalization of the second example above, we consider $\lambda$ of the form $\lambda = ((p-1)n, (p-1)(n-1), \ldots, p-1)$ where $p \in \mathbb{N}$, $p > 1$, is fixed. In this case, the limiting profile
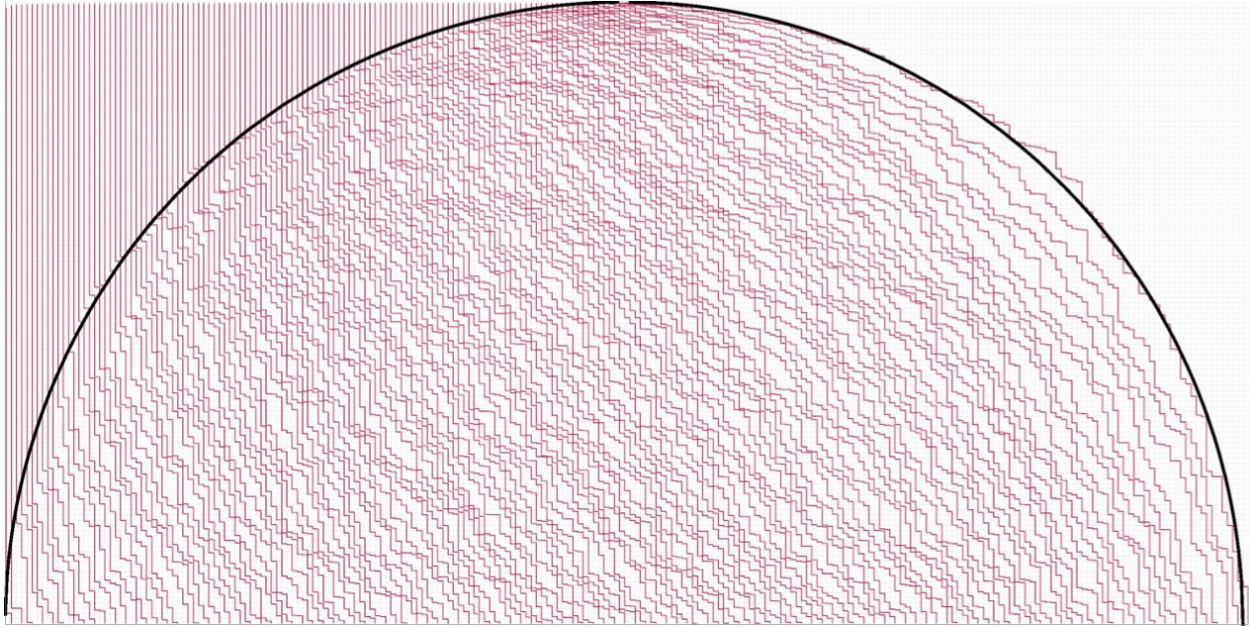
Figure 4.22: A uniformly sampled configuration of paths corresponding to a BLHT of shape $\lambda = ((p-1)n, \ldots, (p-1)n)$, with $p = 4$, $n = 60$, $t = 120$. In black is the computed Arctic curve.

is $\alpha(u) = p(1 - u)$. Computing the parameterization we have

$$I(x) = e^{-\int_0^1 du \frac{1}{x-p+pu}} = \left(\frac{x-p}{x}\right)^{\frac{1}{p}}$$

with $x \in (-\infty, 0] \cup [p, \infty)$. This gives

$$X(x) = \frac{x}{x-p+1}$$

$$Y(x) = \tau \frac{x-p}{x-p+1} \left(\frac{x}{x-p}\right)^{\frac{1}{p}}. \tag{4.4.30}$$

Eliminating the parameter leaves us with the Arctic curve

$$Y = \tau \frac{X-p}{1-p} \left(\frac{(p-1)X}{X-p}\right)^{\frac{1}{p}}$$

or

$$\left((1-p)\frac{Y}{\tau}\right)^{p-1} = X(X-p)^{p-1}.$$

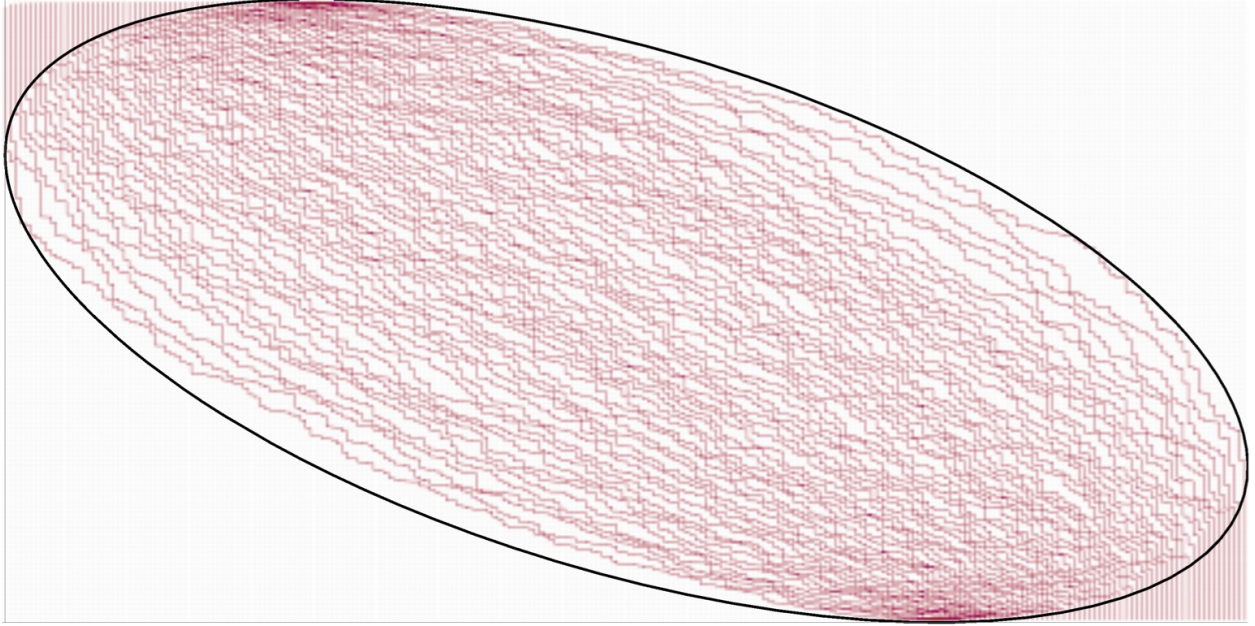Note that this example can provide algebraic curves of degree higher than 2. See Figure .
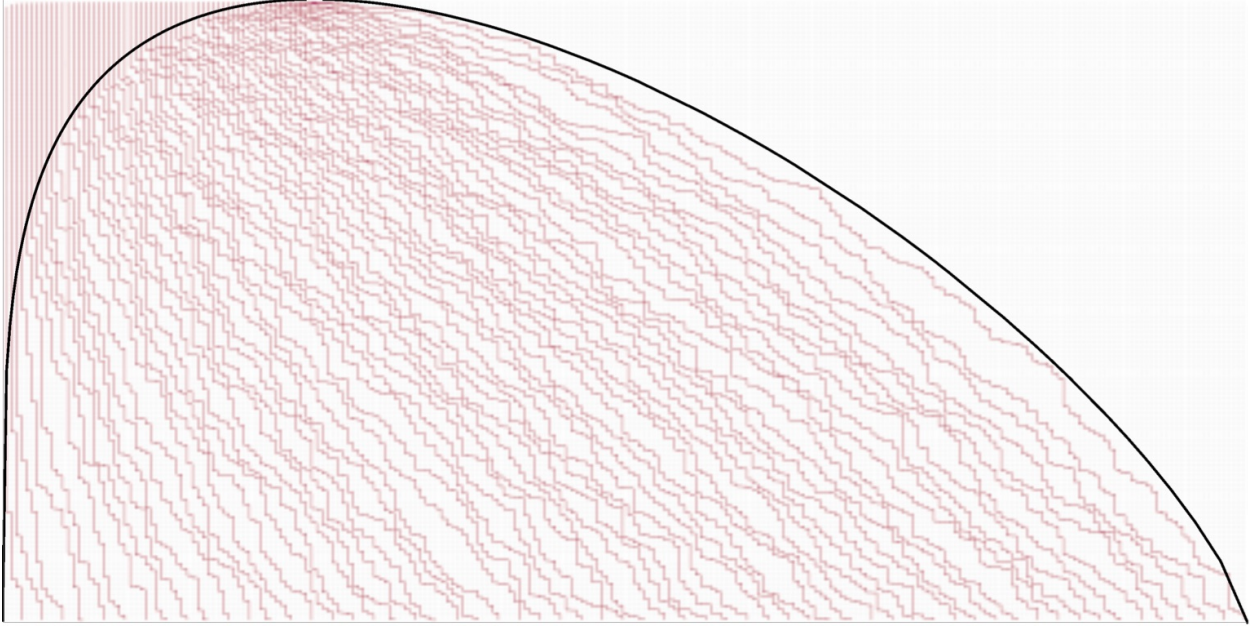
Figure 4.23: A uniformly sampled configuration of paths corresponding to a BLHT of shape $\lambda = ((p-1)n, (p-1)(n-1), \ldots, p-1)$, with $p = 4$, $n = 60$, $t = 120$. In black is the computed Arctic curve.

## Freezing Boundaries

Besides the outer boundary, other portions of the Arctic curve can exist at the so called "freezing boundaries". These occur when the choice of partition freezes a section of paths near the bottom boundary of the domain. When this occurs there will be a new portion of Arctic curve separating this frozen region from the disordered region in the bulk. For example, taking $\lambda = (2n, \ldots, 2n, n, n-1, \ldots, 1)$ where $\lambda$ has $2n$ parts with $n$ having value $2n$, we see a frozen region of no paths resulting in an Arctic curve taking the form of a cusp. See Figure 4.24. In general, these frozen regions will come from a macroscopic jump in either the description of the partition $\lambda$, or of the conjugate partition $\lambda'$. That is, either $\lambda_k - \lambda_{k+1}$ or $\lambda'_k - \lambda'_{k+1}$ are linear in $n$, for some row or column of $\lambda$. The following analysis is very similar to that of [29].

*Remark* 4.4.12. In the analogous problem on the square grid, there are three possible types of frozen region: empty (no paths), horizontal paths, and vertical paths. The parameterization of these freezing boundaries was worked out in [29]. In our case, the lecture hall tableaux do not appear to develop frozen regions of horizontal paths.

### Boundary of an empty region

Consider a BLHT of shape $\lambda$ such that $\lambda$ induces a frozen region of no paths along the bottom boundary of the domain. This means, for some $k$, we must have that $\lambda_{k-1} - \lambda_k$ is
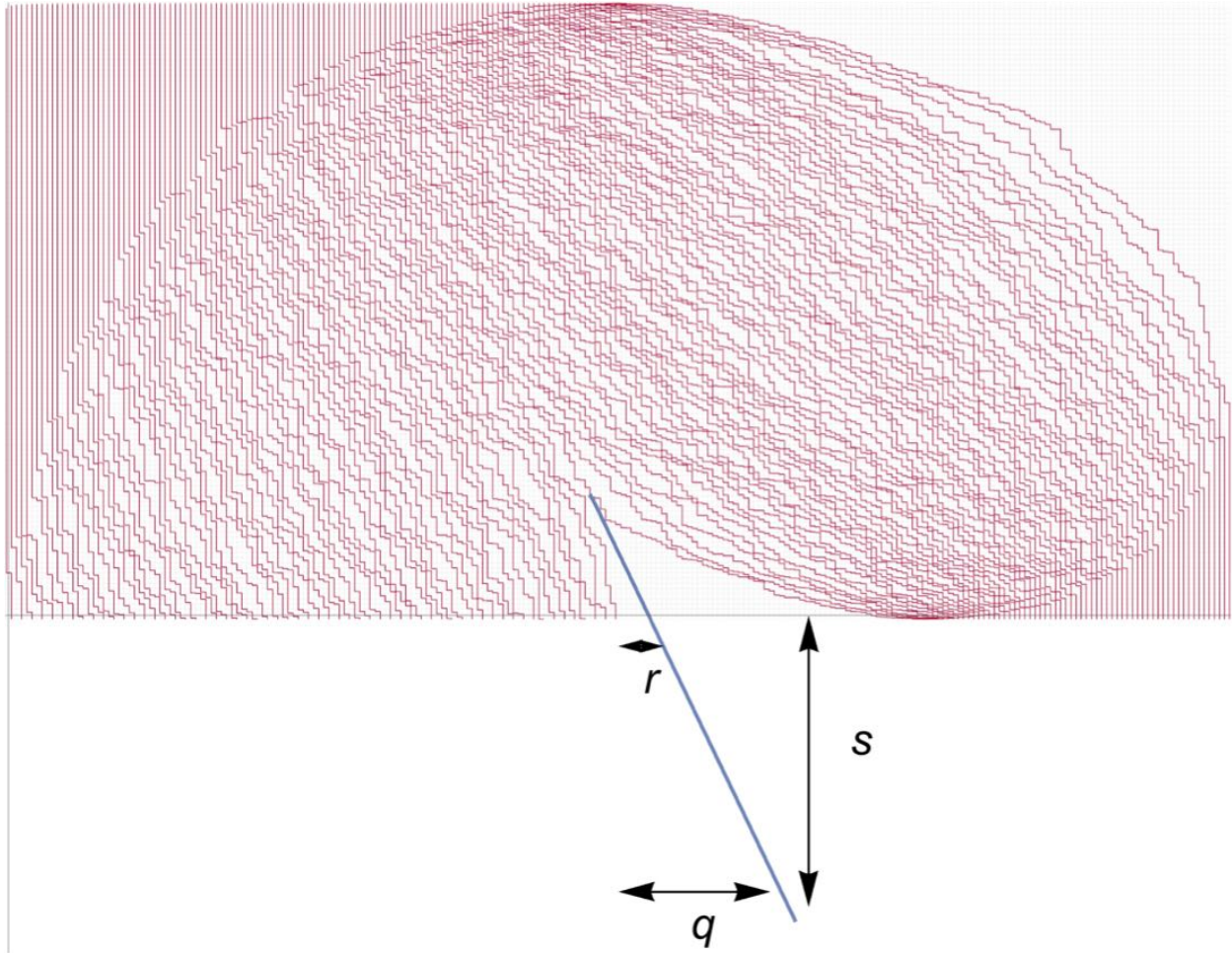
Figure 4.24: A configuration of paths corresponding to a BLHT of shape $\lambda = (2n, \ldots, 2n, n, \ldots, 1)$. The blue curve represents the trajectory of the extended $k^{th}$ path, which ends at $(n + \lambda_k - k + q, -s)$ and passes through $(n + \lambda_k - k + r, 0)$.

linear in $n$. In terms of the paths this means that the endpoints of the $(k-1)^{st}$ and $k^{th}$ path satisfy $a_{k-1} - a_k$ being linear in $n$. As the region is empty in the thermodynamic limit, the left-most portion of the Arctic curve will follow the path ending at $(n + \lambda_k - k, 0)$. By varying the endpoint of this path we will be able to parameterize the Arctic curve bounding this frozen region. See Figure 4.24 for a diagram.

To implement the tangent method, we follow the same procedure as for the outer boundary. Let the total number of configurations be $Z$. Define $\Delta$ through $a_{k-1} - a_k \sim n\Delta$. It is the asymptotic size of the jump between the endpoints of the $(k-1)^{st}$ and $k^{th}$ path. Suppose we move the ending point of the $k^{th}$ path to $(n + \lambda_k - k + r, 0)$ where $r \in [0, n\Delta)$. Call the

new partition function $Z_r$. The ratio of partition functions is

$$\frac{Z_r}{Z} = t^r \prod_{1 \leq i \leq k-1} \frac{\lambda_i - \lambda_k - r + k - i}{\lambda_i - \lambda_k + k - i} \prod_{k+1 \leq j \leq n} \frac{\lambda_k + r - \lambda_j + j - k}{\lambda_k - \lambda_j + j - k}$$

$$= t^r \prod_{1 \leq j \leq n, j \neq k} \frac{\lambda_k + r - \lambda_j + j - k}{\lambda_k - \lambda_j + j - k}. \tag{4.4.31}$$

Now suppose the $k^{th}$ path is extended to end at $(n + \lambda_k - k + q, -s)$ with $q \in [0, \infty)$. Call the partition function $Z_{qs}$. As before, we can write $Z_{qs}$ as

$$\frac{Z_{qs}}{Z} = \sum_{r=0}^{\min(q, n\Delta)} \frac{Z_r}{Z} s^{q-r} \binom{n + \lambda_k - k + q}{q - r}$$

$$= \sum_{r=0}^{\min(q, n\Delta)} t^r s^{q-r} \prod_{1 \leq j \leq n, j \neq k} \frac{a_k - a_j + r}{a_k - a_j} \binom{a_k + q}{q - r}. \tag{4.4.32}$$

**Lemma 4.4.13.** *Consider the limit $n \to \infty$, for parameters scaling as $t = n\tau$, $s = n\sigma$, $r = n\rho$, $q = nz$, $a_i = \lfloor n\alpha(\frac{i}{n}) \rfloor$, $a_{k-1} - a_k = n\Delta$, and $\frac{k}{n} = v$ . In this limit, the $k^{th}$ path passes though the point $(\alpha(v) + \rho, 0)$, with $\rho$ related to $z$ by*

$$z = (\alpha(v) + \rho) \frac{\sigma}{\tau} e^{-\int_0^1 du \frac{1}{\alpha(v) + \rho - \alpha(u)}} + \rho. \tag{4.4.33}$$

*Proof.* In the $n \to \infty$ limit, equation (4.4.32) takes the form

$$\frac{Z_{qs}}{Z} \sim \sqrt{\frac{n}{2\pi}} e^{n z \ln(n)} \int_0^\Delta d\rho \sqrt{\frac{\alpha(v) + z}{(\alpha(v) + \rho)(z - \rho)}} e^{n S(\rho)} \tag{4.4.34}$$

where

$$S(\rho) = \rho \ln(\tau) - (z - \rho) \ln(\sigma) - (\alpha(v) + \rho) \ln(\alpha(v) + \rho) - (z - \rho) \ln(z - \rho)$$

$$+ \int_0^1 du \ln\left(\frac{\alpha(v) + \rho - \alpha(u)}{\alpha(v) - \alpha(u)}\right).$$

The critical point occurs when

$$\frac{\tau}{\sigma} \frac{z - \rho}{\alpha(v) + \rho} e^{\int_0^1 du \frac{1}{\alpha(v) + \rho - \alpha(u)}} = 1.$$

Rearranging we arrive at equation (4.4.33). $\qquad\qquad\qquad\qquad\qquad\qquad\qquad\qquad\square$

Using Lemma 4.4.13, we get a parameterization of the desired portion of the Arctic curve.

**Theorem 4.4.14.** *Assuming the tangent method holds, the portion of the Arctic curve bounding such a frozen region is parameterized by*

$$X(x) = \frac{x^2 I'(x)}{I(x) + x I'(x)}$$

$$Y(x) = \tau \frac{1}{I(x) + x I'(x)}$$

(4.4.35)

*with $x \in [\alpha(v), \alpha(v) + \Delta]$.*

*Proof.* From the points $(\alpha(v) + z, -\sigma)$, $(\alpha(v) + \rho, 0)$, and Lemma 4.4.13 we have a family lines

$$\frac{x}{\tau} I(x) Y + X - x = 0$$

with $x = \alpha(v) + \rho$. Taking the derivative with respect to $x$, we get the system of equations

$$\frac{x}{\tau} I(x) Y + X - x = 0$$

$$\frac{1}{\tau}(I(x) + x I'(x)) Y - 1 = 0$$

which can be solved to yield the desired parameterization. Note that since $\rho \in [0, \Delta)$, the range of $x$ is $[\alpha(v), \alpha(v) + \Delta]$. $\qquad\square$

### Boundary of a vertically frozen region

Now suppose we have a frozen region of vertical paths. In terms of the partition $\lambda$, there exists integers $1 \le a < b \le n$ such that $\lambda_a = \lambda_{a+1} = \ldots = \lambda_b$, and $b - a$ is proportional to $n$. In terms of the dual partition, this means there exists $k$ such that $\lambda'_k - \lambda'_{k+1}$ is proportional to $n$.

In the path description we see a frozen region of vertical paths, which in the dual paths description becomes an empty frozen region whose left boundary follows the $k^{th}$ dual path in the large $n$ limit. See Figure 4.25 for an example such a frozen region and Figure 4.26 for a diagram.

Let $\lambda$ be a partition such that $\lambda'_k - \lambda'_{k+1} \sim n\Delta$. First extend $\lambda$ to $(\lambda_1, \ldots, \lambda_n, 0, \ldots, 0)$ by adding $m$ parts of zero to the end of $\lambda$. Call $Z_r$ the partition function with the starting point of the $k^{th}$ dual path moved to the right by $r$. In terms of the original partition, moving the starting point of the $k^{th}$ dual path to the right by $r$ corresponds to changing $\lambda_i$ to $\lambda_i - 1$ for $i = b, b - 1, \ldots, b - r + 1$. Call the resulting partition $\mu$.

From the product formula we have

$$\frac{Z_r}{Z} = t^{|\mu| - |\lambda|} \prod_{1 \le i < j \le n+m} \frac{\mu_i - \mu_j + j - i}{\lambda_i - \lambda_j + j - i}$$

$$= t^{-r} \prod_{\substack{1 \le i \le b-r \\ b-r+1 \le j \le b}} \frac{\lambda_i - (\lambda_j - 1) + j - i}{\lambda_i - \lambda_j + j - i} \prod_{\substack{b-r+1 \le i \le b \\ b+1 \le j \le n+m}} \frac{(\lambda_i - 1) - \lambda_j + j - i}{\lambda_i - \lambda_j + j - i}$$

Figure 4.25: A configuration of paths with the corresponding dual paths for a BLHT of shape $\lambda = (2n, 2n - 1, \ldots, n + 1, n, \ldots, n)$.


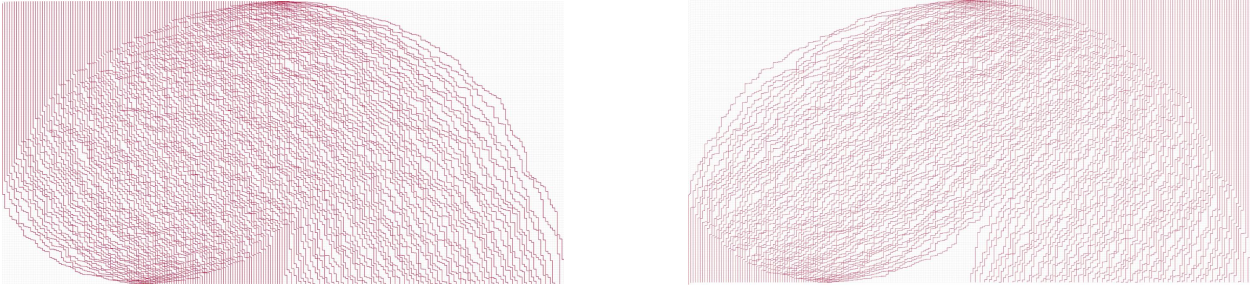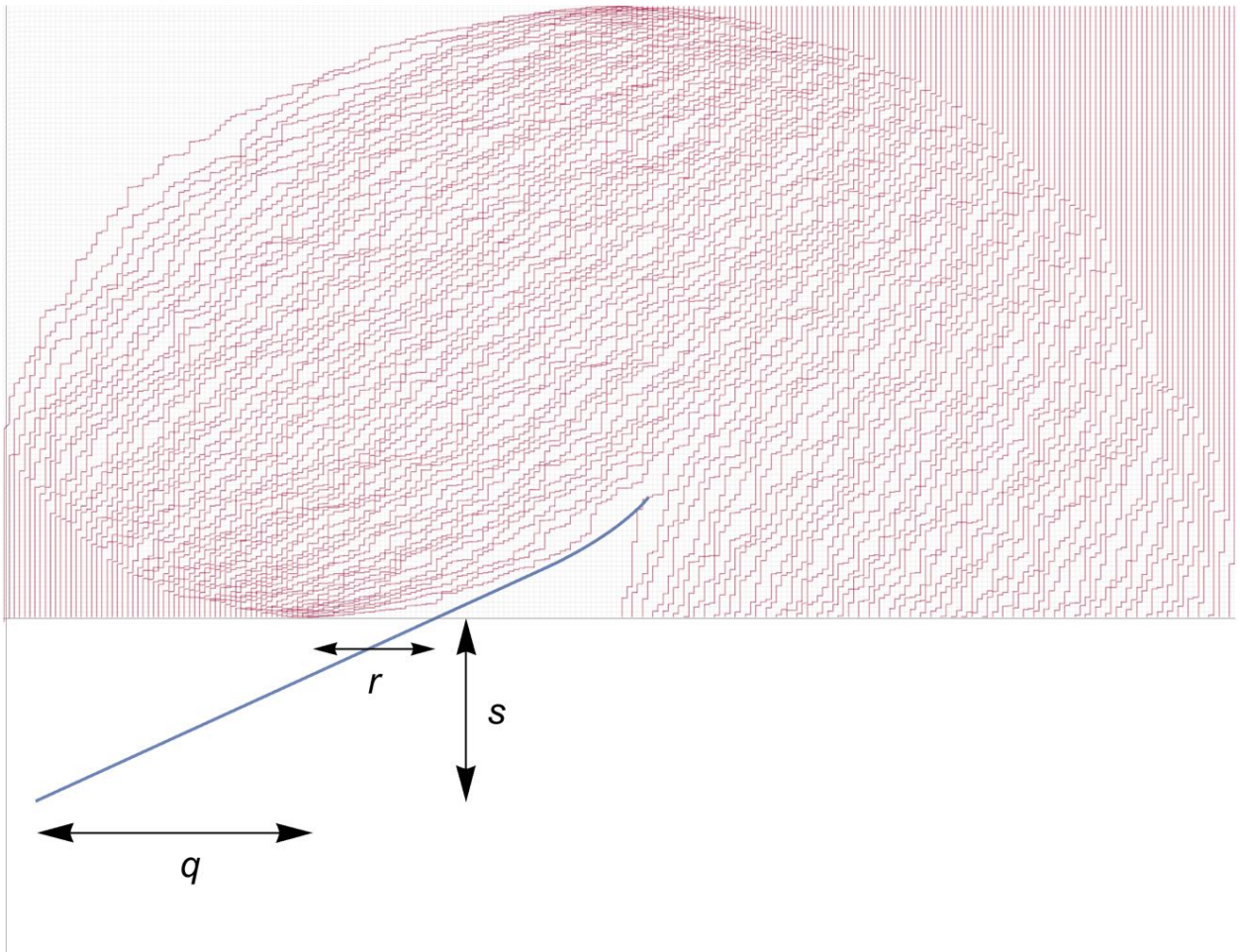
Figure 4.26: A configuration of dual paths corresponding to a BLHT of shape $\lambda = (2n, 2n - 1, \ldots, n+1, n, \ldots, n)$. The blue curve represents the trajectory of the extended $k^{th}$ dual path, which starts at $(2n - \lambda'_k + q - 1, -s - \frac{1}{(2n-\lambda'_k+q)^2})$ and passes through $(2n - \lambda'_k + r - 1, 0)$.

where the other other terms in the product are one. Both remaining terms in the product are telescoping and we have

$$\frac{Z_r}{Z} = t^{-r} \prod_{1 \le i \le b-r} \frac{\lambda_i - \lambda_b + b + 1 - i}{\lambda_i - \lambda_b + b - r + 1 - i} \prod_{b+1 \le j \le n+m} \frac{\lambda_b - \lambda_j + j - (b+1)}{\lambda_b - \lambda_j + j - (b-r+1)}.$$

We can rewrite the above as follows

$$\frac{Z_r}{Z} = t^{-r} \prod_{\substack{1 \le i \le n+m \\ i \ne b-r+1}} \frac{\lambda_i - \lambda_b + b + 1 - i}{\lambda_i - \lambda_b + b - r + 1 - i} \prod_{b-r+2 \le i \le b} \frac{\lambda_i - \lambda_b + b - r + 1 - i}{\lambda_i - \lambda_b + b + 1 - i}$$

$$= t^{-r}(-1)^{r-1} \prod_{\substack{1 \le i \le n+m \\ i \ne b-r+1}} \frac{\lambda_i - \lambda_b + b + 1 - i}{\lambda_i - \lambda_b + b - r + 1 - i}.$$

Now extend the $k^{th}$ dual path to begin at $(2n - 1 - \lambda'_k + q, -s - \frac{1}{(2n-\lambda'_k+q)^2})$, with $q \in (-\infty, \Delta]$. Call the corresponding partition function $Z_{qs}$. Note that $\lambda_b = k$ and $\lambda'_k = b$. $Z_{qs}$ can be written

$$\frac{Z_{qs}}{Z} = \sum_{r=\max(q,0)}^{\Delta} \frac{Z_r}{Z} s^{r-q} \binom{m+n-1+k-\lambda'_k+r}{m+n-1+k-\lambda'_k+q}$$

$$= \sum_{r=\max(q,0)}^{\Delta} t^{-r}(-1)^{r-1} \prod_{\substack{1 \le i \le n+m \\ i \ne b-r+1}} \frac{\lambda_i - \lambda_b + b + 1 - i}{\lambda_i - \lambda_b + b - r + 1 - i} s^{r-q} \binom{m+n-1+\lambda_b-b+r}{m+n-1+\lambda_b-b+q}$$

$$= \sum_{r=\max(q,0)}^{\Delta} t^{-r} s^{r-q}(-1)^{r-1} \prod_{\substack{1 \le i \le n+m \\ i \ne b-r+1}} \frac{a_i - a_b + 1}{a_i - a_b - r + 1} \binom{m-1+a_b+r}{m-1+a_b+q}. \tag{4.4.36}$$

**Lemma 4.4.15.** *Consider the limit $n \to \infty$, for parameters scaling as $t = n\tau$, $s = n\sigma$, $r = n\rho$, $q = nz$, $m = nM$, $\lambda'_k - \lambda'_{k+1} = n\Delta$, $b = n\beta$, and $a_i = \lfloor n\alpha(\frac{i}{n}) \rfloor$. In this limit, the $k^{th}$ dual path passes through the point $(\alpha(\beta) + \rho, 0)$, with $\rho$ related to $z$ by*

$$z = (\alpha(\beta) + \rho)\frac{\sigma}{\tau} e^{-p.v. \int_0^1 du \frac{1}{\alpha(\beta)+\rho-\alpha(u)}} + \rho. \tag{4.4.37}$$

*Proof.* Taking the limit $n \to \infty$

$$\frac{Z_{qs}}{Z} \sim \sqrt{\frac{n}{2\pi}} e^{-nz \ln(n)} \int_{\max(z,0)}^{\Delta} d\rho \sqrt{\frac{M + \alpha(\beta) + \rho}{(M + \alpha(\beta) + z)(\rho - z)}} e^{n S(\rho)}$$

where

$$S(\rho) = (\rho - z) \ln(\sigma) - \rho \ln(\tau) + (M + \alpha(\beta) + \rho) \ln(M + \alpha(\beta) + \rho) - (M + \alpha(\beta) + z) \ln(M + \alpha(\beta) + z)$$

$$-(\rho - z) \ln(\rho - z) + i\rho\pi + \int_0^{\beta-\rho-\epsilon} du \ln\left(\frac{\alpha(u)-\alpha(\beta)}{\alpha(u)-\alpha(\beta)-\rho}\right) + \int_{\beta-\rho+\epsilon}^{1+M} du \ln\left(\frac{\alpha(u)-\alpha(\beta)}{\alpha(u)-\alpha(\beta)-\rho}\right)$$

with $\epsilon = \frac{1}{n}$ tending to 0.

The sole critical point of $S$ occurs when

$$-\frac{\sigma}{\tau}\frac{M + \alpha(\beta) + \rho}{\rho - z}e^{\int_0^{\beta-\rho-\epsilon}\frac{1}{\alpha(u)-\alpha(\beta)-\rho}du + \int_{\beta-\rho+\epsilon}^{1+M}\frac{1}{\alpha(u)-\alpha(\beta)-\rho}du} = 1.$$

This can be simplified to

$$z = (\alpha(\beta) + \rho)\frac{\sigma}{\tau}e^{-p.v.\int_0^1 du\frac{1}{\alpha(\beta)+\rho-\alpha(u)}} + \rho$$

where we use that

$$e^{\int_1^{1+M}\frac{1}{\alpha(u)-\alpha(\beta)-\rho}du} = e^{\int_1^{1+M}\frac{1}{1-u-\alpha(\beta)-\rho}du} = \frac{\alpha(\beta) + \rho}{M + \alpha(\beta) + \rho}.$$

$\square$

**Theorem 4.4.16.** *Assuming the tangent method holds, the portion of the Arctic curve bounding such a frozen region is parameterized by*

$$\begin{aligned}
X(x) &= \frac{x^2 I'(x)}{I(x) + xI'(x)} \\
Y(x) &= \frac{\tau}{I(x) + xI'(x)}
\end{aligned} \tag{4.4.38}$$

*where $I(x) = e^{-p.v.\int_0^1 du\frac{1}{x-\alpha(u)}}$ and $x \in [\alpha(\beta), \alpha(\beta) + \Delta]$. Recall $\lambda_k' = b \sim n\beta$ and $\lambda_k' - \lambda_{k+1}' \sim n\Delta$.*

*Proof.* From the points $(\alpha(\beta) + z, -\sigma)$, $(\alpha(\beta) + \rho, 0)$, and Lemma 4.4.15 we have a family of lines

$$\frac{x}{\tau}I(x)Y + X - x = 0$$

with $x = \alpha(\beta) + \rho$. Taking the derivative with respect to $x$, we get the system of equations

$$\begin{aligned}
&\frac{x}{\tau}I(x)Y + X - x = 0 \\
&\frac{1}{\tau}(I(x) + xI'(x))Y - 1 = 0
\end{aligned}$$

which can be solved to yield the desired parameterization. Note that since $\rho \in [0, \Delta]$, the range of $x = \alpha(\beta) + \rho$ is $[\alpha(\beta), \alpha(\beta) + \Delta]$. $\square$

## Examples

$\lambda = (2n, \ldots, 2n, n, \ldots, 1)$

As an example of a BLHT whose Arctic curve contains a freezing boundary, consider the partition $\lambda = (2n, \ldots, 2n, n, \ldots, 1)$. The limiting profile is

$$\alpha(u) = \begin{cases} 4 - 2u & 1 < u \leq 2 \\ 4 - u & 0 \leq u \leq 1 \end{cases}.$$

From this we have

$$I(x) = \frac{x-4}{x-3}\sqrt{\frac{x-2}{x}}$$

and

$$I'(x) = \frac{2x^2 - 9x + 12}{(x-3)^2 x^2}\sqrt{\frac{x}{x-2}}.$$

Plugging this into equation (4.1.1), we get

$$X(x) = \frac{x(2x^2 - 9x + 12)}{x^3 - 7x^2 + 17x - 12}$$

$$Y(x) = \frac{\tau\, x(x-3)^2}{x^3 - 7x^2 + 17x - 12}\sqrt{\frac{x-2}{x}}$$

with $x \in (-\infty, 0] \cup [2, \infty)$. The portion of the Arctic curve corresponding to the freezing boundary is $x \in [2, 3]$. See Figure 4.27.

$\lambda = (2n, 2n-1, \ldots, n+1, n, \ldots, n)$

In the case $\lambda = (2n, 2n-1, \ldots, n+1, n, \ldots, n)$ the limiting profile is

$$\alpha(u) = \begin{cases} 3 - u & 1 < u \leq 2 \\ 4 - 2u & 0 \leq u \leq 1 \end{cases}.$$

We have

$$I(x) = \frac{1}{x-1}\sqrt{(x-4)(x-2)}$$

and

$$I'(x) = \frac{2x-5}{(x-1)^2}\sqrt{\frac{1}{(x-2)(x-4)}}$$

The gives the parameterization

$$X(x) = \frac{x^2(2x-5)}{x^3 - 5x^2 + 9x - 8}$$

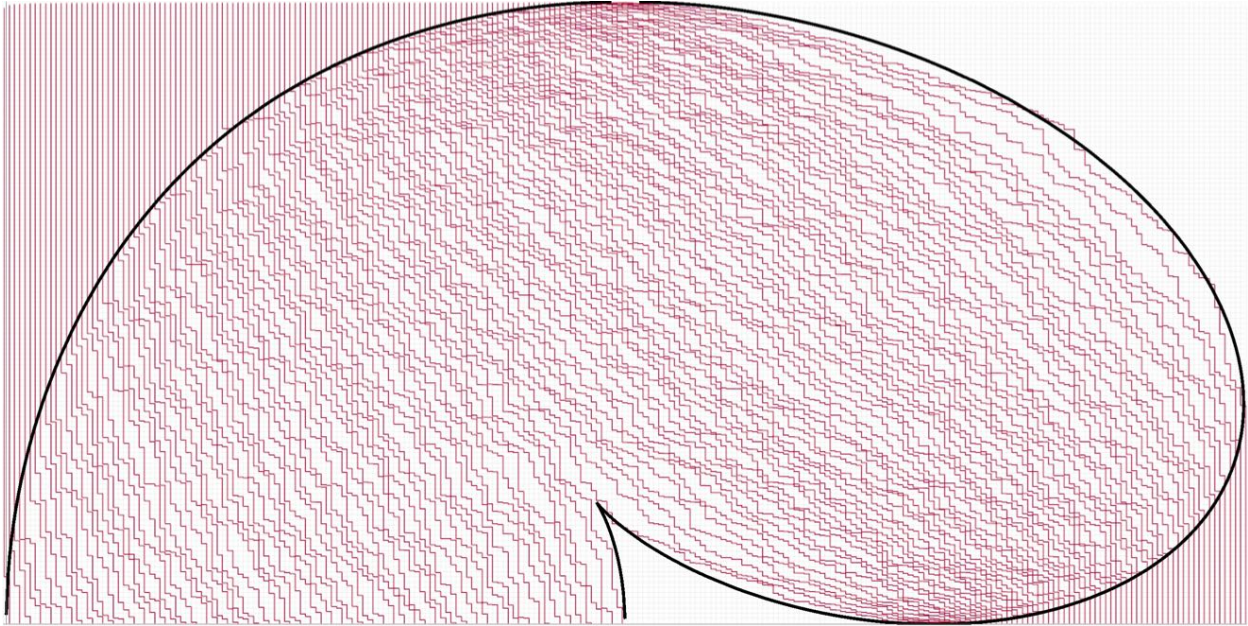$$Y(x) = \tau \frac{(x-1)^2}{x^3 - 5x^2 + 9x - 8}\sqrt{(x-4)(x-2)}$$

Figure 4.27: A uniformly sampled configuration of paths corresponding to a BLHT of shape $\lambda = (2n, \ldots, 2n, n, \ldots, 1)$, with $n = 60$ and $t = 120$. In black is the computed Arctic curve.

for $x \in (-\infty, 2] \cup [4, \infty)$. The portion of the Arctic curve corresponding to the freezing boundary is $x \in [1, 2]$. See Figure 4.28.

More complex examples can be dealt in a similar way. An example with three internal jumps, for which we do not illustrate the calculations here, is shown in Figure 4.29.

## 4.5  Conclusion

In this chapter, we compute Arctic curves for bounded lecture hall tableaux using the tangent method. This method is not fully rigorous, nevertheless we conjecture that the true Arctic curves is is in fact given by our formula, Theorem 4.4.3.

It would be interesting to study rigorously the dimer model on this lattice made of hexagons and octagons. On this lattice (or the lecture hall graph) we can define a height function $h_n(x, y)$ on the faces of the graph. Given a configuration of $n$ paths starting at $(n - i, t - 1/(n - i + 1))$ and ending at $(\lambda_i + n - i, 0)$, the height of a face is the number of paths to the southwest of the face. We give an example of the height function of Figure 4.30 for $\lambda = (2, 2)$.

When $n \to \infty$ and $\lambda_i + n - i = n\alpha(i/n)$, let $h(x, y) = \lim h_n(x, y)/n$ be the limiting height function. Based on strong numerical evidence and on the structural similarities between this dimer model and $\mathbb{Z}^2$-periodic dimer models, it seems possible that many of the results pertaining to $\mathbb{Z}^2$-periodic dimer models could be extended to the BLHT dimer model.
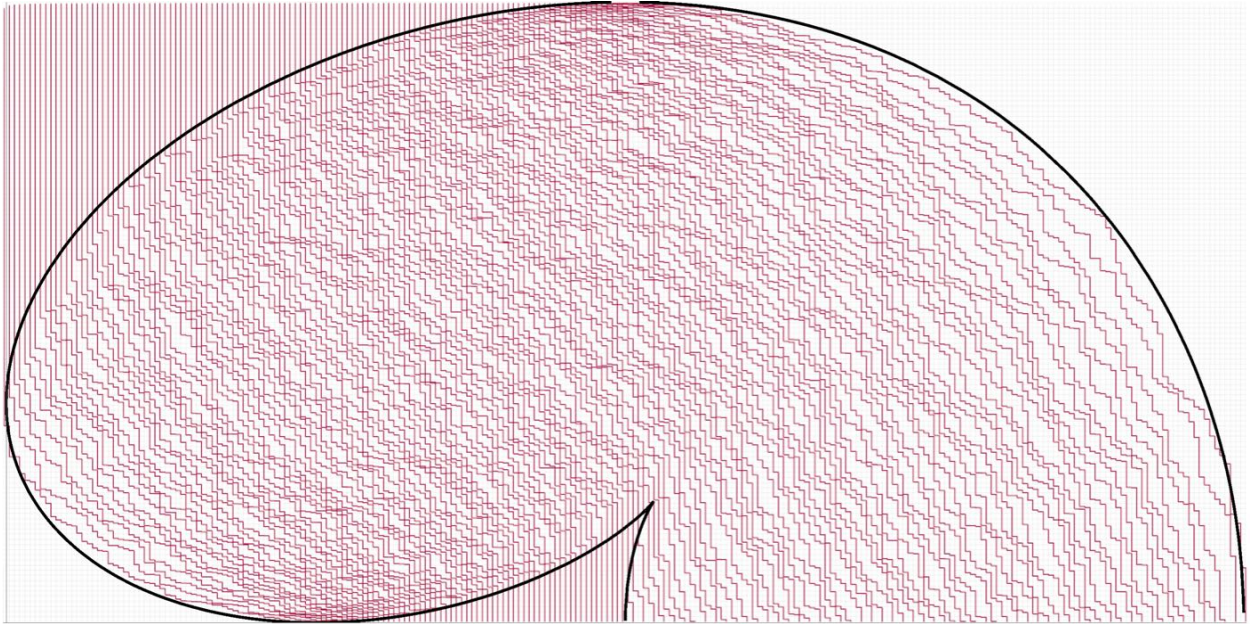
Figure 4.28: A uniformly sampled configuration of paths corresponding to a BLHT of shape $\lambda = (2n, 2n-1, \ldots, n+1, n, \ldots, n)$, with $n = 60$ and $t = 120$. In black is the computed Arctic curve.
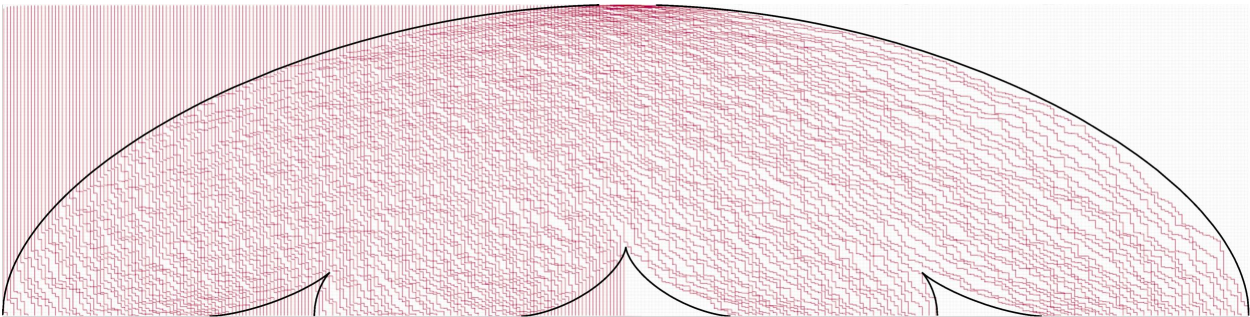


Figure 4.29: A uniformly sampled configuration of paths corresponding to a BLHT of shape $\lambda = (6n, \ldots, 5n+1, 4n, \ldots, 3n+1, 2n, \ldots, 2n, 2n, \ldots, n+1, n, \ldots, n, n, \ldots, 1)$, with $n = 30$ and $t = 60$. In black is the computed Arctic curve.

When we impose that the hexagons and the octagons have all the same area and shape, we get a non-planar lattice made of fans of hexagons separated by line of octagons. This observation is due to N. Reshetikhin. On Figure 4.31, we draw one fan of hexagons and the its line of octagons.

We could also compute the asymptotic behavior of the lecture hall tableaux without the bounded condition. In this case we have an infinite number of tableaux. When $q < 1$, we can compute the generating function of lecture hall tableaux of shape $\lambda$ where each tableau gives the contribution $q^{|T|}$ where $|T| = \sum_{i,j} T_{i,j}$. In [26], Corteel and Kim computed the
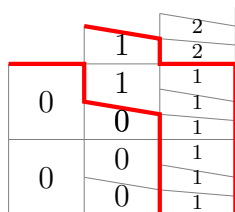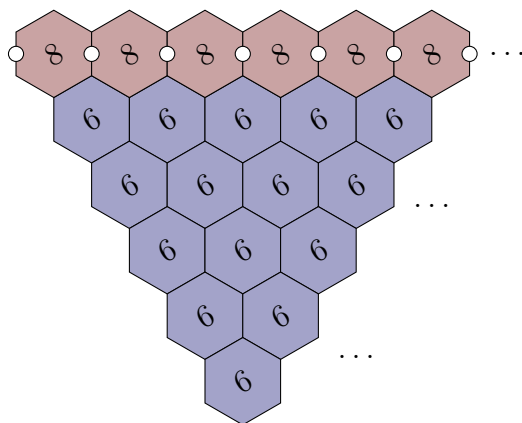
Figure 4.30: Height function for paths of $\mathcal{G}_2$



Figure 4.31: Another way of drawing a horizontal strip of the lecture hall lattice

corresponding generating function which is :

$$\prod_{1 \leq i < j \leq n} \frac{q^{\lambda_j + n - j} - q^{\lambda_i + n - i}}{q^{i-1} - q^{j-1}} \prod_{i=1}^{n} \frac{(-q^{n-i+1})_{\lambda_i}}{(q^{2n-i+1})_{\lambda_i}}.$$

with $(a)_k = \prod_{i=0}^{k-1}(1 - aq^i)$. The fact that this generating function has a beautiful product formula makes us think that we could build the right algebraic tools to study the asymptotics of these unbounded tableaux. In [31], the authors consider the case of $q$-weighted lozenge tilings for which a single path will asymptotically travel along a geodesic (not necessarily a straight line). It would be interesting to consider the same for lecture hall tableaux. It would also be very interesting to define a "lecture hall Schur process". See for example [74] for the classical case and all the follow-up papers.

Last but not least, the tangent method could be made rigorous in our case [3] at least for the computation of some parts of the curves (i.e. the ones that correspond to the trajectory of the first or the last path). This would require some detailed computations.

# Chapter 5

# Random tilings on the GPU

## 5.1 Introduction

The study of tilings of planar regions by dominos, lozenges, and other shapes has a long history in mathematics, physics, and computer science. In the recent decades, the discovery of Arctic circles, limit shapes, and other phenomena in random tilings of large regions has sparked a renewed excitement into their investigation. For a survey of these developments, see [57].

A remarkable tool in the study of tilings has been the use of various computer programs to generate and visualize random tilings. For example, in the previous chapter numerical simulations played an important role in showing that the bounded lecture hall tableaux exhibited the limit shape phenomenon, and in showing that the conjectured formulas for the Arctic curves matched with what was observed. A variety of powerful algorithms and techniques for sampling tilings have been developed and studied (see for example [69, 93, 4, 90, 81]), and their standard implementations are widely available and well-utilized by researchers in the field.

On the other hand, the recent years have seen the advent of many new tools and techniques in high performance computing. In particular is the resurgence of parallel computing, driven by the fact that as speeds of single processors reach their physical limits, computers increasingly rely on multicore processors for performance and efficiency. So, while previously the sole purview of supercomputing, parallel computing is now-a-days essential to fully exploit modern computational power.

At the cutting-edge of multicore hardware is the graphics processing unit (GPU). Designed specifically for certain computations in 3D computer graphics, GPUs employ a massively-parallel architecture with up to thousands of limited-functionality processing cores working synchronously. Thanks to the popularity of video games, powerful GPUs are now commonplace on nearly all personal computers, as well as Playstations, XBoxes, and other devices. Utilizing these computational resources for tasks beyond computer graphics is a tantalizing prospect. Indeed, GPUs have proven to be well-suited for many other types of problems,

and general purpose computing with the GPU (GPGPU) has become increasingly popular and successful in many fields. For an overview of applications of GPUs to other Monte Carlo simulations see [92].

The main purpose of this chapter is to demonstrate the use of GPUs to generate random tilings. These results are presented in [53]. Our approach is based on the Glauber dynamics Markov chains where Markov moves are local "flips" of the tiling. For parallelization, we consider non-local updates consisting of clusters of flips, which when chosen according to a domain decomposition, can be generated and executed independently and in parallel on GPU cores. We implemented the program with C++ and OpenCL, and have made our source code available [54].

The structure of the remainder of the chapter is as follows: in the first section, we recall the basics of domino tilings and Markov chain algorithms for generating random tilings. We briefly discuss generalizations to some other models. In the second section, after reviewing some important aspects of graphics hardware architecture and programming, we explain our implementation of the Markov chain algorithm on the GPU. In the conclusion, we present the results of some experiments we conducted to test the program.

## 5.2   Random Tilings

### Domino Tilings

By the *square lattice* we mean the planar graph embedded in the Euclidean plane with vertices at coordinates $(i, j) \in \mathbb{Z}^2$ and edges joining all pairs of vertices unit distance apart. A *domain* $\mathcal{D}$ is the union of a finite set of faces of the square lattice. We assume that $\mathcal{D}$ is simply-connected.

A *domino* is the union of two square lattice faces that share an edge. A *tiling* $\mathcal{T}$ of $\mathcal{D}$ is a set of dominos whose interiors are disjoint and whose union is $\mathcal{D}$. We denote by $\Omega_\mathcal{D}$ the set of tilings of $\mathcal{D}$. A domino tiling $\mathcal{T}$ can equivalently be viewed as *perfect matching* or *dimer cover* $\mathcal{T}^*$ of the dual graph, or as a lattice routing as shown in Figure 5.1.



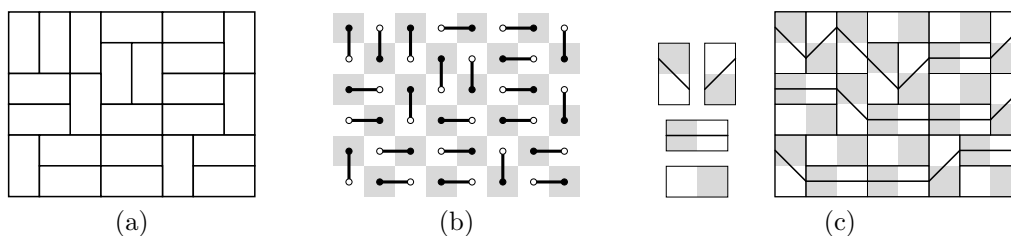(a)                                    (b)                                    (c)

Figure 5.1: (A) A domino tiling of a rectangular domain. (B) The corresponding perfect matching of the dual graph. (C) The corresponding routing, obtained by drawing paths through dominos as shown.
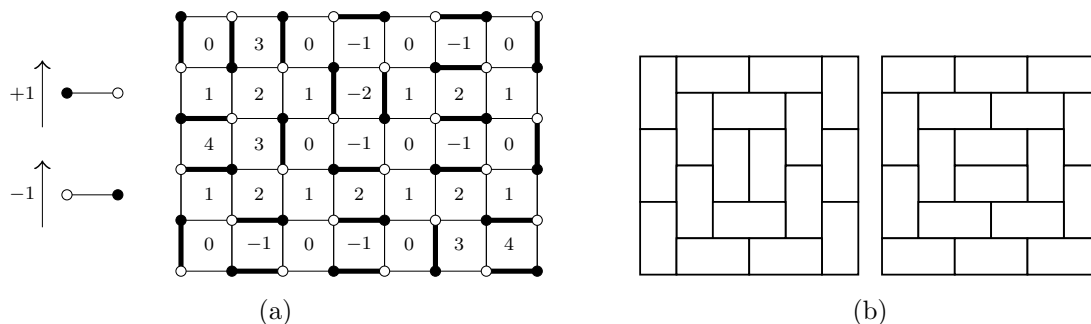
Figure 5.2: (A) The height function is defined by first fixing the height at a reference face (say the bottom-most, left-most face) to zero and then propagating the height function across unmatched edges according to the rules at left. (B) The maximal and minimal tilings of a square domain.

By identifying tilings with perfect matchings of a bipartite graph, each tiling $\mathcal{T}$ can be associated with an integer valued *height function* $h_{\mathcal{T}}$ on vertices $v \in \mathcal{D}$, according to the rules shown in Figure 5.2. Height functions induce a partial ordering on tilings, where $\mathcal{T} < \mathcal{T}'$ if $h_{\mathcal{T}}(v) < h'_{\mathcal{T}}(v)$ for all $v \in \mathcal{D}$. Moreover, the point-wise maxima (or minima) of two height-functions also defines a height function and a corresponding tiling, which endows $\Omega_{\mathcal{D}}$ with the structure of a distributive lattice. We denote by $\mathcal{T}_{max}$ and $\mathcal{T}_{min}$ the unique maximal and minimal elements of $\Omega_{\mathcal{D}}$, see Figure 5.2.

We say a domain $\mathcal{D}$ is *tileable* if $\Omega_{\mathcal{D}}$ is non-empty. An efficient algorithm due to [91] determines the tileability of a domain and returns a maximum (or minimum) tiling in time proportional to the size of the domain.

## Weights

It is often important to consider various probability measures on $\Omega_{\mathcal{D}}$. Gibbs measures originate from models of statistical physics, in which dimer covers of the lattice correspond to bond configurations in crystals.

These measures are defined by an *edge weights* that assign to each dual edge $e$ a positive number $w_e$, and to each tiling $\mathcal{T}$ a weight $W(\mathcal{T}) = \prod_{e \in \mathcal{T}^*} w_e$. A tiling $\mathcal{T}$ then has the probability

$$P[\mathcal{T}] = \frac{1}{Z} W(\mathcal{T}), \qquad Z = \sum_{\mathcal{T} \in \Omega} W(\mathcal{T}).$$

Equivalently, the Gibbs measure can be defined by *volume weights* that assign to each vertex $v$ a positive real number $q_v$, and to each tiling $\mathcal{T}$ the weight $W(\mathcal{T}) = \prod_{v \in \mathcal{D}} q_v^{h_{\mathcal{T}}(v)}$. Choosing all weights to be 1 gives the uniform distribution on $\Omega$.

## Moves on Tilings

We say a tiling $\mathcal{T}$ is *rotateable* at a vertex $v$ if the faces adjacent to $v$ are covered by two parallel dominos. An *elementary rotation* at $v$ rotates the dominos in place, as shown in Figure 5.3. More precisely, an up-rotation replaces two horizontal dominos by two vertical dominoes, and down rotation does the opposite. We denote by $R_{\pm v} : \Omega_{\mathcal{D}} \to \Omega_{\mathcal{D}}$ the function that maps a tiling $\mathcal{T}$ to the tiling obtained from $\mathcal{T}$ by rotating up/down at $v$ if possible. Here we adopt the convention of formally signing vertices to denote up and down rotations.
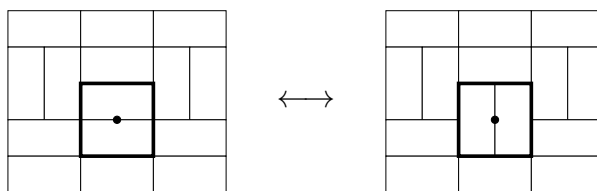


Figure 5.3: An elementary rotation at a vertex.

A theorem of [91] states that any two tilings $\mathcal{T}$ and $\mathcal{T}'$ of a domain $\mathcal{D}$ are connected by a sequence of elementary rotations.

It is natural to consider simultaneous rotations on clusters of faces. Note that if two signed vertices $v$ and $v'$ are not adjacent, then $R_v \circ R_{v'} = R_{v'} \circ R_v$. We call a subset of signed vertices $S$ an *admissible cluster* if no two of its vertices are adjacent. Then the cluster rotation $R_S = \prod_{v \in S} R_v$ is well defined. In practice, a convenient class of admissible clusters is found by fixing a vertex coloring, and choosing subsets of vertices of the same color.

## Markov Chain on Tilings

A random walk on $\Omega_D$ is defined by an initial tiling $\mathcal{T}^{(0)}$ and a sequence of randomly chosen admissible clusters $\{S_i\}_{i=1\cdots\infty}$, where the $n$th step is,

$$\mathcal{T}^{(n)} = R^{(n)}(\mathcal{T}) \qquad R^{(n)} = R_{S_n} \circ \cdots \circ R_{S_1}. \tag{5.2.1}$$

In other words, at each step, the Markov chain chooses a random cluster $S$ and moves to $R_S(\mathcal{T})$. It is straightforward to check that this Markov chain is irreducible and aperiodic, from which it follows that in the limit $n \to \infty$ the random tiling $\mathcal{T}^{(n)}$ is uniformly distributed.

In reality, the Markov chain is run for a finite but large time determined by the rate of convergence or *mixing time*. Although mixing times of Markov chains on tilings have been studied by many, see for example [69, 93, 65], and upper bounds rigorously established in many particular settings, very little is known in general. In practice, the mixing times can often be estimated empirically by heuristic techniques such as a self-consistent analysis of autocorrelation times.

**Perfect Sampling with Coupling From the Past**

When statistical soundness is paramount, exact sampling can be accomplished using the *coupling-from-the-past* algorithm [81], which effectively simulates running the Markov chain for an infinite time. It works as follows: given a sequence of random clusters $\{S_i\}_{i=1\cdots\infty}$, define the backwards walk

$$\mathcal{T}^{(n)} = R^{(n)}(\mathcal{T}) \qquad R^{(-n)} = R_{S_1} \circ R_{S_2} \circ \cdots \circ R_{S_n}$$

Almost surely there exists an $n$ for which $|R^{(-n)}(\Omega_{\mathcal{D}})| = 1$ (and in fact for all earlier times $m \geq n$). The Markov chain is then said to have *collapsed* and the unique element in the range of $R^{(-n)}$ is distributed according to the stationary distribution.

For Markov chains with large state spaces, checking for collapse can be impractical. However, in the case that the state space is partially ordered and the Markov moves monotone, as is the case for domino tilings, the state space collapses if and only if $R^{(-n)}(\mathcal{T}_{max}) = R^{(-n)}(\mathcal{T}_{min})$. Consequently, it is sufficient to check only the maximal and minimal states.

## Other Models

The machinery described above for domino tilings can be generalized to a variety of other models. Let us briefly describe a few examples:

**Lozenge Tilings**

Lozenge tilings are the triangular-lattice analog of domino tilings, see Figure 5.4. Lozenge tilings correspond to dimers on the hexagonal lattice, whose bipartite structure allows the introduction of a height function at vertices (which is easy to visualize by imagining a tiling as a stack of cubes), which in turn induces a partial order and lattice structure on the set of tilings. The set is connected elementary rotations at vertices of the triangular lattice as shown below. Cluster rotations can be generated by three-coloring the triangular lattice.
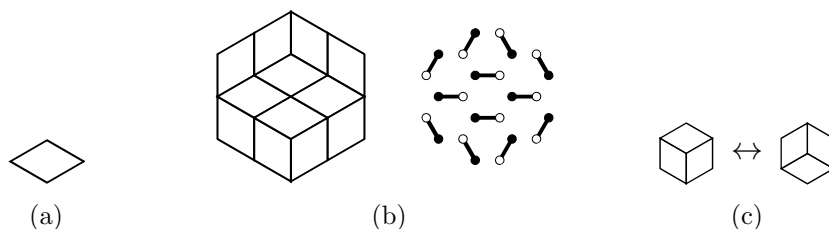


(a)        (b)        (c)

Figure 5.4: (A) A lozenge is a pair of equilateral triangles glued along a side. (B) A lozenge tiling and the corresponding matching on the hexagonal lattice. (C) An elementary rotation.

**Bibone tilings**

Bibone tilings are the hexagonal-lattice analog of domino tilings, see Figure 5.5. While they correspond to dimers on the triangular lattice, techniques for bipartite dimers do not apply;

for example, bibone tilings do not admit height functions. Nonetheless, [55] showed the connectedness of the set of tilings under three types of elementary moves as shown in Figure 5.5. For parallelization, we consider clusters of the same type of move, with a different domain decomposition for each type.



(a)                                    (b)                                    (c)
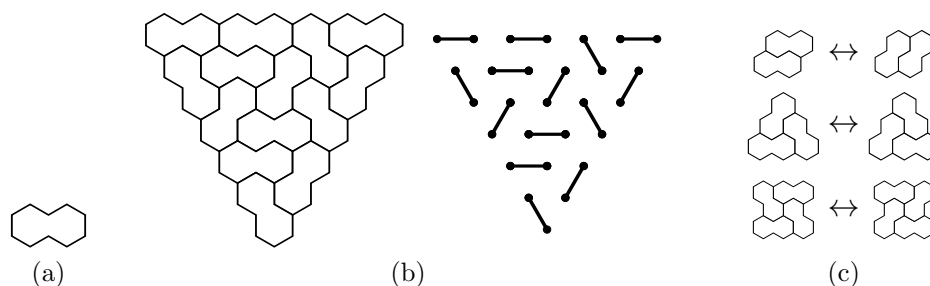
Figure 5.5: (A) A bibone is a pair of hexagons glued along an edge. (B) A bibone tiling and the corresponding matching on the triangular lattice. (C) Up to orientation and reflection, there are three types of elementary moves.

## Rectangle-triangle tilings

Rectangle-triangle tilings were studied by B. Nienhuis, [71]. The tiles are isosceles triangles and rectangles with side lengths 1 and $\sqrt{3}$. We focus on tilings of domains of the triangular lattice. Like lozenge tilings, rectangle-triangle tilings can be visualized in 3D as stacks of half-cubes, which gives a partial ordering to the set of tilings. It is easy to check that the set of tilings is connected by an elementary move at vertices as shown in Figure 5.6. In practice, we allow many other local moves to improve the mixing rate.



(a)                                    (b)                                    (c)
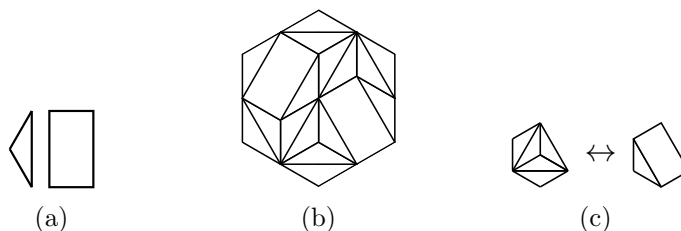
Figure 5.6: (A) Rectangle and triangle tiles. (B) A rectangle-triangle tiling. (C) Up to orientation and reflection, there is one elementary move.

Local weights can be introduced by assigning to each face of the triangular lattice a weight depending on the tiles that cover the face [71]. Up to orientation, there are four possibilities, as shown below: (A) covered by triangles, (B) covered by a rectangle and triangle, (C) covered by rectangles. These cases are assigned weights $t$, $c$, and $r$ respectively; the weight of the tiling is given by the product of all weights of faces.

(a)        (b)        (c)
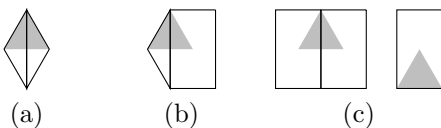
## The six-vertex model

The six-vertex model is defined on a domain $\mathcal{D}$ of the square lattice. A configuration $S$ of the model is an assignment of "occupied" or "unoccupied" to each edge in $\mathcal{D}$ that satisfies the condition that at every vertex $v$ in the interior of $\mathcal{D}$, the edges adjacent to $v$ must be one of six local configurations shown in Figure 5.7. A boundary condition for the six-vertex model fixes the state of edges intersecting the boundary of $\mathcal{D}$.
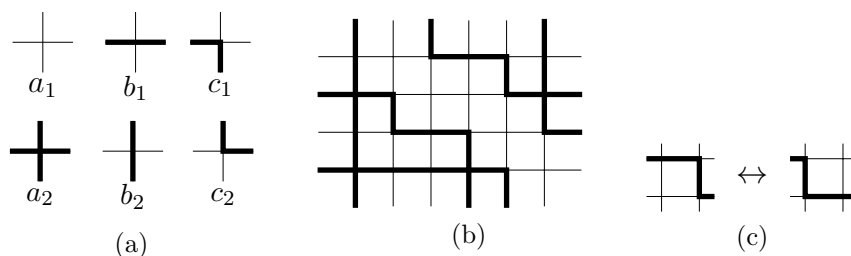


Figure 5.7: (A) The six vertex types with six weights. (B) A six-vertex configuration. (C) A local move.

Six-vertex configurations correspond bijectively to height functions, as shown in Figure 5.8. This endows the set of configurations with a partial ordering and the structure of a distributive lattice.



Figure 5.8: The height function for the six-vertex model.
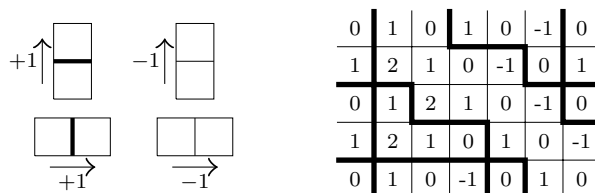
Gibbs measures are defined by assigning positive real weights to each of the six vertex types. The weight of a configuration $S$ is $W(S) = \prod_{v \in \mathcal{D}} w(v, S)$ where $w(v, S)$ is the weight of the vertex $v$ in the configuration $S$ depending on the vertex type. The probability of $S$ is then

$$P[S] = \frac{1}{Z} W(S) \qquad Z = \sum_{S \in \Omega} W(S)$$

The weights $a = 1, b = 1, c = 1$ give the uniform distribution on configurations.

With fixed boundary conditions, the set of configurations is connected by elementary $c$-flips at faces, as shown in Figure 5.7. In general, variations of $c$-flips for boundary faces are also required. For parallelization, cluster moves can be generated by coloring faces according to both the parity of the $x$- and $y$- coordinate of the face.

It can be checked that the local moves preserve the partial order only if the weights satisfy $a \leq c$ and $b \leq c$; this means that coupling-from-the-past can only be used for these weights, although the standard Markov chain sampling can be used for all weights. For the weights $(a = 1, b = 1, c = 1)$, a much faster program is possible due to the combinatorial nature of the model, although we do not pursue it here.

## 5.3   Implementation

### Graphics Processing Units

Certain properties of graphics hardware have great significance in the design and implementation of efficient algorithms for the GPU. Let us briefly mention a few important aspects, and refer the reader to [45] for details.

### GPU Design and Architecture

Many tasks in 3D computer graphics involve carrying out an identical sequence of operations independently on a large set of input primitives. Rendering a surface for instance could require: for each pixel drawn to the screen, computing the local surface normal, computing directions to the viewer and light sources, and finally computing the color according to some lighting and shading model. These types of tasks are often called *data parallel*, and the routine executed on each input called a shader or *kernel*.

GPUs are designed specifically for data parallel tasks. At the hardware level, a typical GPU consists of a number of *compute units*, each containing an instruction block, shared memory caches, and a number of *processing elements* that carry out arithmetic computations. A parallel computation is organized by issuing a *thread* for each kernel execution instance; the threads are divided into blocks and distributed to compute units for execution. Each compute unit executes the kernel in *single instruction multiple data* (SIMD) fashion, by issuing at each time-step the same kernel instruction to every processing element to carry out in a different thread.

For tasks well-suited to this architecture, GPUs can perform up to hundreds of times faster than conventional CPUs.

Performance can drastically suffer, however, when programs are not tuned for the graphics hardware. Due to the SIMD execution model, GPU performance can be severely affected by *branch divergences*, which occur when conditional expressions in the kernel cause different threads to follow different execution paths. Furthermore, compared to conventional processors, GPUs have little hardware dedicated to speed-up the execution of sequential code.

In particular, GPU cores have relatively smaller memory caches and limited bandwidth for memory access. While GPUs hide memory-access latency by multithreading, their performance is nonetheless sensitive to the pattern of memory-access and organization of data in memory.

**The OpenCL Framework**

In early years, general purpose computing with GPUs required reformulating a task in terms of graphics primitives and operations. Since then, GPUs have evolved into highly flexible and easily programmable processors. Frameworks such as NVidia's Compute Unified Device Architecture (CUDA) and the Open Computing Language (OpenCL), define C-type kernel programming languages and provide C/C++ libraries to access GPU devices.

For this work, we chose to use OpenCL.

In the OpenCL framework, a computing platform consists of a *host* (typically the CPU) and any number of *devices* (typically GPUs). Kernel source code is loaded and compiled for devices by OpenCL at run-time. The host issues commands to the device, such as kernel executions and data transfers, via a command queue. Before launch, the set of kernel execution threads is arranged by the user into a grid of *work-items*. The grid coordinates of a work-item can be accessed from within the kernel program and used to identify the thread. The grid is further divided into *work-groups*, each of which is executed on one compute unit of the GPU, and whose work-items can communicate via shared local memory and can synchronize with barriers.

A typical OpenCL host program first initializes the platform, then loads and compiles the kernel source, transfers relevant data to the device, sets up and launches the kernel on the device, and finally reads back the output data from the device.

## Random Domino Tilings with the GPU

Having laid the necessary foundations, let us now explain our implementation.

To each vertex $v$ we associate an integer *state* representing the tiling of the faces adjacent to $v$ as follows: enumerating the edges adjacent to $v$ in the order North, South, East, West, the tilestate $s_v$ is defined as

$$s_v = e_0 + 2\,e_1 + 4\,e_2 + 8\,e_3$$

where $e_i$ is 1 if a domino of $\mathcal{T}$ crosses edge $i$ and 0 otherwise. A vertex $v$ is rotateable if its state $s_v = 12$ or $s_v = 3$.

A tiling is represented by the state of every vertex of the domain $\mathcal{D}$, as in Figure 5.9. Assuming the domain $\mathcal{D}$ is contained in an $N \times N$ square domain in the first quadrant of the Euclidean plane, we store a tiling $\mathcal{T}$ as an array $N \times N$ array $T$, where the $(i,j)$th entry of $T$ is the state of the vertex with coordinate $(i,j)$.

To optimize kernel occupancy and memory transfer speed, we divide the tiling into the sub-arrays $T_b$, $T_w$ of black and white vertices, and store each contiguously in the GPU device

memory. For simplicity, we assume $N$ is even, so that for example the $(i,j)$th component of the array $T_b$ corresponds to the state of the vertex $(i, 2j + i \bmod 2)$ in $\mathcal{D}$. Moreover, to avoid special cases at the boundary we assume all arrays are sufficiently zero-padded.

In our implementation, the primitives of GPU operations are the vertices of the domain $\mathcal{D}$. We define a kernel function that rotates a vertex $v$ with some fixed probability, and kernel functions that check the neighbors of $v$ and recomputes its state. More precisely,

- The kernel *Rotate* takes as a parameter a tiling sub-array $T$. The work-item $(i,j)$ first generates a pseudo-random number, and then with fixed probability attempts to either rotate up or down the state $T[i,j]$. The state can be rotated up if $T[i,j] = 3$ with rotating accomplished by setting $T[i,j] = 12$, and similarly for down-rotation.
- The kernels *UpdateBlack* and *UpdateWhite* take as parameters both sub-arrays $T_b, T_w$. The work-item $(i,j)$ of *UpdateBlack* recomputes the state of the vertex with index $(i,j)$ in $T_b$ in terms of the neighboring vertices in $T_w$. This can be done efficiently with bitwise operations, as follows

$$T_b[i,j] = \frac{1}{2}(T_w[i-1,j] \,\&\, 2) \;+\; 2(T_w[i+1,j] \,\&\, 1)+$$
$$\frac{1}{2}(T_w[i,j+i \bmod 2 - 1] \,\&\, 8) \;+ 2(T_w[i,j+i \bmod 2] \,\&\, 4)$$

The *UpdateWhite* kernel is defined similarly.

Other kernels used to generate pseudo-random numbers are discussed in Section 5.3.

A random cluster rotation is accomplished by launching *Rotate* on all black vertices and *Update* on all white vertices, or *Rotate* on all white vertices and *Update* on all black vertices. We define the following host functions:

- The function *RandomWalk* takes as parameters a tiling $\mathcal{T}$, a random number seed $s$, and a natural number *nSteps*. The function first divides $\mathcal{T}$ into the two sub-arrays $T_b$ and $T_w$ and loads them to the GPU memory. It then seeds all pseudo-random number generators with $s$. Then, looping *nSteps* times, with equal probability it either runs *Rotate* with all black vertices and *Update* on all white vertices, or vice versa. Finally, after the loop is complete, it reads back $T_b$ and $T_w$, and recombines the two sub-arrays into the tiling $T$.
- The function *DominoTilerCFTP* generates a random tiling using the coupling-from-the-past algorithm. The pseudo-code is:
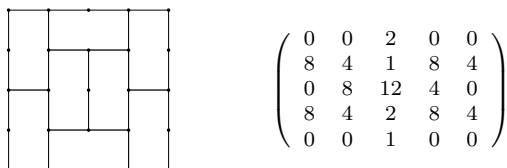


$$\begin{pmatrix} 0 & 0 & 2 & 0 & 0 \\ 8 & 4 & 1 & 8 & 4 \\ 0 & 8 & 12 & 4 & 0 \\ 8 & 4 & 2 & 8 & 4 \\ 0 & 0 & 1 & 0 & 0 \end{pmatrix}$$

Figure 5.9: A tiling and its tilestate (without zero padding).

**D**ominoTilerCFTP:

Compute the extremal tilings $\mathcal{T}_{max}$ and $\mathcal{T}_{min}$.

Initialize a list *seeds* with a random real number.

Repeat:

    Initialize $\mathcal{T}_{top} = \mathcal{T}_{max}$

    Initialize $\mathcal{T}_{bottom} = \mathcal{T}_{min}$

    For $i = 1$ to length of *seeds*:

        Set $\mathcal{T}_{top} = RandomWalk(\mathcal{T}_{top}, seeds_i, 2^i)$

        Set $\mathcal{T}_{bottom} = RandomWalk(\mathcal{T}_{bottom}, seeds_i, 2^i)$

    If $\mathcal{T}_{top} = \mathcal{T}_{bottom}$, return $\mathcal{T}_{bottom}$.

    Else, push a new random number to the beginning of *seeds*.

### Pseudo-random Number Generators

Random number generators for massively parallel computing is an active area of research. Most applications require a stream of pseudo-random numbers for each thread, with good statistical properties both within each stream and across different streams. The statistical independence is crucial in our application to ensure that the set of tilings is connected by the cluster moves generated by the *Rotate* kernel.

For our implementation, we adopted a variant of the well-known *Mersenne Twister* pseudo-random number generator known as TinyMT [86]. Although compared to the Mersenne Twister, the period of TinyMT is relatively small ($2^{127}$), the TinyMT admits a large number (up to $2^{48}$) of internal parameter values that ensure statistical independence (see [86]) of generators with different parameter values. For tilings with fewer than $2^{48}$ vertices, it is convenient to simply instantiate a TinyMT generator with a unique parameter value for each vertex of the domain.

## 5.4 Conclusion

We tested our implementation using a few different graphics cards: an Intel Integrated HD 510, an NVidia Tesla P100, and an AMD Radeon Pro 555. Although a rigorous performance comparison of GPU algorithms and CPU algorithms can be a delicate matter (see [66]), we nevertheless compared our implementation with standard CPU algorithms, see Figure 5.10. We found that for smaller domains, the processing time is dominated by memory transfer time and other overheads, and the CPU is often faster. For larger domains, the parallelism pays off and we found significant speed-ups, of at least an order of magnitude depending on the quality of the graphics hardware.
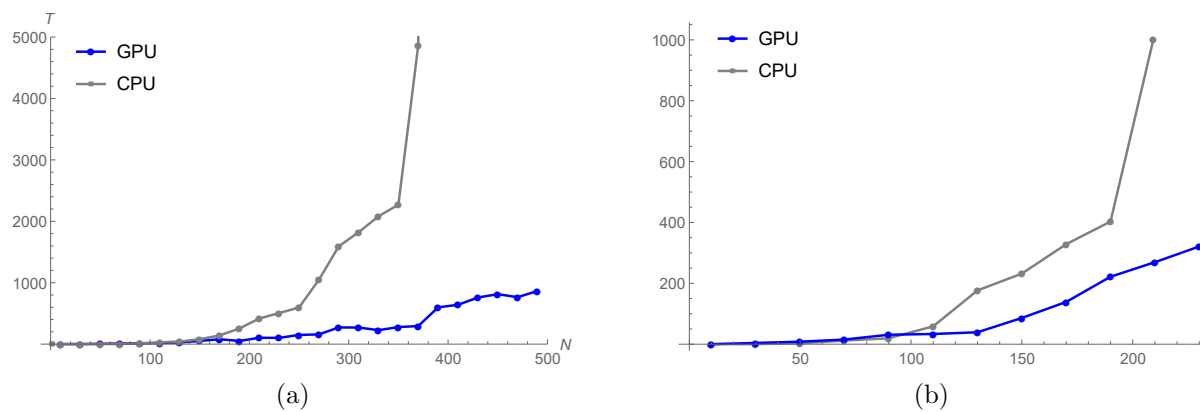
Figure 5.10: (A) The time $T$ in seconds to generate, with coupling-from-the-past, a random configuration of the six-vertex model on an $N \times N$ sized domain with domain wall boundary conditions and weights $(a, b, c) = (1, 1, 1)$. We used an Nvidia Tesla P100 GPU and a 2.2 GHz Intel Xeon E5 CPU. (B) The time to generate a random domino tiling of an $N \times N$ square. Here we used a laptop with an Intel 510 Integrated GPU and 2.10 GHz Pentium CPU.
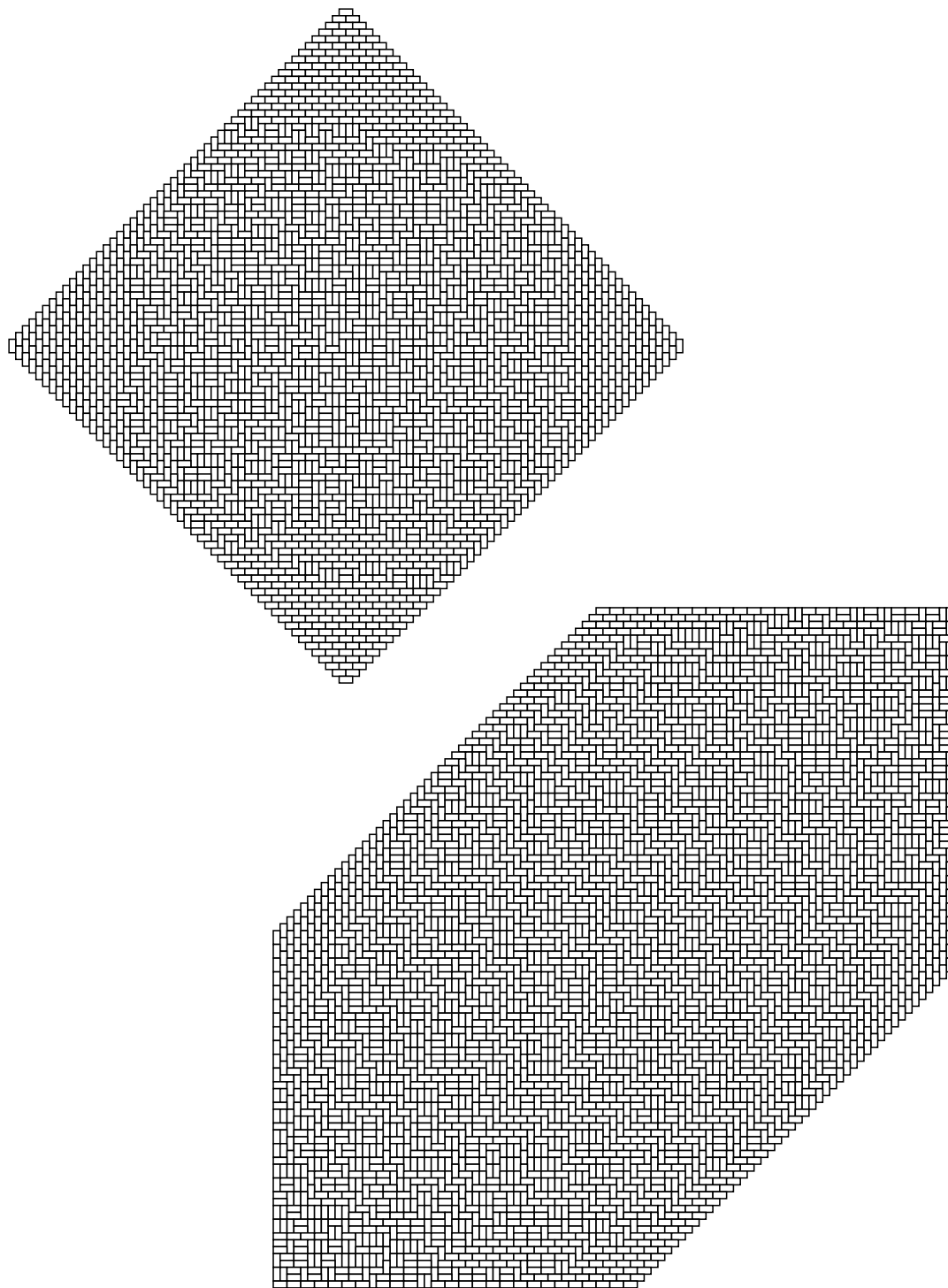
## 5.5 Examples
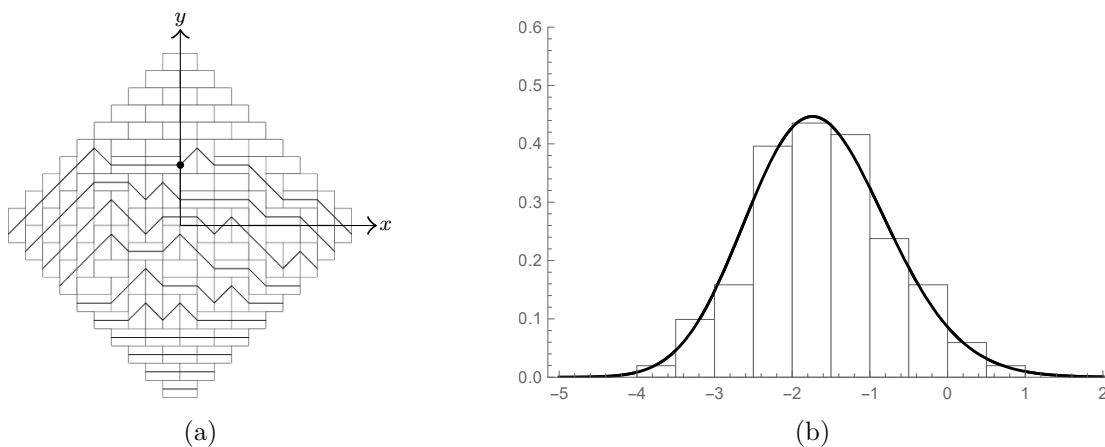
Figure 5.11: Some domino tilings.

(a)

(b)

Figure 5.12: [49] showed that the fluctuations of the top-most path, above which all tiles are horizontal, converges to the Airy process. In particular, the $y$-intercept of the path as shown in (A), after appropriate rescaling, converges to the Tracy-Widom distribution $F_2$. (B) shows a normalized histogram of the $y$-intercept computed from 100 random tilings of an Aztec diamond of size 300, with the distribution $F_2$ superimposed in bold.
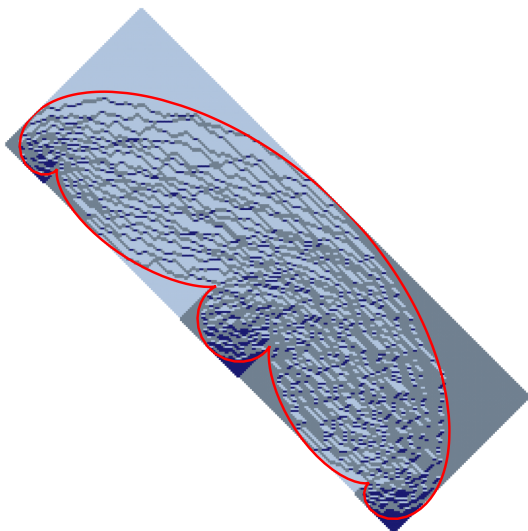


Figure 5.13: A tiling of a rectangular Aztec diamond, with the Arctic curve computed by [17] superimposed in red.
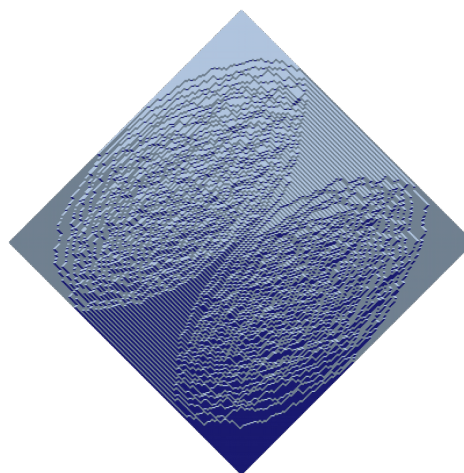


Figure 5.14: A random tiling of the Aztec diamond with volume weights (see Section 5.2) $q = 20$ for all black vertices and $q = 1/20$ for all white vertices. See [8] for details.
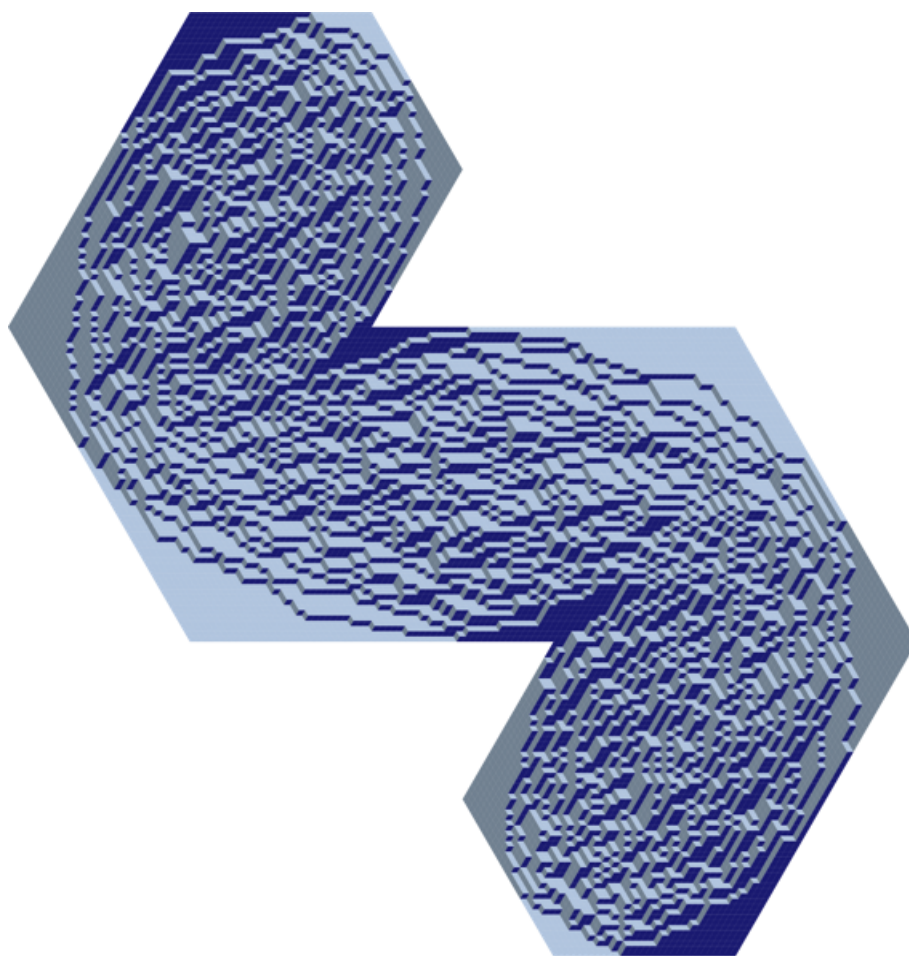
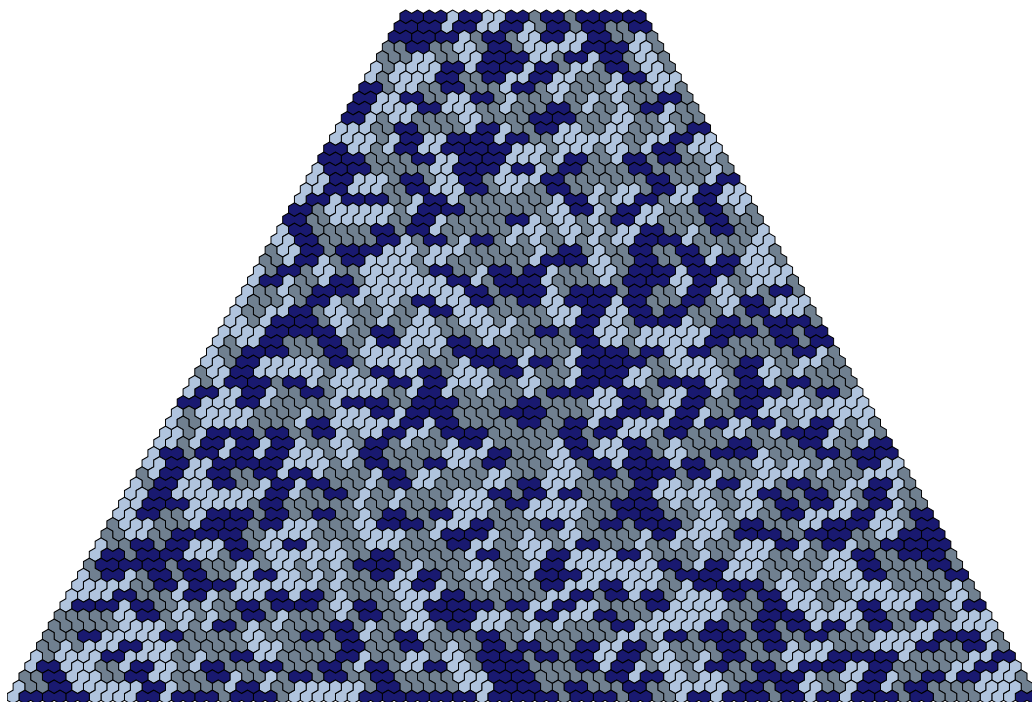Figure 5.15: A random tiling of a weird region by lozenges.

Figure 5.16: A tiling of a trapezoid by bibones. Bibone tilings, which correspond to dimers on the triangular lattice, seem not to develop Arctic curves or limit shapes.
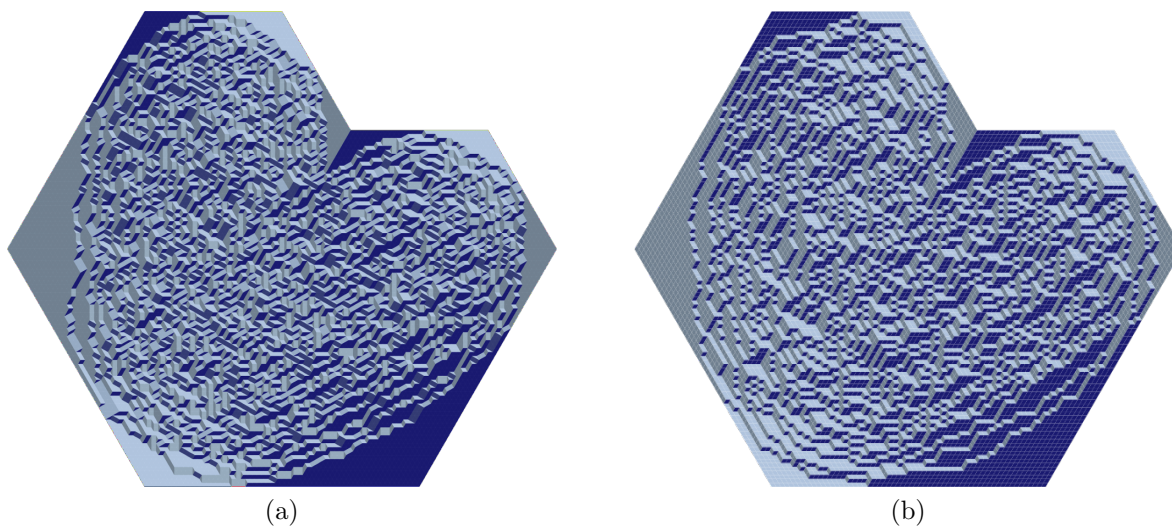


| (a) | (b) |

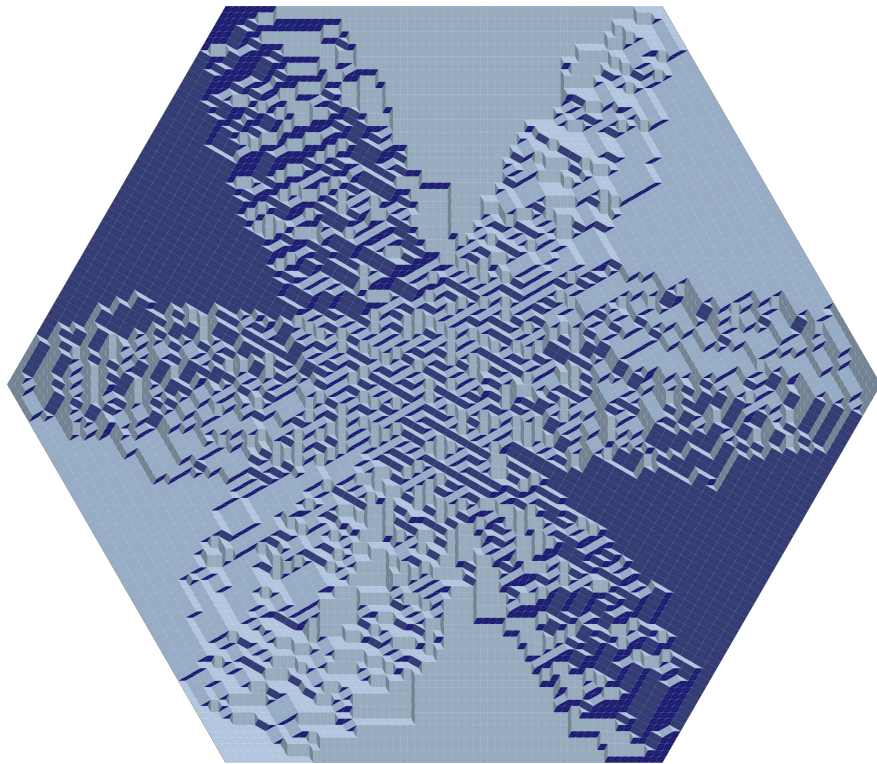Figure 5.17: A tiling of a partial hexagon (A) by rectangles and triangles, and (B) by lozenges.

Figure 5.18: Choosing weights $t = .5, r = 1, c = 1$ (see Section 5.2) produces tilings that look like snowflakes. We observed large fluctuations in the boundaries of the arms as compared to Arctic curves of lozenge tilings.

(a)


(b)


(c)


(d)


(e)
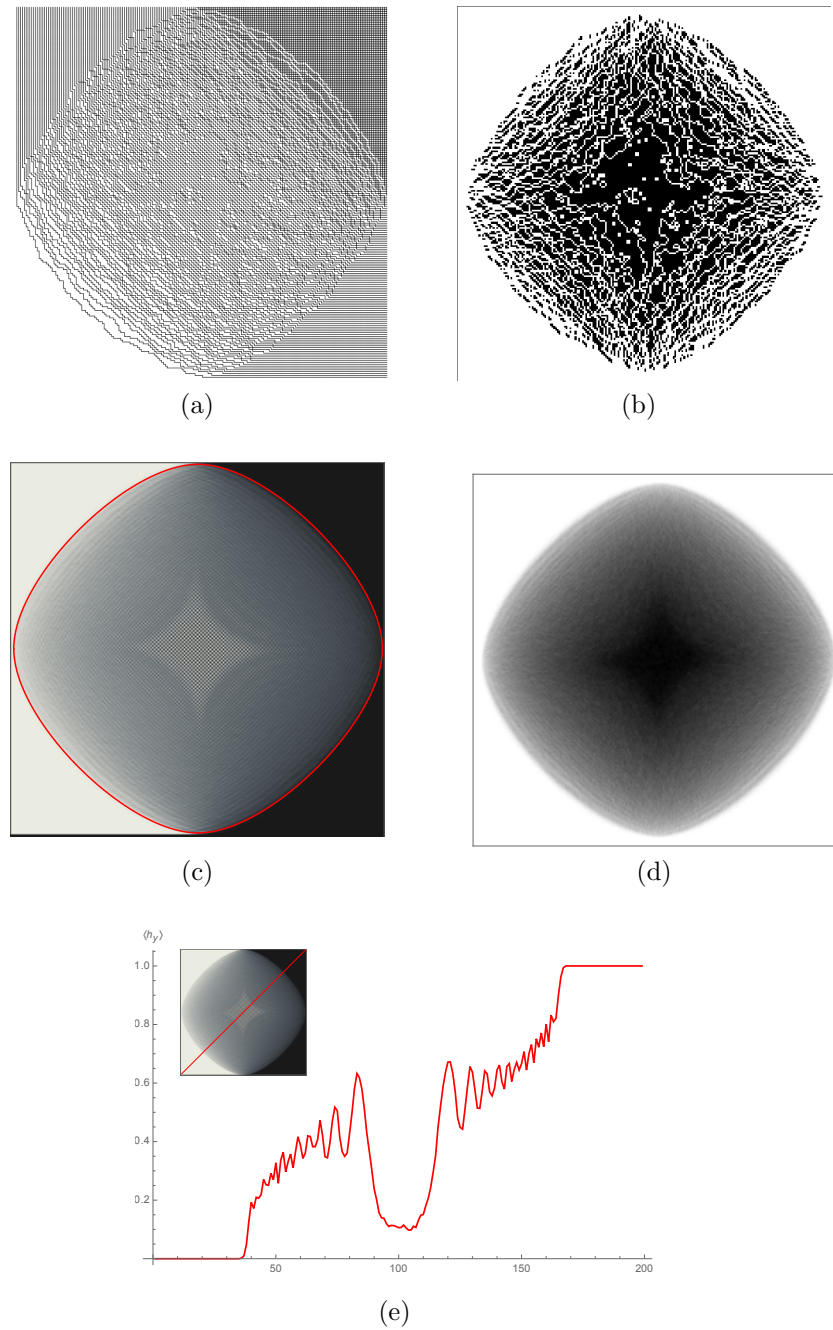
Figure 5.19: The six-vertex model with weights $a = 1, b = 1, c = \sqrt{8}$, $(\Delta = -3)$, in a square with DWBC. (A) shows a random configuration and (B) shows the $c$-vertices of the random configuration in black. (C) shows the average density of horizontal edges computed, with 1000 random configurations. The Arctic curve computed by [22] is superimposed in red. (D) shows the average density of $c$-vertices. (E) shows the cross-section profile of the horizontal edge density along a diagonal slice, which was studied in [64].
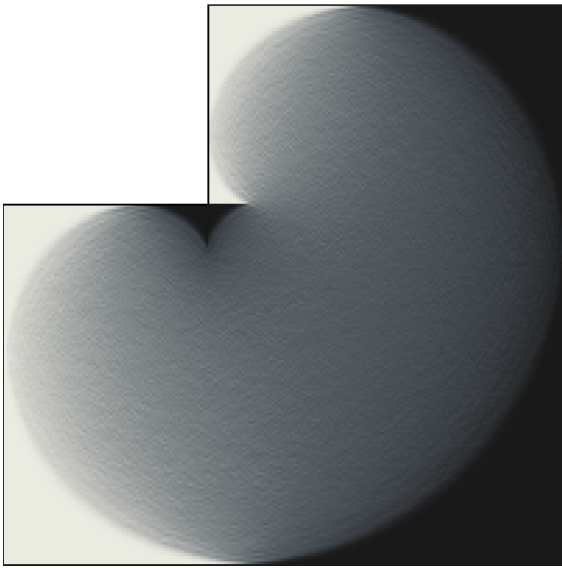
Figure 5.20: The average density of horizontal edges in with weight $\Delta = 0$ in an L-shaped region with domain wall type boundary conditions, computed with 1000 samples.
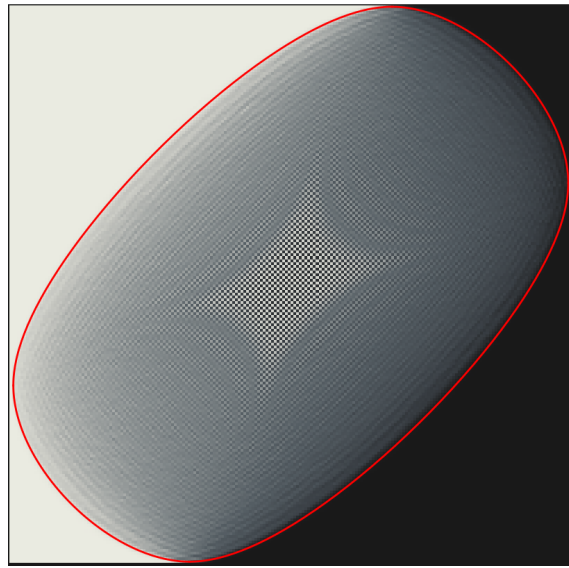


Figure 5.21: The average density of horizontal edges with weights $a = 2b$, $\Delta = -3$, computed with 1000 samples. The red curve is the Arctic curve computed by [22].

(a)  (b)
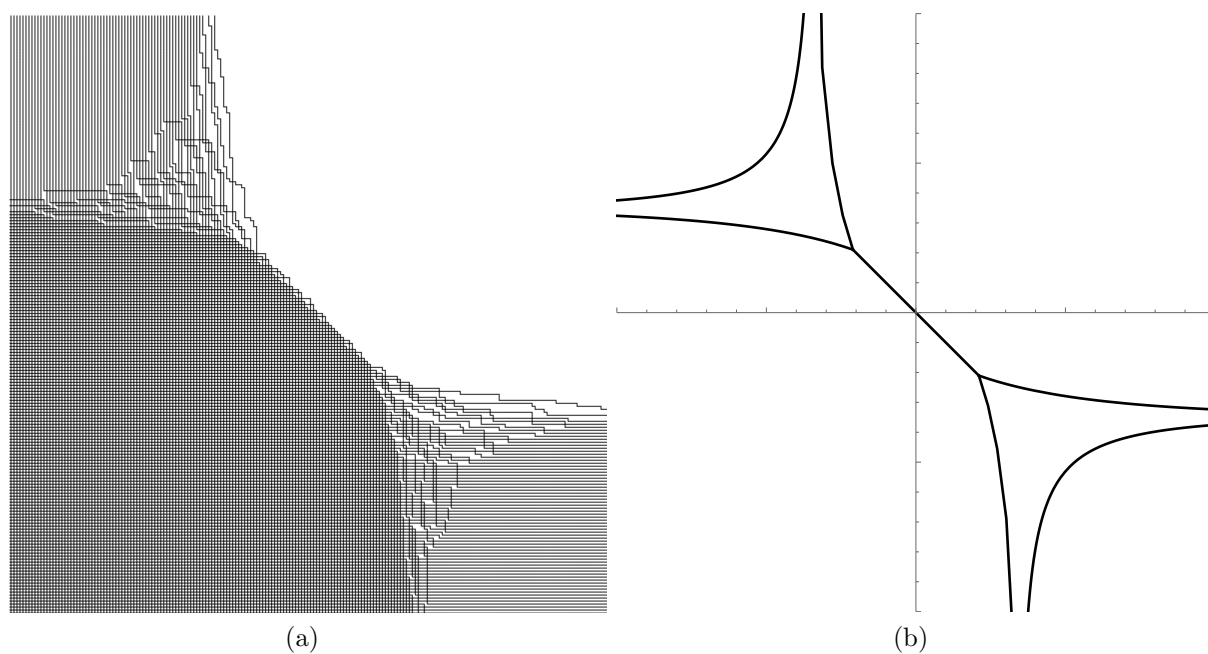
Figure 5.22: By the Wulff construction, the toroidal free energy $f(H, V)$ is the limit shape of the volume-constrained model with special boundary conditions. Figure A shows a random configuration with weights $a = 2$, $b = 1$, $c = .8$ and volume weights. Figure B shows the free energy phase diagram for the same weights [76].

(B)

(C)

(A)
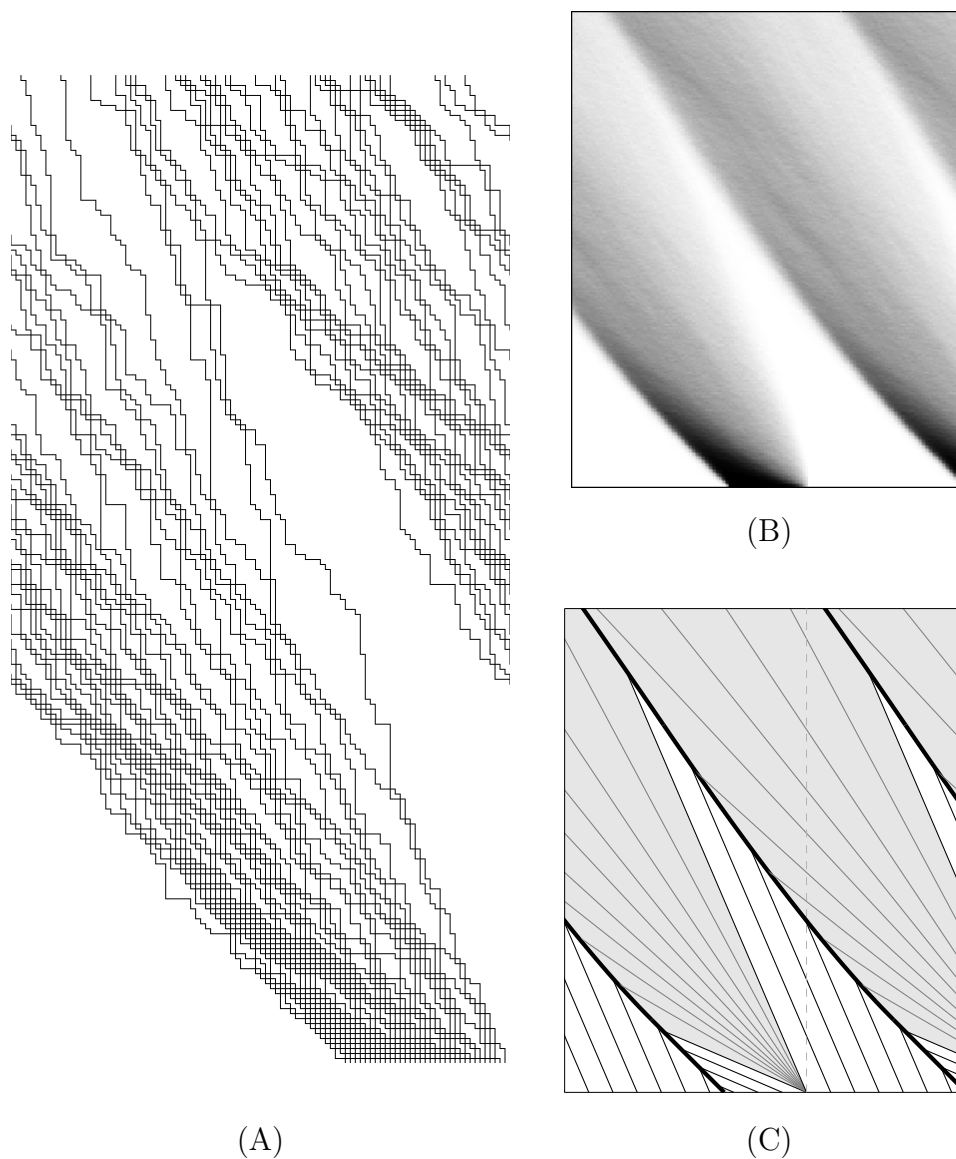
Figure 5.23: The six-vertex model at the stochastic point with weights $(a_1, a_2, b_1, b_2, c_1, c_2) = (1, 1, .3, .7, .3, .7)$ on a cylinder with fixed step boundary conditions at the bottom and free boundary conditions at the top. For details about the stochastic six vertex model, see [43, 10, 84]. (A) shows a random configuration on the cylinder. (B) shows the average density of paths, taken over 100 sample, with empty space shaded in white. In the thermodynamic limit, the density of paths is described by a Burgers-type equation that can be solved by characteristics. (C) shows the characteristic lines, with shocks drawn in bold and the rarefaction fans shaded in grey.

# Bibliography

[1]   A. Aggarwal. "Arctic Boundaries of the Ice Model on Three-Bundle Domains." *Invent. math.* 220, 611-671 (2020). arXiv:1812.03847 [math.PR].

[2]   A. Aggarwal, "Limit Shapes and Local Statistics for the Stochastic Six-Vertex Model." *Preprint* (2019), arXiv:1902.10867

[3]   A. Aggarwal, Private communication, March 2019.

[4]   D. Allison, N. Reshetikhin. "The 6-vertex model with fixed boundary conditions." *Annales de l'institut Fourier.* Vol. 55. No. 6. (2005), arXiv:cond-mat/0502314.

[5]   R.J. Baxter, *Exactly Solved Models in Statistical Mechanics*, 1982 , Dover Publications, London.

[6]   Baxter, R. J. "Solvable eight-vertex model on an arbitrary planar lattice." *Philos. Trans. Roy. Soc. London Ser. A* 289 (1978), no. 1359, 315-346.

[7]   V. Bazhanov, V. Mangazeev. "Analytic Theory of the Eight Vertex Model." *Nuclear Physics B* 775 [FS] (2007): 225-282.

[8]   D. Betea, C. Boutillier, J. Bouttier, G. Chapuy, S. Corteel, M. Vuletic. "Perfect sampling algorithm for Schur processes." *Markov Processes And Related Fields,* Polymat Publishing Company, 2018, 24 (3), pp.381-418, arXiv:1010.5011v1 [math-ph].

[9]   H. Bethe. "Zur Theorie der Metalle." *Z. Physik* 71, 205?226 (1931).

[10]  A. Borodin, I. Corwin, V. Gorin. "Stochastic six-vertex model." *Duke Math. J.* 165, no. 3 (2016), 563-624.

[11]  A. Borodin, G. Olshanski. "Stochastic dynamics related to Plancherel measure on partitions." *Representation Theory, Dynamical Systems, and Asymptotic Combinatorics. Amer. Math. Soc.*, Translations - Series 2, vol. 217 (2006) 9-22, arXiv:math-ph/0402064.

[12]  A. Borodin, M. Wheeler. "Coloured stochastic vertex models and their spectral theory." *Preprint* arXiv:1808.01866 [math.PR].

[13] M. Bousquet-Mélou and K. Eriksson. "Lecture Hall Partitions." *The Ramanujan Journal*, 1 no. 1 (1997):101-111.

[14] M. Bousquet-Mélou and K. Eriksson. "Lecture Hall Partitions II." *The Ramanujan Journal*, 1 no. 2 (1997):165-186.

[15] M. Bousquet-Mélou and K. Eriksson. "A refinement of the lecture hall theorem." *J. Combin. Theory Ser. A.* 86 (1999) 63-84.

[16] D.J. Bukman and J.D. Shore. "The conical Point in the Ferroelectric Six-Vertex Model." *J. Stat. Phys.* 78, 1277-1309 (1995).

[17] A. Bufetov, A. Knizel. "Asymptotics of random domino tilings of rectangular Aztec diamonds." *Ann. de l'Inst. Henri Poincare*, 2016.

[18] D. Cimasoni, N. Reshetikhin. "Dimers on surface graphs and spin structures." *Commun. Math. Phys.* 275(1), 187-208 (2007), arXiv:0704.0273.

[19] H. Cohn, N. Elkies, and J. Propp. "Local statistics for random domino tilings of the Aztec diamond." *Duke Math. J.*, 85(1), 117-166 (1996), arXiv:math/0008243

[20] H. Cohn, R. Kenyon, J. Propp. "A variational principle for domino tilings." *J. Amer. Math. Soc.* 14, 297-346 (2001).

[21] F. Colomo and A. Sportiello. "Arctic curves of the six-vertex model on generic domains: the tangent method." *J. Stat. Phys.*, 164(6), 1488-1523 (2016).

[22] F. Colomo and A. G. Pronko. "The arctic curve of the domain-wall six-vertex model." *J. Stat. Phys.* 138, 662-700 (2010), arXiv:0907.1264.

[23] F. Colomo, A. G. Pronko and A. Sportiello. "Arctic curves of the free-fermion six-vertex model in an L-shaped domain", *J. Stat. Phys.* 174 (2019).

[24] F. Colomo, A. G. Pronko, P. Zinn-Justin. "The arctic curve of the domain wall six-vertex model in its antiferroelectric regime." *J. Stat. Mech.: Theor. Exp.* (2010) L03002

[25] S. Corteel and J. S. Kim. "Enumeration of bounded lecture hall tableaux." *Preprint* (2019), arXiv:1904.10602

[26] S. Corteel and J. S. Kim. "Lecture hall tableaux", *Advances in Mathematics* 371 (2018), arXiv:1804.02489.

[27] S. Corteel, D. Keating, and M. Nicoletti. "Arctic curves phenomena for bounded lecture hall tableaux." *Commun. Math. Phys.* 382, 1449-1493 (2021), arXiv:1905.02881 [math.CO].

[28] I. Corwin, L. Petrov. "Stochastic higher spin vertex models on the line." *L. Commun. Math. Phys.* 343: 651 (2016), arXiv:1502.07374 [math.PR].

[29] B. Debin, P. Ruelle. "Tangent method for the arctic curve arising from freezing boundaries." *J. Stat. Mech.* (2019) 123105, arXiv:1810.04909

[30] P. Di Francesco, E. Guitter. "Arctic curves for paths with arbitrary starting points: a tangent method approach." *J. Phys. A: Math. Theor.* 51 (2018), arXiv:1803.11463.

[31] P. Di Francesco, E. Guitter, "A tangent method derivation of the arctic curve for $q$-weighted paths with arbitrary starting points." *J. Phys. A: Math. Theor.* 52 (2019), arXiv:1810.07936.

[32] P. Di Francesco, E. Guitter, "The Arctic curve for Aztec rectangles with defects via the Tangent Method." *J. Stat. Phys.* 176, 639-678 (2019), arXiv:1902.06478

[33] P. Di Francesco, M. F. Lapa. "Arctic curves in path models from the tangent method." *J. Phys. A: Math. Theor.* 51 (2018).

[34] P. Di Francesco, R. Soto-Garrido. "Arctic curves of the octahedron equation". *J. Phys. A*, 47(28):285204, 34 (2014), arXiv:1402.4493

[35] R. L. Dobrushin, R. Kotecky, and S. B. Shlosman. *Wulff Construction: A Global Shape from Local Interactions.* AMS Translations of mathematical monographs (1992).

[36] L. Faddeev, N. Reshetikhin, "Integrability of the principal chiral field model in $1 + 1$ dimension." *Ann. Physics*, v.167 (1986), no. 2, 227-256.

[37] L.D. Faddeev, L. A. Takhtajan, *Hamiltonian Methods in the Theory of Solitons*, Springer, 2007.

[38] L.D. Faddeev, L. A. Takhtajan, "The quantum method for the inverse problem and the XYZ Heisenberg model" (Russian), *Uspekhi Mat. Nauk* 34 (1979); no. 5(209), 13-63, 256.

[39] M. Fisher. "Statistical mechanics of dimers on a plane lattice", *Physical Review*, 124(6):1664 (1961).

[40] I. M. Gessel, X. G. Viennot, "Binomial determinants, paths, and hook-length formulas", *Advances in Math.* 58 (1985), 300-321.

[41] I. M. Gessel, X. Viennot. "Determinants, paths, and plane partitions." *Preprint,* (1989), available at `http://www.cs.brandeis.edu/ ira`.

[42] J. de Gier, R. Kenyon, and S. Watson. "Limit shapes for the asymmetric five vertex model." *Preprint* arXiv: 1812.11934v1.

[43] L.-H. Gwa, H. Spohn. "Six-vertex model, roughened surfaces, and an asymmetric spin Hamiltonian." *Physical Review Letters*, 68, no. 6 (1992), 725-728.

[44] W.K. Hastings. "Monte Carlo Sampling Methods Using Markov Chains and Their Applications". *Biometrika.* 57 (1): 97-109 (1970).

[45] J.L. Hennessy, D.A. Patterson, *Computer architecture: a quantitative approach.* Elsevier, 2011. 16142, 2011.

[46] A. Izergin, V. Korepin, and N. Reshetikhin. "Conformal Dimension in Bethe Ansatz Solvable Models." *J. Phys. A: Math. Gen.* 22 (1989): 2615-2620

[47] M. Jimbo, T. Miwa. "Algebraic Analysis of Solvable Lattice Models". *American Mathematical Soc.* Vol. 85 (1994).

[48] W. Jockusch, J. Propp, and P. Shor. "Random domino tilings and the arctic circle theorem", *Preprint* arXiv:math/9801068 [math.CO] (1998).

[49] K. Johansson. "The arctic circle boundary and the Airy Process." *Ann. Probab.* 33, Number 1 (2005), 1-30

[50] P. Kasteleyn. "Graph theory and crystal physics", 1967 *Graph Theory and Theoretical Physics* pp. 43-110 Academic Press, London.

[51] D. Keating, N. Reshetikhin and A. Sridhar, "Conformal limit for Dimer models on the hexagonal lattice", *Zap. Nauchn. Sem. POMI* 473 (2018), 174-193 http://www.pdmi.ras.ru/znsl/2018/v473/abs174.html

[52] D. Keating, N. Reshetikhin, A. Sridhar. "Integrability of Limit Shapes of the Inhomogeneous Six Vertex Model." *Preprint* arXiv:2004.08971 [math-ph].

[53] D. Keating, A. Sridhar, "Random tilings with the GPU", *J. Math. Phys.* 59, 091420 (2018); https://doi.org/10.1063/1.5038732

[54] D. Keating, A. Sridhar. https://github.com/GPUTilings

[55] C. Kenyon. "Perfect matchings in the triangular lattice." *Discrete Mathematics* 152 (1996), 191-210

[56] R. Kenyon. "Height Fluctuations in the Honeycomb Dimer Model." *Commun. Math. Phys.* (2008) 281: 675.

[57] R. Kenyon. "The planar dimer model with boundary: a survey," *Directions in mathematical quasicrystals*, CRM Monograph Series, 13, Providence, RI: American Mathematical Society, pp. 307-328

[58] R. Kenyon. "Lectures on dimers." Statistical mechanics, 191-230, IAS/Park City Math. Ser., 16, Amer. Math. Soc., Providence, RI, 2009.

[59] R. Kenyon, A. Okounkov, "Planar dimers and harnack curves". *Duke Math. J.* 131 (2006), no. 3, 499-524, arXiv:math/0311062 [math.AG].

[60] R. Kenyon, A. Okounkov. "Limit shapes and the complex Burgers equation". *Acta Math.* 199 (2007), no. 2, 263-302, arXiv:math-ph/0507007.

[61] R. Kenyon, A. Okounkov, and S. Sheffield. "Dimers and Amoeba." *Annals of Math.* 163 , no.3, 1019-1056 (2006), arXiv:math-ph/0311005.

[62] R. Kenyon, R. Pemantle, "Double-dimers, the Ising model and the hexahedron recurrence." *J. of Comb. Theory, Series A*, Vol 137 (2016) Pages 27-63.

[63] V.E. Korepin, N.M. Bogolyubov, and A.G. Izergin. *Quantum Inverse Scattering Method and Correlation Functions*, Cambridge University Press, 1993.

[64] V. Korepin, I. Lyberg, and J. Viti. "The density profile of the six vertex model with domain wall boundary conditions." *Preprint* arXiv:1612.06758 [cond-mat.stat-mech].

[65] B. Laslier, F.L. Toninelli. "Lozenge Tilings, Glauber Dynamics and Macroscopic Shape." *Commun. Math. Phys.* (2015) 338: 1287.

[66] V. Lee et al. "Debunking the 100X GPU vs. CPU myth: an evaluation of throughput computing on CPU and GPU." *Proceedings of the 37th annual international symposium on Computer architecture* ACM, 38, no. 3 (2010), 451-460.

[67] E. Lieb, *Phys. Rev.* 162, 162, 1967; E.H. Lieb, *Phys. Rev.* Lett. 18, 1046, 1967; 19, 108, 1967.

[68] E. Lieb, F. Y. Wu,. "Two-dimensional Ferroelectric Models." *Phase Transitions and Critical Phenomena*, Vol. 1, Eds. C. Domb and M.S. Green (Academic Press, 1972) pp. 331-490.

[69] M. Luby, D. Randall, and A. Sinclair. "Markov chain algorithms for planar lattice structures," *SIAM Journal on Computing*, 31(1):167-192, 200.

[70] N. Metropolis, A.W. Rosenbluth, M.N. Rosenbluth, A.H. Teller, and E. Teller. "Equation of State Calculations by Fast Computing Machines." *Journal of Chemical Physics.* 21 (6): 1087-1092 (1953).

[71] B. Nienhuis. "Unfinished Business", *Ingenuity and integrability in statistical mechanics* Conference, Amsterdam, (2017).

[72] J.D. Noh, D. Kim. "Finite size scaling and the toroidal partition function of the critical asymmetric six-vertex model." *Physical Review E* 53.4 (1996): 3225. arXiv:cond-mat/9511001.

[73] I.M. Nolden. "The Asymmetric Six-Vertex Model." *Journal of Statistical Physics,* Vol. 67, (1991) No 1/2, 155-201.

[74] A. Okounkov, N. Reshetikhin. "Correlation function of Schur process with application to local geometry of a random 3-dimensional Young diagram." *J. Amer. Math. Soc.,* 16(3):581-603, 2003, arXiv:math/0107056.

[75] A. Okounkov, N. Reshetikhin, "Random skew plane partitions and the Pearcey process." *Comm. Math. Phys.,* 269 no. 3, February 2007, arXiv math. CO/0503508.

[76] K. Palamarchuk, N. Reshetikhin. "The 6-vertex model with fixed boundary conditions." *Preprint* arXiv:1010.5011 [math-ph].

[77] L. Pauling. "The Structure and Entropy of Ice and of Other Crystals with Some Randomness of Atomic Arrangement." *Journal of the American Chemical Society.* 57 (12): 2680-2684 (1935).

[78] T. K. Petersen, D. Speyer. "An arctic circle theorem for Groves." *J. of Comb. Theory, Series A* 111 (2005) 137-164.

[79] L. Petrov. "Asymptotics of uniformly random lozenge tilings of polygons. Gaussian free field." *Ann. Probab.,* 43 (1) (2014), pp. 1-43 arXiv:1206.5123

[80] B. Pittel, D. Romik. "Limit shapes for random square Young tableaux and plane partitions." *Adv. Appl. Math.* 38 (2): 164-209 (2007), arXiv:math/0405190 [math.PR].

[81] J. Propp, D. Wilson, "Coupling from the past: a user's guide", Microsurveys in discrete probability (Princeton, NJ, 1997), *DIMACS Ser. Discrete Math. Theoret. Comput. Sci.,* 41, Providence, R.I.: American Mathematical Society, pp. 181-192.

[82] N. Reshetikhin. "Lectures on integrable models in statistical mechanics", In: *Exact methods in low-dimensional statistical physics and quantum computing,* Proceedings of Les Houches School in Theoretical Physics, Oxford University Press, 2010, arXiv:1010.5031

[83] N. Reshetikhin, A. Sridhar, "Integrability of Limit Shapes in the Six Vertex Model." *Commun. Math. Phys.* 356, 535-565 (2017), arXiv:1510.01053 [math-ph].

[84] N. Reshetikhin, A. Sridhar. "Limit shapes in the stochastic six-vertex model." *Commun. Math. Phys.* 363, 741-765 (2018), arXiv:1609.01756v1 [math-ph]

[85] C. D. Savage. "The mathematics of lecture hall partitions." *J. Combin. Theory Ser. A,* 144:443-475, 2016.

[86] M. Saito, M. Matsumoto https://github.com/MersenneTwister-Lab/TinyMT

[87] S. Sheffield. PhD Thesis, Standford Univ. 2003.

[88] RP. Stanley. Enumerative Combinatorics, Volume 2. Combinatorics. Cambridge studies in advanced mathematics. (1999).

[89] B. Sutherland, C.N. Yang, C.P. Yang. "Exact solution of a model of two-dimensional ferroelectrics in an arbitrary external electric field." *Phys. Rev. Letters,* v. 19 (1967), n 10, 588-591.

[90] O. Syljuasen, M. Zvonarev. "Directed-loop Monte Carlo simulations of vertex models", *Phys. Rev.* E 70, 016118 (2004)

[91] W.P. Thurston. "Conway's Tiling Group." *Amer. Math. Monthly* (1990) 757-773.

[92] M. Weigel. "Monte Carlo methods for massively parallel computers", in: *Order, Disorder and Criticality*, Vol. 5, ed. Yu. Holovatch (World Scientific, Singapore, 2018), pp. 271-340

[93] D.B. Wilson. "Mixing times of Lozenge tiling and card shuffling Markov chains." *Ann. Appl. Probab.* 14, 274-325 (2004)

[94] C.P. Yang. "Exact solution of a model of two-dimensional ferroelectric in an arbitrary external electric field." *Phys. Rev. Letters*, v. 16 (1967), n10, 586-588.

[95] C.N. Yang, C.P. Yang. "One-Dimensional Chain of Anisotropic Spin-Spin Interactions, I and II." *Phys. Rev.*, v. 150 (1967), n1, 321-339.

[96] P. Zinn-Justin. "The Influence of Boundary Conditions in the Six-Vertex Model", *Preprint* arXiv:cond-mat/0205192.